

Generation of High-Energy Pulses by Managing the Kerr-Nonlinearity in Fiber-Based Laser Amplifiers

Von der Fakultät für Mathematik und Physik
der Gottfried Wilhelm Leibniz Universität Hannover
zur Erlangung des akademischen Grades

Doktor der Naturwissenschaften
– Dr. rer. nat. –

genehmigte Dissertation von

Paul Reppen
geboren am 26. Mai 1991 in Düsseldorf

2021

Referent: Prof. Dr. Uwe Morgner
Korreferenten: Prof. Dr. Detlev Ristau
Prof. Dr. F. Ömer Ilday
Tag der Promotion: 25. Januar 2021

Abstract

Increasing the pulse energy of ultrafast laser systems is an important field of laser development. High pulse energies simplify and accelerate most applications, such as the stimulation of optical parametric effects or the processing of materials. The amplification of ultrashort pulses in glass fibers is a prominent method, as fiber amplifiers are inexpensive, flexible and highly-integrated. Resulting from the strong confinement in the fiber core and the high peak intensities of the laser pulses, the amplification is often limited by the onset of a nonlinear deterioration of the pulses.

Within this thesis, two methods of fiber-based pulse amplification by managing the Kerr-nonlinearity are presented. In the first method, the chirped-pulse amplification, nonlinear effects are suppressed by locally reducing the peak intensity. A chirped-pulse amplifier was realized that generated pulses with energies of 450 nJ and durations of 293 fs, limited by pump power. These pulse parameters were not sufficient for the intended application. In order to further decrease the pulse duration and increase pulse energy, the parameters of the amplified pulses had to be decoupled from the seed pulses. This is achieved in an amplifier based on the second approach. By enforcing the impact of Kerr-nonlinearity, the optical spectrum of self-similar pulses could be broadened by self-phase modulation during the amplification to generate pulses with 1 μ J pulse energy and a compressed duration of 50 fs at which level the amplification was limited by transverse mode instabilities.

This improvement of pulse parameters by nonlinear techniques is also exploited in a pulse regenerator. By feeding back a part of the amplified pulse into a second amplifier, a so-called Mamyshev oscillator is formed. Its principle of alternating spectral filtering between sections of gain and spectral regeneration allowed for the generation of mode-locked pulses. This Mamyshev oscillator was optimized for the generation of high-energy pulses by the analysis of optimum band-pass filter parameters and the implementation of a few-mode gain fiber. A pulse with a maximum energy of 650 nJ and a compressed duration of < 100 fs was achieved. This was the highest pulse energy achieved by a Mamyshev oscillator based on standard Yb-doped fibers to date, even surpassing the performance of state-of-the-art Titanium:Sapphire lasers. A transfer of the Mamyshev oscillator concept to the regime of Thulium-doped gain fibers with the wavelength 2 μ m is challenging due to the anomalous dispersion of the gain fibers which prevents parabolic pulse evolution. Nevertheless, a realization of this design is feasible. Mode-locked pulses with durations of < 200 fs and pulse energies of 6.4 nJ were achieved. At this pulse duration it was the highest output power from a Thulium-doped fiber oscillator to date.

Due to the alteration of the pulse shape in the glass fibers, a characterization of the final pulses is necessary. A recently developed method for the required complete pulse analysis was transferred from the application in solid-state systems to fiber-based systems in this thesis, which involves the management of less precisely defined amounts of dispersion. The complete characterization by dispersion scans based on a grism compressor was achieved by the use of an adequate retrieval algorithm.

Key words: d-scans, chirped-pulse amplification, nonlinear amplification, Mamyshev oscillator

Kurzzusammenfassung

Intensive, ultrakurze Laserpulse sind eine notwendige Voraussetzung für deren Nutzung als Werkzeug in vielen Anwendungen. Die Verstärkung in Glasfasern ist dabei eine weit verbreitete Methode, weil Glasfaserverstärker kostengünstig und flexibel handzuhaben sind. Außerdem ist ein hoher Integrationsgrad möglich. Wegen der Beschränkung der Lichtintensität auf den Kern der Glasfaser und der daraus resultierenden extrem hohen Spitzenleistungen ist die Verstärkung der ultrakurzen Pulse oft durch nichtlineare Effekte begrenzt, durch die die Pulsqualität vermindert wird.

In dieser Arbeit werden zwei Ansätze für die faserbasierte Pulsverstärkung unter kontrolliertem Einfluss von Kerr-Nichtlinearität vorgestellt. Zum einen können nichtlineare Effekte unterdrückt werden, indem die Spitzenintensität lokal reduziert wird. Ein auf diesem Prinzip basierender Verstärker (engl. *chirped-pulse amplifier*) wurde realisiert und ermöglichte Pulsdauern von 293 fs und Pulsenergien von 450 nJ, limitiert durch die Pumpleistung. Um die Pulsdauern für die geplante Anwendung weiter zu verkürzen und die Pulsenergie weiter zu erhöhen, müssen die Parameter der verstärkten Pulse durch einen Verstärker für selbstähnliche (engl. *self-similar*) Pulse von den Eingangspulsen entkoppelt werden. Durch die gezielte Herbeiführung einer spektralen Verbreiterung durch Selbstphasenmodulation, konnten in diesem zweiten Verstärker Pulsenergien von bis zu 1 μ J mit Pulsdauern von 50 fs erzeugt werden.

Diese nichtlineare Verbesserung der Pulsqualität wurde ebenfalls in einem Pulsregenerator ausgenutzt. Durch die Rückkopplung eines Teils des verstärkten Pulses in einen zweiten nichtlinearen Verstärker wurde ein sogenannter Mamyshev Oszillator aufgebaut. Durch das Prinzip der alternierenden spektralen Filterung zwischen Abschnitten der spektralen Regeneration können modengekoppelte Pulse erzeugt werden. Das Konzept des Mamyshev Oszillators wurde für die Erzeugung hoher Pulsenergien optimiert, indem die Parameter der Bandpass-Filter optimiert wurden und eine Verstärkerfaser mit einem Kerndurchmesser von 20 μ m verwendet wurde. Die Erzeugung von Pulsen mit maximalen Energien von 650 nJ und Dauern von < 100 fs war möglich. Mit dieser Pulsenergie übertrifft der Mamyshev Oszillator die Leistung handelsüblicher Titan:Saphir-Oszillatoren deutlich. Ein Wechsel hin zu Thulium-dotierten Verstärkerfasern hatte die Schwierigkeit, dass diese Verstärkerfasern im relevanten Wellenlängenbereich um 2 μ m anomal dispersiv sind, was eine parabolische Pulsentwicklung verhindert. Nichtsdestotrotz war die Erzeugung von modengekoppelten Pulsen möglich und Pulse mit Dauern von weniger als 200 fs und Energien von 6.4 nJ wurden realisiert. Bei dieser Pulsdauer ist das die bis heute höchste Pulsenergie eines Thulium-dotierten Faseroszillators.

Wegen der Änderung der Pulsparameter in den Glasfasern war die vollständige Analyse der ultrakurzen Pulse notwendig. Eine Methode besteht darin, die Dispersion durch den Pulskompressor abzurastern (engl. *dispersion scan*). Die Übertragung dieser eigentlich für Pulse mit wenigen optischen Zyklen (engl. *few-cycle pulses*) entwickelten Methode auf Pulse eines Fasersystems mit Grism-Kompressor wurde durch die Verwendung eines adäquaten Auswertalgorithmus ermöglicht.

Schlagwörter: d-scans, Verstärkung gestreckter Pulse, nichtlineare Verstärkung, Mamyshv Oszillator

Contents

1. Introduction	1
2. Fundamentals of Ultrashort Pulses in Glass Fibers	5
2.1. Optical Glass Fibers	5
2.2. Self-Phase Modulation	12
2.3. Self-Steepening	13
2.4. Stimulated Raman Scattering	14
3. Fundamentals of Fiber-Based Amplification Schemes	15
3.1. Chirped-Pulse Amplification	15
3.2. Optical Wave Breaking	18
3.3. Self-Similar Pulse Evolution	18
3.4. Pulse Generation in Mamyshev Oscillators	20
4. Characterization of Ultrashort Pulses by Dispersion Scans	25
4.1. Dispersion Scans	25
4.2. Experimental Results	27
4.3. Conclusion	29
5. Linear Amplification of Ultrashort Pulses in Glass Fibers	31
5.1. State of the Art	31
5.2. Experimental Results	33
5.3. Conceptual Limitations	41
5.4. Conclusion	42
6. Nonlinear Amplification of Ultrashort Pulses in Glass Fibers	45
6.1. State of the Art	45
6.2. Experimental Realization	46
6.3. Conclusion	54
7. Nonlinear Amplification with Feedback in Normal Dispersion Fibers	55
7.1. Ultrafast Oscillators Based on Ytterbium-Doped Fibers	55
7.2. Experimental Results	57
7.3. Conclusion and Prospects	65
8. Nonlinear Amplification with Feedback in Anomalous Dispersive Fibers	67
8.1. Ultrafast Oscillators Based on Thulium-Doped Fibers	67
8.2. Experimental Results	68
8.3. Numerical Analysis	74
8.4. Conclusion and Prospects	78

Contents

9. Summary and Prospects	81
Appendix	85
A. Mode-locking by Nonlinear Polarization Evolution	85
B. Grating-Prism Compressors	87
C. Established Pulse Analysis Methods	89
D. Numerical Model	91
Bibliography	93
Publications	109
Curriculum Vitae	111

1. Introduction

Ultrafast laser systems allow the emission of very intense light fields in form of ultrashort pulses. Thus, they serve as a universal tool in diverse applications, such as short-time physics [43], optical telecommunication [19], or cutting and marking of biological tissue [35] or metals, ceramics and more [16]. Ultrashort pulse laser systems are continuously optimized for specific applications with the target of increasing the pulse energy, reducing the pulse duration or the complexity and cost of the system.

Ultrashort laser pulses are usually generated in a master-oscillator, providing the required spectral bandwidth and repetition rate of the pulse train for applications with a low pulse energies. Because of the relatively low intensities in the seed oscillator, the pulse parameters can be adequately controlled. In a power-amplifier the pulse energy is subsequently scaled up to the required level. During and after amplification the stronger influence of nonlinear effects must be managed, which have an impact e. g. on the optical spectrum or the spectral phase and, therefore, pose a potential to deteriorate the pulses.

State-of-the-art solid-state lasers, e. g. based on Titanium:Sapphire (Ti:Sa), currently allow the generation of the highest pulse peak powers and pulse energies [73] and are the dominant platform for the generation of femtosecond pulses for scientific applications. Ti:Sa-lasers have the drawbacks to be very complex, expensive and unreliable for many applications and are thus rarely found outside of research laboratories. The use of optical fibers is a prominent approach to simplify beam guidance and generation of ultrashort pulses. Optical fibers doped with rare earth elements like Ytterbium or Thulium provide small-signal gains of up to 40 dB and long upper energy level life times, up to milliseconds [101]. Furthermore, optical fibers in general can easily be bent, have excellent guiding properties, and are inexpensive due to the production in large quantities for the telecommunications market.

Resulting from the strong confinement, the high peak intensities of light, and the long interaction length of light and glass in fibers, nonlinear effects have a much higher significance on the pulse evolution in glass fibers than in solid-state systems [2]. Pulse alterations by nonlinear effects can be circumvented by locally reducing the peak power and thereby amplifying the pulses in a linear regime [129]. In chirped-pulse amplifiers, the pulses are temporally stretched, amplified, and then recompressed. The development of this technique has been awarded with the Nobel Prize in Physics in 2018¹ and has become a well-established technique by now. In solid-state laser systems, i. e. crystal-based systems, the amount of dispersion that is required for pulse chirping can be controlled quite precisely, because besides the intended chirping element, the other components hardly induce any dispersion. Furthermore, the threshold of the nonlinear limitation can be increased, as the laser beam diameter can be strongly enlarged. In fiber-based systems, the optical fibers must be considered as a source of dispersion, as well as a source of potential nonlinear phase that must both be compensated. Sophisticated pulse

¹“All Nobel Prizes in Physics”, <https://www.nobelprize.org/prizes/lists/all-nobel-prizes-in-physics/>, accessed September 7, 2020.

1. Introduction

compressors that can compensate the group velocity dispersion as well as higher order dispersion individually, were developed with great effort. Nonlinear effects are most efficiently suppressed by the local reduction of the laser intensity in time and space. The temporal intensity distribution is achieved by dispersion, spatial distribution in fibers with large core diameters in the range of 20 – 40 μm . In large core fibers, transversal mode instabilities must be considered that strongly limit the beam quality.

Pulse alterations by nonlinear effects can be enforced in order to improve the pulse parameters. While the chirped-pulse amplification in presence of strong gain is ultimately limited to ≈ 120 fs-pulses in the wavelength-regime of Ytterbium-doped fibers due to gain narrowing [70], the pulses can be shortened by an order of magnitude when properly managing the nonlinearities [53]. Applied in a controlled manner, self-phase modulation can be used to increase the spectral width and establish a linear spectral phase on the pulse so that the pulse can easily be compressed temporally [30]. This amplification based on nonlinear effects is enabled by the self-similar pulse propagation in normal dispersive fibers. Under ideal conditions, in the absence of higher order dispersion or higher order nonlinear effects like self-steepening, the energy scaling would be unlimited.

Concatenating two nonlinear amplifiers with a feedback enables the design of a new type of oscillator concept, called the Mamyshev oscillator [39]. This design has drawn much research attention lately, because of the possible high output pulse energies in combination with very broad spectra, that even exceed the performance of commercial Ti:Sa-lasers². The exceptional performance of this laser design results from alternating spectral filtering between sections of spectral regeneration by nonlinear effects. In comparison to the routinely applied nonlinear polarization evolution mode-locking mechanism, the Mamyshev oscillator does not show an output pulse limitation due to the nonlinear overdrive of the saturable absorption, which makes it an extremely attractive concept for use as a high-power seed source in a master-oscillator power-amplifier system.

Self-similar amplification depends on normal dispersive fibers. This limited the realization of Mamyshev oscillators to the use of Ytterbium- and Erbium-doped gain fibers so far. In order to set up high power seed sources in the regime of Thulium-doped gain media, the concept must be transferred to the 2 μm wavelength range, in which the gain fibers are anomalous dispersive and self-similar pulse evolution is not possible.

Following from the complexity of the pulse's spectral phase after amplification and compression, reliable methods for pulse analysis must be available. The complete characterization of pulses is challenging due to their short duration. Several methods have been proposed, relying on a self-referencing of the pulses [137]. A recent development for the complete characterization of ultrashort pulses is the d-scan method, an abbreviation for dispersion scan [89]. This method takes advantage of the compressor and enables a retrieval of the pulse shape by analyzing a nonlinear signal with different amounts of dispersion. Although initially developed for the use in few-cycle systems, the application in fiber-based laser systems with longer pulse durations is also promising and its exploitation of the pulse compressors for both, compression and characterization, allows for a high integration level.

²"Vitara-Family by Coherent Inc.", <https://www.coherent.com/lasers/laser/vitara-family>, accessed September 8, 2020.

In this thesis, multiple aspects for the amplification of ultrashort pulses in glass fibers are discussed. In the beginning, a theoretical introduction is given in Chapters 2 and 3, presenting the fundamentals of glass fibers and their impact on the evolution of ultrashort pulses, respectively. As mentioned above, due to the presence of nonlinear effects and dispersion, the pulse shape is altered, thus requiring a reliable means for pulse analysis. In Chapter 4, the d-scan method is introduced and its application for the use in combination with a grating-prism compressor is demonstrated. Furthermore, the principle of autocorrelation and a standard, well-established method for the complete pulse characterization, the frequency-resolved optical gating, are presented in the Appendix C. In Chapter 5, the chirped-pulse amplification is analyzed, regarding scaling potential and limitations. As an alternative, a nonlinear amplification scheme is presented in Chapter 6. Here, nonlinearities were exploited in order to improve the pulse parameters compared to those achieved from the chirped-pulse amplification. The possibility of linking two nonlinear amplifiers with a feedback also enables the generation (rather than the mere amplification) of ultrashort, mode-locked pulses. This is the principle of the Mamyshev oscillator, which will be introduced in Chapter 7. The Mamyshev oscillator is optimized to generate high pulse energies in order to evaluate the potential omission of one or more amplification stages. In order to address further wavelength ranges, the concept of the Mamyshev oscillator is transferred to the Thulium-regime. The advantages as well as the challenges are discussed in Chapter 8. The thesis ends with a conclusion and prospects in Chapter 9.

2. Fundamentals of Ultrashort Pulses in Glass Fibers

Optical glass fibers¹ are widely used and very versatile in their occurrence due to their established use in telecommunications and as beam delivery devices in laser systems. Despite the advantages in light guiding, in laser systems glass fibers can show “side effects” when guiding ultrashort pulses. Due to the tight confinement of the pulse energy, the high peak intensity and the long interaction of light and glass, the material response to the intense field is nonlinear. On the other side, those nonlinear effects can also be expedited and exploited for shaping, regeneration or the improvement of pulses. Furthermore, due to the broad optical spectrum, the pulse shapes are altered by dispersion.

In this chapter, the fundamentals of pulse propagation in glass fibers are introduced. In Section 2.1, the categorization of and pulse manipulation in glass fibers will be thematized. In Section 2.2, the self-phase modulation as the nonlinear effect with the strongest impact on ultrashort pulses will be introduced in particular. Following self-phase modulation, self-steepening is introduced in Section 2.3, as an example for a nonlinear effect that becomes significant for very short pulses.

2.1. Optical Glass Fibers

The most common type of glass fibers is the step-index fiber. The step-index fiber guides light by total internal reflection: A glass core with a refractive index n_{co} is surrounded by a glass cladding with a lower refractive index n_{cl} . The refractive index of the glass core can be increased by doping it with an additional material, e. g. Germanium. According to Snell’s law

$$n_1 \cdot \sin(\alpha_1) = n_2 \cdot \sin(\alpha_2), \quad (2.1)$$

the light is confined in the core due to total internal reflection for angles larger than the critical angle α_c

$$\alpha_c = \arcsin\left(\frac{n_2}{n_1}\right) = \arcsin\left(\frac{n_{\text{cl}}}{n_{\text{co}}}\right), \quad n_1 > n_2. \quad (2.2)$$

The acceptance angle of total reflection at the interface of core to cladding in the fiber depends on the refractive index difference of core and cladding. This can be determined by the numerical aperture (NA) [116]:

$$\text{NA} = \sqrt{n_{\text{co}}^2 - n_{\text{cl}}^2}. \quad (2.3)$$

¹The terms “optical fiber”, “glass fiber” and “optical glass fiber” are used synonymously within this thesis.

Transverse Fiber Modes The boundary conditions of the light propagation in glass fibers depend on the refractive index difference. In the case of standard step-index fibers the difference is usually small, i. e. $n_{\text{co}} \approx n_{\text{cl}}$, so that the guided rays are approximately parallel to the fiber axis [116]. Small angle variations of the light in the fiber form interference patterns that are dominated in shape by the wave nature of the light [115]. The longitudinal components of the electromagnetic field can be neglected for the description of the intensity distribution of the mode. Due to the transverse components of the electromagnetic field, the linear polarization in x and y -direction forms orthogonal polarization states, and the mode is hence referred to as linear polarized (LP) mode [116]. The fundamental intensity distribution in the glass fiber (LP₀₁-mode) is very close to the intensity distribution in a Gaussian beam. Under the correct boundary conditions, fibers can be optimized to only guide the fundamental mode, which leads to excellent beam qualities. By the V -number, it can be determined, if the boundary conditions for single-mode guidance are matched. It is defined as [124]

$$V = \frac{2\pi a}{\lambda} \cdot \sqrt{n_{\text{co}}^2 - n_{\text{cl}}^2}, \quad (2.4)$$

with the fiber core-diameter a and the operating wavelength λ . Fibers guide the fundamental mode exclusively, if the V number is below the critical value of $V_c = 2.4045$. Fundamental mode guidance is, therefore, a compromise between a large core (less nonlinearities) and a large NA (easy fiber handling). For decreasing wavelengths, the fiber can guide multiple modes again, the cutoff wavelength λ_c is given by

$$\lambda_c = \frac{2\pi a}{V_c} \cdot \sqrt{n_{\text{co}}^2 - n_{\text{cl}}^2}. \quad (2.5)$$

Fibers with a V -number only slightly higher than V_c also support higher order modes, which can be efficiently suppressed by coiling of the fiber [87, 68].

Polarization Maintaining Fibers Strictly speaking, a single-mode fiber can support two modes; the fundamental mode in two orthogonal polarization states. Those two modes are degenerate in terms of the propagation constant. If the cylindrical symmetry of the fiber is broken, e. g. by stress on the fiber, the degenerate modes can decouple. Stress on the fiber induces birefringence, leading to a higher refractive index in one axis. Due to the refractive index difference between the two axes, the group velocities in the axes differ from each other. The axes are referred to as *fast* and *slow axis*. The group velocity difference leads to a polarization-dependent modal dispersion. Randomly induced stress on the fiber decreases the degree of polarization as the light is split at an arbitrary angle to the axes. Stress can also be induced intentionally, e. g. by stress rods in the cladding. This leads to a strong decoupling between the polarization modes. If the light is launched along one polarization axis, the propagation of light in one polarization can be preserved, despite minor imperfections due to coiling of the fiber or deviations in the cylindrical symmetry from the manufacturing process. These fibers are called polarization maintaining (PM) fibers.

If the two polarization states propagate simultaneously in the fiber, energy is transferred periodically between the two polarization states. The length of the period is called polarization beating length L_B [2], with

$$L_B = \frac{\lambda}{|n_x - n_y|} \quad (2.6)$$

depending on the wavelength λ and the difference of the refractive indices of the two axes. The intentionally induced birefringence usually causes a difference of the refractive index of roughly $|n_x - n_y| \approx 10^{-4}$. This results in a polarization beating length of $L_B \approx 1$ cm at a wavelength of $1 \mu\text{m}$.

Dispersion Besides the polarization-induced dispersion, light propagating in glass fibers experiences dispersion from various sources. The propagation speed of light results from the frequency-dependent refractive index of the medium in which the propagation takes place. This is referred to as *chromatic dispersion*. In the presence of a broadband optical spectrum, e. g. from ultrashort pulses, the different propagation constants must be considered. For the mathematical description of the chromatic dispersion, the propagation constant $\beta(\omega) = n(\omega) \cdot \omega/c$ is expanded in a Taylor series around the central angular frequency ω_0 of the light [2]:

$$\begin{aligned} \beta(\omega) &= \sum_{k=0}^{\infty} \frac{1}{k!} \frac{d^k \beta(\omega)}{d\omega^k} (\omega - \omega_0)^k \\ &= \beta_0 + \beta_1(\omega - \omega_0) + \frac{1}{2}\beta_2(\omega - \omega_0)^2 + \frac{1}{6}\beta_3(\omega - \omega_0)^3 + \dots \end{aligned} \quad (2.7)$$

In this expansion, β_0 is a phase shift of the electrical field. This phase shift determines the carrier envelope offset (CEO) and is only important for few-cycle pulses. The term including β_1 describes a linear spectral and temporal phase on the pulse and corresponds to a time shift of the pulse. The group velocity v_g , i. e. the speed of the pulse envelope, is given by $\beta_1 = 1/v_g$. The second order or group velocity dispersion (GVD), β_2 , describes a quadratic spectral and temporal phase that is induced to the pulse. The frequency components of the pulse are rearranged linearly from red to blue (red being the faster frequency component) in case of normal dispersion ($\beta_2 > 0$) and from blue to red (blue being the faster frequency component) in the case of anomalous dispersion ($\beta_2 < 0$). The quadratic temporal phase on the pulse is also referred to as linear chirp, due to the linear rearrangement of the frequency components. Usually, in order to achieve pulse durations down to ≈ 200 fs, it is sufficient to consider GVD for dispersion compensation. For pulse durations less than ≈ 200 fs, also the third order dispersion (TOD), β_3 , must be compensated [93]. TOD introduces a cubic phase to the pulse, corresponding to a quadratic chirp. By TOD, the frequency components are rearranged such that red and blue frequency components overlap and interfere. This generates a characteristic train of satellite pulses, which can be used to verify uncompensated TOD on the pulse. The effects of GVD and TOD on the pulse are also depicted in Figure 2.1. The electric field is shown in Figure 2.1 (a) and (c), with the corresponding intensity, instantaneous frequency and phase distribution over the pulse in Figure 2.1 (b) and (d). The instantaneous frequency ν_{inst} results from the negative derivative of the temporal phase $\phi(t)$ [138].

The total chromatic dispersion consists of the components resulting from the material dispersion, which is a material property, and the waveguide dispersion, which results from the fact, that core and cladding of a fiber are different materials. The fiber mode always sticks out from the fiber core into the cladding. As the phase velocity of the light field is different in core and cladding, the group velocity of the mode is altered [116]. The type of dispersion (normal or anomalous) depends on the fiber material and the wavelength of the light. In fused silica fibers for instance, the zero-dispersion wavelength is around

2. Fundamentals of Ultrashort Pulses in Glass Fibers

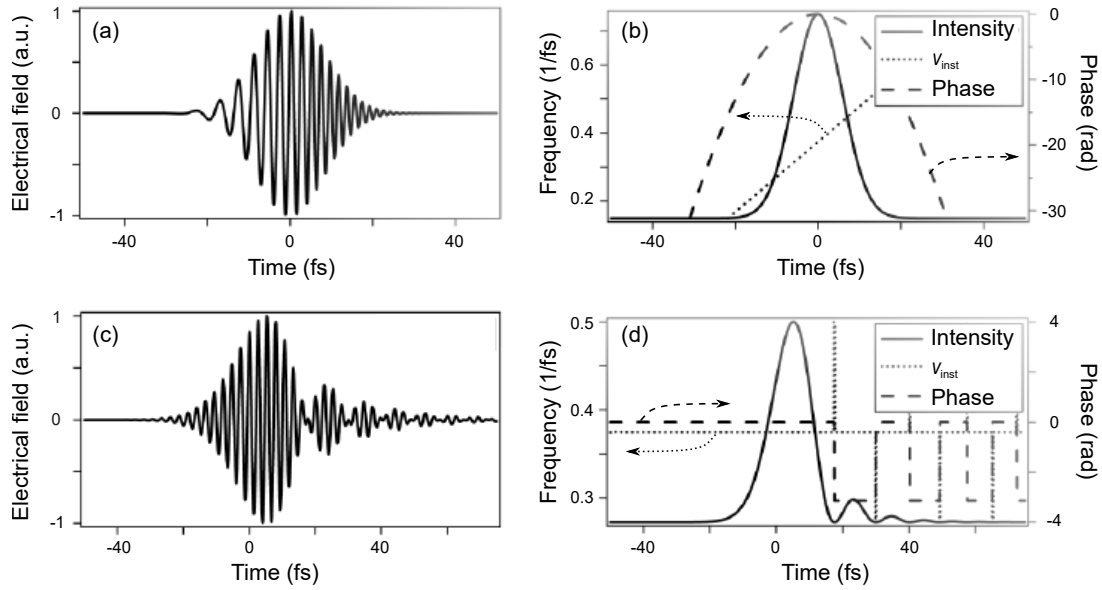


Figure 2.1.: Effect of the dispersion on the pulse: rearrangement of the electrical field following (a) second and (c) third order dispersion, variation of intensity, instantaneous frequency ν_{inst} , and temporal phase, following (b) second and (d) third order dispersion [138].

1300 nm. Shorter wavelengths underlie normal dispersion, longer wavelengths anomalous dispersion. The waveguide dispersion can be manipulated by a reduction, respective increase, of the core diameter, such that a larger, respective smaller, part of the light is guided in the cladding. If the waveguide dispersion is sufficiently high, it dominates the material dispersion. This way, fused silica fibers can also be normal dispersive at wavelengths larger than 1300 nm.

Photonic Crystal Fibers The *photonic crystal fiber* (PCF) was developed by the group of P. Russell in the 1990s [66, 12, 140]. Nowadays, PCFs exist in various versions, with different applications and optimization goals. They can be roughly divided into two types: high-index core fibers and low-index core fibers².

Low-index core fibers have a core with a lower index than that of the cladding. The low refractive index is usually realized as a hollow core filled with air or a gas. As light is not guided in this structure by total internal reflection, guidance relies on the photonic band gap effect. The photonic band gap results from a wavelength-scale periodic structure that generates areas (the cladding) of forbidden light propagation [115]. Due to the wavelength-scale dimensions, Bragg reflection appears, confining the light in the fiber core [8]. Properly designed as two-dimensional structures, e. g. air holes surrounding the core, waveguide properties can be achieved. An analogy in material physics is the band gap between two different energy bands of a solid. As the energy band gap in a solid can be surpassed by the correct energy, the photonic band gap fibers also requires light at a matching photon energy, i. e. wavelength, to be guided. The hollow core along with the strong boundary conditions allows for interesting applications, such as the transport of high pulse energies with a low influence of nonlinear effects (due to the hollow core) and

²"NKT Photonics", <https://www.nktphotonics.com/>, accessed: September 21, 2020.

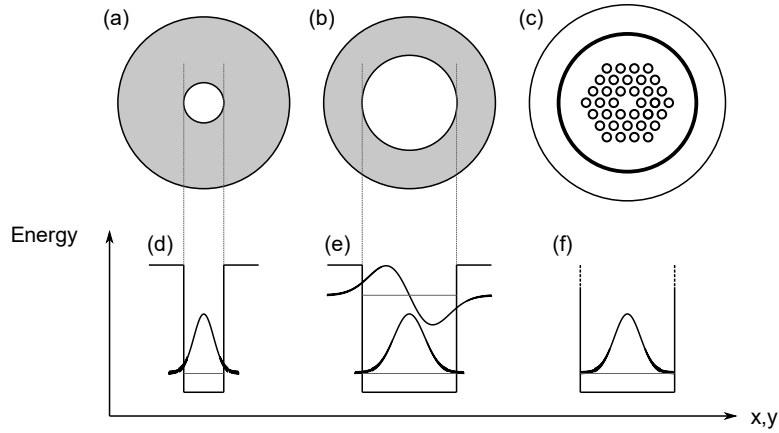


Figure 2.2.: Illustration of different fiber types (a)-(c) as an analogon to the quantum well (d)-(f). Single-mode fibers (a), (d) correspond to a narrow, finite quantum well in which only a single energy state or mode can be confined. The lower refractive index of the cladding is indicated gray. Following from the finite barriers, the mode-field is larger than the core area, i. e. a part of the intensity is guided in the cladding. Multi-mode fibers (b), (e) correspond to a broad, finite quantum well. In the broad well, several energy states (modes) can be confined. The photonic crystal fiber (c), (f) corresponds to an infinite quantum well. As the electrical field cannot be guided in the cladding, the core diameter can be much larger before a higher order mode can be confined.

very small losses to a small bending radius. Loading the fiber with a gas can also lead to an enhancement of nonlinear effects. A noble gas such as Argon or Xenon has a relatively high nonlinear coefficient and a high threshold for ionization [9]. This can be used for self-compression of ultrashort pulses.

Opposed to the low-index core fibers, the core in high-index core fibers usually consists of pure silica. The cladding is composed of an air-hole structure. Resulting from the structure with the forbidden zones and the clear pathways, the fiber acts as a “sieve” for different modes: The fundamental mode is confined in the core, while higher order modes fall through the sieve [115]. As depicted in Figure 2.2, standard fibers require a smaller core-diameter to prevent the guidance of higher order modes (Fig. 2.2 (a), (b)). Due to the stronger suppression of the light guidance in the cladding of the PCF, the mode-field can be increased without the potential guiding of higher order modes (Fig. 2.2 (c)).

Solid core PCFs can also be approximated as step-index fibers, because the average refractive index of the cladding is merely reduced by the air holes in the pure silica host. By the use of the air holes, the effective index of the cladding is only very slightly reduced relative to the core-index. This enables a low NA, while simultaneously allowing for a large mode-field diameter. In analogy to the V number in step index fibers (cf. Eq. (2.4)), an effective V_{eff} number for the single-mode guidance of PCFs can be defined [12]:

$$V_{\text{eff}} = \frac{2\pi\Lambda}{\lambda} \cdot \sqrt{n_0^2 - n_{\text{eff}}^2}. \quad (2.8)$$

Here, Λ is the hole-spacing (also called pitch), λ the wavelength, n_0 is the refractive index of the core, and n_{eff} the average (effective) refractive index of the hole-structure region (cladding).

2. Fundamentals of Ultrashort Pulses in Glass Fibers

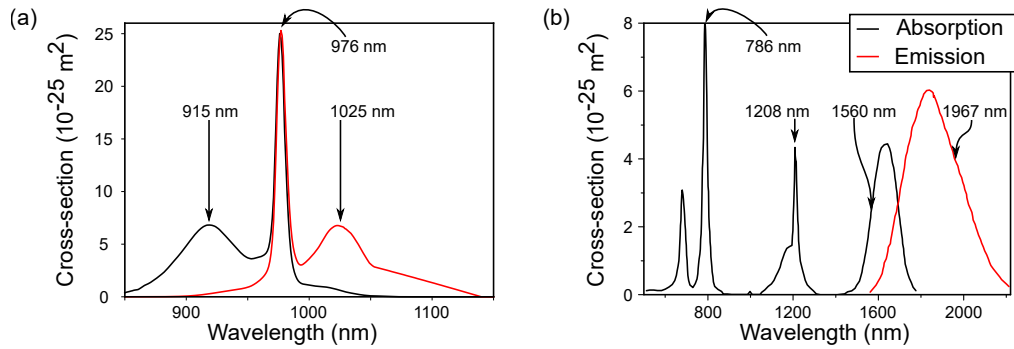


Figure 2.3.: Absorption and emission cross-sections of (a) Yb-doped glass fibers, from [101], and (b) Tm-doped glass fibers, from [1].

The integrity of the airhole-structure of the PCFs is critical for its guiding performance. Splicing of standard fibers to PCFs is difficult, because the holes in the PCF may collapse during the process. Photonic crystal fiber components were reported, but are usually lossy [71]. Therefore, signal light often coupled to the PCF via a free-space section.

Active Fibers Besides the passive transportation of light, glass fibers can be used to manipulate the signal amplitude as well. The doping of the fiber core with rare earth materials allows the amplification of light in various spectral regions. Most common dopants are Ytterbium (Yb) for the amplification at $\approx 1 \mu\text{m}$, Erbium (Er) for the spectral region around $1.5 \mu\text{m}$ wavelength and Thulium (Tm) and Holmium (Ho) for the amplification of light with wavelengths around $2 \mu\text{m}$. Due to the amorphous structure of the glass host material, the emission and absorption are very broadband, as shown in Figure 2.3. Yb-doped fibers have a very narrow but significant absorption peak at 976 nm (Fig. 2.3 (a)). High gain can be achieved by pumping at this wavelength with a semiconductor-based laser diode. The strongest emission wavelength is around 1030 nm. Tm-doped gain fibers have a broad absorption cross-section (Fig. 2.3 (b)). It can be pumped at 1550 nm, i. e. with an Er-based fiber laser or alternatively at 793 nm, which is covered by commercially available high-power laser diodes. Pumping at the wavelength 793 nm can lead to a 2-for-1 emission, where two signal photons are generated from one pump photon. This scheme results in a very high quantum efficiency despite the large quantum defect. The emission cross-section of Tm-doped fibers is very broad, but with a significant overlap with the absorption. As a result, the main emission wavelength of Tm-doped fibers depends on the inversion level of the active medium. The broad gain bandwidths make the rare earth doped fibers attractive active media for the generation of ultrashort pulses.

As the absorption and emission bands overlap in both, Yb and Tm-doped fibers, the effective gain bandwidth is reduced. The gain bandwidth for Yb from $\approx 1010 \text{ nm} - 1060 \text{ nm}$, corresponding to 14.0 THz is comparable to the effective bandwidth of Tm from $\approx 1800 \text{ nm} - 1950 \text{ nm}$, corresponding to 12.8 THz. The amplification of laser light in glass fibers has several advantages compared to crystal gain media, as e. g. the long interaction length between active medium and light. Furthermore, the relation of surface to volume is large, which simplifies the cooling of the active medium.

Nonlinear Effects The response of the glass fiber to an intense light field is nonlinear. This nonlinearity results from the motion of the bound electrons in the glass fibers. In the presence of a strong field the motion becomes anharmonic, i. e. nonlinear [2]. The resulting nonlinear effects are categorized in different orders, depending on the amount of photons that are required for the specific interaction. The second-order nonlinearity for instance causes second-harmonic generation or sum-frequency generation. Due to the inversion symmetry of silica molecules, the second-order nonlinearity is zero in fused silica fibers [2]. Fiber nonlinearities are dominated by third-order nonlinearities. Third-order nonlinearities cause third-harmonic generation, four-wave mixing, and, most importantly for the pulse propagation, an alteration of the refractive index n , which is increased in the presence of an intense field, following the relation

$$n(\omega) = n_0(\omega) + n_2 I. \quad (2.9)$$

Here, $n(\omega)$ is the total refractive index depending on the frequency of the light, n_0 is the linear part of the refractive index and n_2 the nonlinear refractive index, scaling with the intensity I . The nonlinear refractive index is relatively small. In the case of fused silica at the wavelength of 1030 nm, the nonlinear refractive index is $n_2 = 2.19 \cdot 10^{-20} \text{m}^2/\text{W}$ [54]. Due to the tight confinement of the light in the fiber and the high peak intensities of ultrashort pulses, the nonlinear refractive index becomes significant for the propagation in fibers.

An important measure for the impact of nonlinearity to a pulse is the accumulated nonlinear phase, quantified by the B-integral:

$$B(z) = \int_0^L \gamma(z) P(z) dz \quad (2.10)$$

The B-integral depends on the propagation length L along the fiber, the pulse peak power and the fiber-dependent nonlinear coefficient γ with [2]

$$\gamma(\omega_0) = \frac{n_2 \omega_0}{c A_{\text{eff}}}. \quad (2.11)$$

Here, c is the speed of light and A_{eff} the effective area of the fiber core. Values of the B-integral of less than π , such as in chirped-pulse amplification systems (cf. Chapter 5), are usually classified as linear.

The propagation of ultrashort pulses in glass fibers is influenced by nonlinearities through the high peak powers and by dispersion effects due to the broad spectrum. The significance of the respective effects is determined by the interaction length, the spectral width and the pulse duration. To evaluate which effect dominates the pulse propagation is defined by the dispersive length L_D and the nonlinear length L_{NL} .

$$L_D = \frac{T_0^2}{|\beta_2|} \quad (2.12)$$

$$L_{\text{NL}} = \frac{1}{\gamma P_0} \quad (2.13)$$

The length L_D depends on the initial pulse duration T_0 and the second order dispersion β_2 . The length L_{NL} depends on the peak power P_0 of the pulse and the nonlinear coefficient

2. Fundamentals of Ultrashort Pulses in Glass Fibers

γ . At L_{NL} , the nonlinear phase shift $\phi_{\text{NL}} = 1$. If the (fiber) length $L \ll L_{\text{NL}}$ and $L \approx L_{\text{D}}$, nonlinear effects only have a minor impact on the pulse. The pulse temporally broadens by dispersion which further decreases P_0 and consequently increases L_{NL} . For the opposite case $L \ll L_{\text{D}}$ and $L \approx L_{\text{NL}}$, high local intensities, i. e. short pulses and small fiber cores, are required. Here, the pulse evolution is governed by nonlinear effects such as the nonlinearity of the refractive index. The most significant manifestation of the intensity-dependent refractive index variation is the self-phase modulation.

2.2. Self-Phase Modulation

At high intensities, the refractive index of media like fused silica or air increases as a result of the Kerr effect (cf. Eq. (2.9)). Thereby, an intense laser beam with a Gaussian spatial distribution focusses itself, because the intensity, and simultaneously the refractive index, is higher in the center of the beam. Self-phase modulation (SPM) can be described as the temporal analogue to self-focussing [2]. Phenomenologically, SPM can be described like the following: The instantaneous frequency depends on the index of refraction, which means that e. g. the frequency is lower in a material with a higher refractive index. As the refractive index changes rapidly during the propagation of an ultrashort pulse, a frequency shift can be observed in the course of the pulse. The spectral modulation results from the fast increase and decrease of the intensity along the pulse. The change of the refractive index shifts the phase of the pulse, which is expressed by a frequency chirp.

Mathematically, the nonlinear phase ϕ_{NL} can be described as a part of the field amplitude A . The accumulated nonlinear phase ϕ_{NL} follows the temporal pulse shape, which can be put into concrete terms by the nonlinear length L_{NL} (cf. Eq. (2.13)) [2].

$$A(L, t) = A(0, t) \exp\{i\phi_{\text{NL}}(L, t)\} \quad (2.14)$$

$$\phi_{\text{NL}}(L, t) = |A(0, t)|^2 \frac{L_{\text{eff}}}{L_{\text{NL}}} \quad (2.15)$$

Here, L_{eff} is the effective fiber length, which comprises the effect of fiber losses for the nonlinear effects: $L_{\text{eff}} = (1 - \exp\{-\alpha L\})/\alpha$, with the losses α (inverse gain) and the fiber length L .

The frequency chirp results from a variation of the phase shift. The difference of the instantaneous optical frequency $\delta\omega$ from the central frequency ω_0 can be expressed by

$$\delta\omega = -\frac{\partial\phi_{\text{NL}}}{\partial t} = -\left(\frac{L_{\text{eff}}}{L_{\text{NL}}}\right) \frac{\partial}{\partial t} |A(0, t)|^2 \quad (2.16)$$

in the dispersionless case.

It can be seen that the phase shift depends on the changes of the intensity and, therefore, on the pulse shape; the phase shift is the negative derivative of the pulse shape. The steeper the edges of the pulse, the stronger is the phase shift, as shown in Figure 2.4. This means that the frequency chirp due to SPM is stronger for a pulse with a Supergaussian shape than for a pulse with a Gaussian shape. On the other hand, a temporal interval without change of intensity results in a part of the pulse without any phase shift, leaving a strongly nonlinear phase (cf. Fig. 2.4 (b)).

In the case of an unchirped Gaussian pulse, the frequency chirp is negative at the rising slope of the pulse. Therefore, the frequency components at the leading edge are

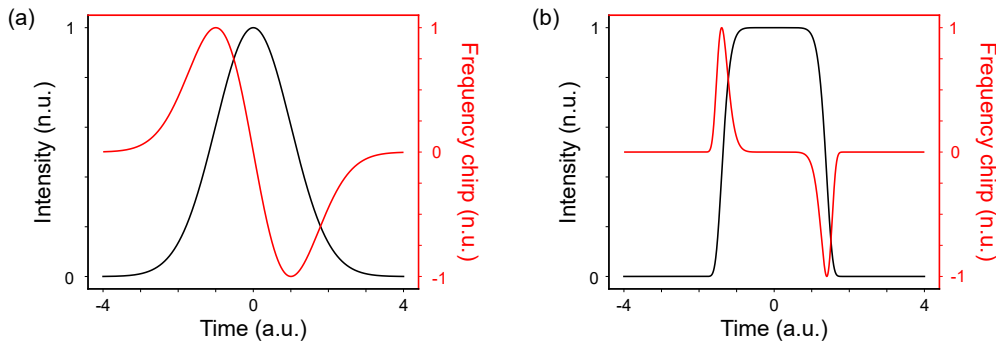


Figure 2.4.: Illustration of the frequency chirp (red), acting on a (a) Gaussian and a (b) super-Gaussian pulse shape (black). The chirp is inversely proportional to the derivative of the intensity.

red-shifted. The intensity decays on the trailing edge and the frequency chirp is positive, i. e. the frequency components are blue-shifted.

The optical spectrum of an ultrashort pulse can be broadened by SPM, if the pulse is either unchirped or up-chirped. The up-chirp is usually achieved by propagation through a normal dispersive medium, e. g. a standard glass fiber in the case of a central wavelength < 1300 nm. An initial down-chirp on the other hand means that the blue frequency components of the pulse are on the leading edge. These components are red-shifted, while the components on the trailing edge are blue-shifted; the result is a spectral narrowing.

If the effect of SPM is achieved by the interaction of two or more separate pulses, this effect is referred to as cross-phase modulation (XPM). In practice, XPM can be distinguished from SPM as the spectral changes are usually asymmetric for XPM, while SPM alters the spectrum symmetrically.

2.3. Self-Steepening

Asymmetry of the optical spectrum is not necessarily generated by XPM, but can also result from the impact of self-steepening. This nonlinear effect must be considered for pulses with durations of < 1 ps [2]. It derives from the intensity dependence of the group velocity. Due to the Kerr effect, the refractive index is increased at higher intensities, which leads to a reduction of the group velocity for the pulse peak. As the pulse wings are faster, the pulse peak is shifted to a temporally later point. The leading edge of the pulse, therefore, flattens, while the trailing edge steepens.

This altered temporal pulse shape has an impact on the spectral broadening by SPM: while SPM is weaker on the leading edge, it gets stronger on the trailing edge. That induces an asymmetry in the broadened spectrum. In the case of normal dispersive fibers, the red frequency components are on the leading edge, the blue frequency components are on the trailing edge of the pulse. The effect of spectral broadening by SPM is, therefore, stronger on the blue side than on the red side, which, in turn, leaves the red-shifted peaks with a higher intensity than the blue-shifted peaks.

The effect on the pulse is illustrated in Figure 2.5. In that simulation, a pulse with an energy of 5 nJ and an initial pulse duration of 100 fs is propagated over 5 cm and 8 cm of standard single-mode fiber with zero dispersion and a mode-field diameter of 6 μm ,

2. Fundamentals of Ultrashort Pulses in Glass Fibers

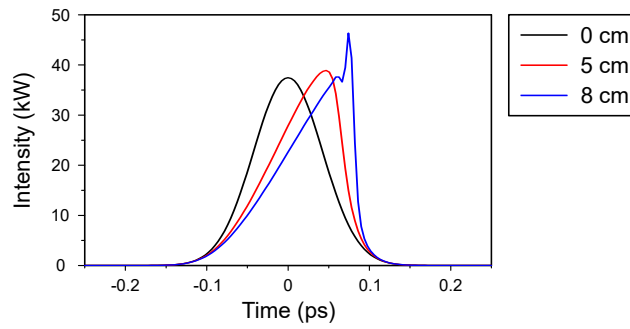


Figure 2.5.: Self-steepening of a Gaussian pulse after the propagation of 0 cm, 5 cm, and 8 cm in fiber.

underlying only self-steepening. In the temporal domain, the steeper side on the right can be clearly seen. After 8 cm of propagation, the pulse edge would be infinitely steep. In this case, the pulse wings overtake the peak, leading to the generation of multiple pulses by interferences. This situation is described by optical wave breaking (cf. Sec. 3.2).

2.4. Stimulated Raman Scattering

Raman scattering describes the inelastic scattering of a photon at a material structure. A part of the photon's energy is transferred to the material. In the material, the energy is transformed to characteristic mechanical vibrations, while the photon is emitted with the remaining energy. In glass fibers, the characteristic Raman shift has a broad peak with a maximum around 13 THz below the signal frequency, which corresponds to a shift from 1030 nm to 1078 nm [74] for Yb-based fiber amplifiers. If there is a sufficient number of shifted photons, this effect can also be stimulated. The stimulated Raman scattering limits the amplified pulse quality, because it reduces the pulse's compressibility, owing to the strong nonlinear phase that is accumulated along the amplification stage. Furthermore, it caused nonlinear optical pulse breaking, because the Raman scattering has a significant impact on the parabolic pulse shape [37].

3. Fundamentals of Fiber-Based Amplification Schemes

Nonlinear effects and dispersion as introduced in the previous chapter cause alterations of the ultrashort pulses. The nonlinear effects need to be considered and handled in order to generate pulses with both high energy and high compressibility. Thus, different paths leading to amplified pulses with different parameters can be followed.

Nonlinear effects can be avoided by temporally spreading the pulse intensity, following the concept of chirped-pulse amplification, introduced in Section 3.1. Chirped-pulse amplification is a prominent amplification method as the excessive accumulation of nonlinear phase may cause a serious deterioration of the pulse quality, e. g. by optical wave breaking (Sec. 3.2). With suitable preconditions, however, the threshold for the onset of nonlinear optical wave breaking can be drastically increased. These preconditions are introduced in Section 3.3.

The most salient advantage of self-similar nonlinear amplifiers is the improvement of pulse parameters, such as the generation of a broadband spectrum from a narrowband seed pulse. As there are almost no requirements for these seed pulses, small portions from the amplified output of nonlinear amplifiers can be used as the seed pulse. This pulse reproduction leads to a pulse source with outstanding output parameters as introduced in Section 3.4.

3.1. Chirped-Pulse Amplification

The influence of nonlinear effects scales with the optical intensity. In order to keep the amplification of the pulses in a linear regime, the peak intensity of the ultrashort pulses must be reduced spatially or temporally. Reversible temporal stretching can be achieved by chromatic dispersion. For chirped-pulse amplification (CPA), a pulse is temporally stretched prior to its amplification in a dispersive delay line and compressed afterwards. This enables a linear amplification, because of the lower pulse peak power during the amplification process, as schematically depicted in Figure 3.1. Stretching and compression

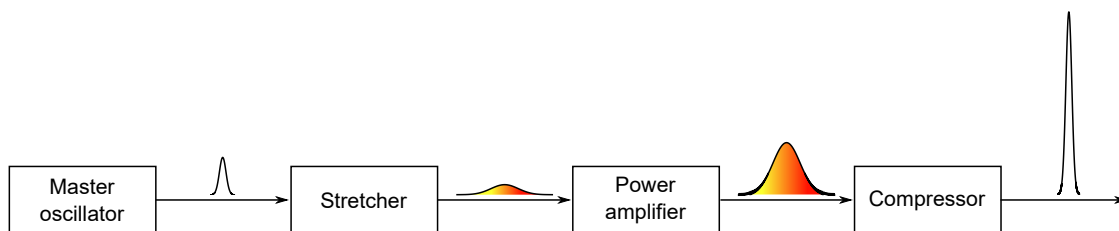


Figure 3.1.: Schematic representation of the pulse peak intensity increase by chirped-pulse amplification.

3. Fundamentals of Fiber-Based Amplification Schemes

of pulses by dispersive delay lines was first described by D. Strickland and G. Mourou in 1985 [129] and awarded with the Nobel prize in physics in 2018¹.

The overall dispersion on the pulse behind seed laser, stretcher, amplifier, and compressor should be as close to zero as possible in the classical case without any nonlinearities, in order to receive the shortest pulse. The most significant amount of dispersion is induced by stretcher and compressor. Optimally, the exact opposite amount of dispersion induced by the stretcher is induced in the compressor, i. e. stretcher and compressor should be well matched.

For the amplification of chirped femtosecond pulses with a duration below ≈ 200 fs, second and third order dispersion, for very short pulses (≈ 20 fs) also the fourth order dispersion must be compensated. The individual management of different dispersion orders increases the complexity of the system. Various combinations for stretchers and compressors have been developed with respective advantages and disadvantages. The most common designs for the induction of positive and negative dispersion are introduced in the following.

Diffraction Gratings Diffraction gratings can be used in a compressor to compensate second order dispersion (group velocity dispersion, GVD, β_2), which usually represents the most significant dispersion on the pulse [136]. Light is diffracted at different angles at the grating, according to the particular wavelength. This wavelength-dependent angle can be used to manipulate the optical path lengths. The angular distribution of the diffracted wavelength components is almost linear, resulting in an appropriate compensation of GVD by a grating compressor. Besides a negative GVD, the grating compressor applies a small amount of positive third order dispersion (TOD, β_3) and, with decreasing significance, higher orders of dispersion to the pulse. For pulses with a Fourier transformed duration of several hundreds of femtosecond, this dispersion has hardly any impact on the final pulse duration. For shorter pulses, however, TOD must also be handled.

This can be achieved by using a grating stretcher-compressor combination. Expanding two diffraction gratings by a telescope adds a degree of freedom to the setup. This allows for the introduction of positive β_2 [105, 88]. Furthermore, the TOD that is introduced by the grating stretcher matches the opposite amount of TOD induced by the grating compressor. Fine tuning of the dispersion can be obtained by varying the grating period and the angle of incidence on the gratings [61, 127].

The setup of the grating stretcher is, however, complex, as the grating separation and the telescope adjustment are critical. Furthermore, the grating stretcher poses a free-space component, which is prone to mechanical disturbances. Therefore, a fiber-based approach is often desirable.

Chirped Bragg-Gratings As the pulse energy before amplification is relatively low, fiber-based stretchers can be applied, allowing a fiber-integrated setup from oscillator to amplifier. Besides the material and waveguide dispersion from the fiber itself, periodic (or aperiodic) refractive index variations in the fiber can have a wavelength-dependent effect on the pulse shape [44, 100]. In chirped fiber Bragg-gratings, light is reflected at different spatial positions in the grating structure in the fiber. The exact reflection position in

¹“All Nobel Prizes in Physics”, <https://www.nobelprize.org/prizes/lists/all-nobel-prizes-in-physics/>, accessed September 7, 2020.

the Bragg-grating can be precisely tailored to match the sum of oscillator, amplifier and compressor, such that also higher dispersion orders can be compensated in the overall setup.

Chirped fiber Bragg-gratings can be photoimprinted into the fiber core by exposing the fiber to ultraviolet (UV)-light. The periodic grating structure is achieved by a phase mask that diffracts the UV-light to form a high-contrast intensity pattern [45]. The freedom in the production of the chirped fiber Bragg-grating makes a customized production necessary, usually resulting in high costs of this component. Chirped fiber Bragg-gratings cannot be tuned in such a wide range as grating-based stretchers, but tuning is possible, e. g. via a temperature management.

As the confinement of high pulse energies in small fiber cores in the case of fiber Bragg-gratings can cause severe pulse deformations, the fiber Bragg-grating cannot be used as a compressor. The corresponding counterpart as free-space component is the chirped volume Bragg-grating, which is enscribed into bulk material. In free-space, the peak power can be reduced by increasing the beam diameter.

Fiber Bragg-gratings as well as volume Bragg-gratings can be customized in order to compensate arbitrary combinations of higher order phase terms. This way, they are a very powerful tool for pulse stretching and compression. The major drawback of these components is the missing tunability, along with a high cost for the customization. This hinders the wide use in research laser systems.

Prism-Grating Combinations Chromatic dispersion can be induced by an optical fiber, in which the GVD is the most significant portion of the fiber dispersion. Using a fiber as pulse stretcher is advantageous, because of the simplicity of the setup. The GVD of a standard optical fiber is normal (positive) in the 1 μm wavelength range up to 1.3 μm . For longer wavelengths such as 2 μm , specifically designed dispersion-compensation fibers can be used to achieve normal dispersion, as described in Section 2.1. In order to achieve significant stretching of the pulse, a long fiber section is required, often in the range of hundreds of meters. The most obvious problem of using a fiber stretcher is, therefore, the accumulation of TOD along the fiber that needs to be compensated. Solely using the grating compressor results in seriously deformed pulse shapes due to cumulative TOD, as also stated above. This effects becomes more salient the broader the pulse spectrum is [93].

Combining a prism and a grating in a grism-compressor introduces additional degrees of freedom to the compressor, regarding the induced dispersion. On the one hand, the dispersion properties of the grism rely on the diffraction at the gratings and the refraction in the prisms, thus manipulating and delaying the frequency components differently and allowing for TOD compensation. On the other hand, the additional elements in the compressor can be individually adjusted, thus allowing for a precise control of the relation of β_3/β_2 [59]. A more precise introduction to grism compressors is presented in Appendix B.

Grisms can be used as pulse compressors as well as pulse stretchers [59]. Owing to the various degrees of freedom, the pulses can be pre-shaped for amplification in order to solely use reflective optical components (e. g. reflective gratings) after amplification, which is advantageous for the pulse quality of high energy pulses [21].

Compared to fiber Bragg-gratings or volume Bragg-gratings, the major advantage of a grism compressor is its tunability. It can linearize dispersion up to the third order, which

3. Fundamentals of Fiber-Based Amplification Schemes

is sufficient for the pulse durations that are handled within the scope of this work. The grism compressor is, however, limited when nonlinear components of the phase need to be compensated. These can arise when the pulses are insufficiently chirped.

3.2. Optical Wave Breaking

Opposed to the concept of CPA, in nonlinear amplifiers, pulses are amplified while they are close to their transform-limit. Short pulses with high peak intensities underlie optical wave breaking during propagation in a normal dispersive glass fiber. Optical wave breaking severely degrades the pulse's quality, i. e. the possibility to recompress the pulse, and hence represents a nonlinear limitation for the pulse amplification.

During propagation, the pulse spectrum and thereby the pulse shape are altered by several nonlinear effects. SPM for instance acts on the high-intensity center part of the pulse and shifts the frequency components of the leading and the trailing edge to the red and the blue, respectively. The pulse shape evolves into a nearly rectangular form, with a linear frequency chirp [5]. At some point, the shifted frequency components temporally pass the unaffected pulse wings (unaffected by SPM due to the low intensity) as a result of the normal dispersion of the fiber and interfere with the wings. The temporal interference causes side lobes in the spectrum and also alters the pulse shape, which again results in SPM-induced changes of the pulse. The breaking of the single pulse peak into multiple interference fringes is the characteristic of optical wave breaking. This effect can be verified by a temporal analysis of the pulse, e. g. in an autocorrelation (AC) trace.

Comparing the group velocity of the newly generated frequency components with the group velocity of the wings leads to the distance x_{wb} , in which wave breaking occurs [6]:

$$x_{wb} = -\frac{1}{\beta_2 d\omega_c/dt}. \quad (3.1)$$

Here, β_2 is the group velocity dispersion (GVD) and $\omega_c = -\partial\phi/\partial t$ stands for the variation of the frequency chirp. It can be seen that the length x_{wb} is shorter, the stronger the changes resulting from GVD and nonlinear effects are. Therefore, amplified ultrashort pulses require very short fiber lengths and a reduction of the local peak intensity, e. g. by an increase of the fiber core diameter, in order to maintain the pulse quality. An important exception is presented in the following section.

3.3. Self-Similar Pulse Evolution

Anderson *et al.* determined in 1992 that a pulse with a monotonically varying chirp $\omega_c(t)$ would not show optical wave breaking [6]. The combination of a monotonic chirp and absence of a nonlinear limit is interesting for a pulse amplification scheme, as this promises the generation of intense pulses, which are easily compressible by compensation of the linear chirp. This is realized in a self-similar pulse amplifier.

The concept of self-similarity is an approach for the simplification of a mathematical problem, if the spatial distribution of a time-developing phenomenon at different moments in time can be derived from one another by a similarity transformation [10]. The mathematical simplification results from reducing the number of degrees of freedom by

symmetry reduction to obtain an asymptotic solution of a partial differential equation. A self-similar propagation and amplification of pulses in optical glass fibers can be achieved by parabolic pulse shapes. Under the correct preconditions (e. g. negligible TOD, broadband gain cross-section), a parabolic pulse propagating in an amplification stage underlies normal dispersion and SPM as well as an exponential amplitude scaling [30] and maintains the parabolic shape. Additionally, the chirp is linear over the whole pulse which allows for compression by a grating compressor. For the self-similar evolution, a relatively low gain over a relatively long active fiber is beneficial.

Mathematically, the self-similar propagation can be approached via the nonlinear Schrödinger equation (NLSE) with gain g [30] and second order dispersion.

$$i\frac{\partial\Psi}{\partial z} = \frac{\beta_2}{2}\frac{\partial^2\Psi}{\partial T^2} - \gamma|\Psi|^2\Psi + i\frac{g}{2}\Psi \quad (3.2)$$

Here, $\Psi(z, T)$ is the slowly varying pulse envelope in a co-moving frame with the time variable T denoted by $T = t - z/v_g$ with the group velocity v_g of the pulse envelope, γ is the nonlinearity parameter and g is the gain coefficient. The envelope Ψ can be separated into a real amplitude A and a phase ϕ . The symmetry reduction is used to reduce the degrees of freedom in order to search for an asymptotic self-similar solution of the NLSE for $z \rightarrow \infty$ [150]:

$$A(z, T) = A_0(z)\sqrt{1 - (T/T_0(z))^2} \cdot \exp\{i\phi(z, T)\} \quad (3.3)$$

$$\text{with } \phi(z, T) = \phi_0 + \frac{3\gamma}{2g}A_0^2(z) - \frac{g}{6\beta_2}T^2 \quad (3.4)$$

in the case of normal dispersion, a gain $g \neq 0$, an arbitrary constant ϕ_0 , and with $A(z, T) = 0$ for $|T| > T_0(z)$. The pulse envelope from Equation (3.3) corresponds to a parabolic intensity profile with an exponentially increasing amplitude A_0 . The temporal change of the phase (Eq. (3.4)), represents the linear chirp:

$$-\frac{\partial\phi}{\partial T} = \frac{g}{3\beta_2}T. \quad (3.5)$$

As the gain is positive in an active fiber ($g > 0$), the amplitude $A_0(z) = A(z, 0)$ and the effective pulse duration $T_0(z)$ increase exponentially while propagating self-similarly, i. e. the parabolic shape is preserved.

Often, low-intensity pulse wings can be found that deviate from the ideal parabolic intensity profile. These decay over time, as the parabolic intensity profile is the *asymptotic* solution for the NLSE [150]. By the same effect, also pulses with small perturbations in their shapes develop towards the parabolic intensity profile. Therefore, initial disturbances are reduced during amplification.

The parabolic pulse form is wave breaking-free. An initially unchirped Gaussian pulse quickly evolves into a parabolic shaped pulse, owing to positive GVD, and evolves self-similarly afterwards.

Simulations show that for a constant, flat gain and including GVD and SPM, the amplification is not limited. The pulse shape and phase do not experience wave breaking. When choosing a smaller fiber core diameter, the SPM becomes stronger; the parabolic shape is obtained faster and spectral width and pulse duration are increased faster. The

3. Fundamentals of Fiber-Based Amplification Schemes

pulse energy at the end of the fiber line is independent from the fiber core diameter. A small amount of TOD in the simulation causes a reshaping of the spectrum such that the intensity on the blue side of the spectrum is a little stronger than on the red side.

In real systems, the self-similar pulse propagation is limited or perturbed by gain saturation, a gain bandwidth that might be lower than the pulse's spectral bandwidth and the finite gain fiber length.

The self-similar evolution process is directly related to the gain fiber parameters, such as dispersion (mostly β_2), the nonlinear coefficient γ , the amplitude gain g and the fiber length, and the input pulse parameters, including the pulse amplitude A , the intensity profile and the effective pulse duration T . From these parameters, a characteristic length z_c can be defined, after which the pulse shape has reached a parabolic shape:

$$z_c(N) = \frac{3}{2g} \ln \left(\frac{Ng}{6|\gamma|A^2} \right). \quad (3.6)$$

The constant N can be seen as a merit value for the pulse shape. The higher N is, the closer the pulse shape is to the (optimum) parabola, which is the asymptotic solution. For a value of $N > 100$, the pulse is well evolved into a parabolic shape [150].

3.4. Pulse Generation in Mamyshev Oscillators

A Mamyshev oscillator (MO) consists of two concatenated nonlinear amplifiers, separated by offset spectral filtering. A MO can be used as a source for mode-locked pulses. In this section, the pulse evolution in a MO is first described experimentally, a theoretical concept for self-starting is given afterwards.

Pulse Shaping The MO is based on the concept of the Mamyshev regenerator [38]. It was proposed by P. Mamyshev in 1998 for the regeneration of telecommunication data in fibers [86]. The principle of a Mamyshev regenerator is schematically illustrated in Figure 3.2. A spectrally narrow (band-pass filtered) pulse propagating through a nonlinear medium, e. g. an Yb-doped, normal dispersive fiber, is amplified and spectrally broadened by self-phase modulation (SPM). After spectral broadening, the pulse is band-pass filtered at a wavelength that is offset to its central wavelength. The filter bandwidth has (ideally) no spectral overlap with the initially launched narrowband spectrum. Therefore, only newly generated wavelength components are passed through this band-pass filter (BPF). Again, the spectrally narrow pulse is amplified and spectrally broadened by SPM. The next BPF is again offset to the central wavelength of the pulse, such that, again, only newly generated wavelength components pass the BPF. Feeding back the two regenerator outputs into each other, forms the Mamyshev *oscillator*. As the generation of new wavelength components depends on the nonlinear effect SPM, the new wavelength components are coherent, which enables locking the longitudinal modes over the whole oscillator. Furthermore, due to the dependence of the generation of new wavelength components on the nonlinear effect, the loss at the BPFs is lower for higher intensities, i. e. nonlinear. For insufficient pulse peak power, i. e. insufficient SPM, propagation is inhibited at the offset BPF (dashed lines in Fig. 3.2). Therefore, the offset spectral filtering acts as an artificial saturable absorber.

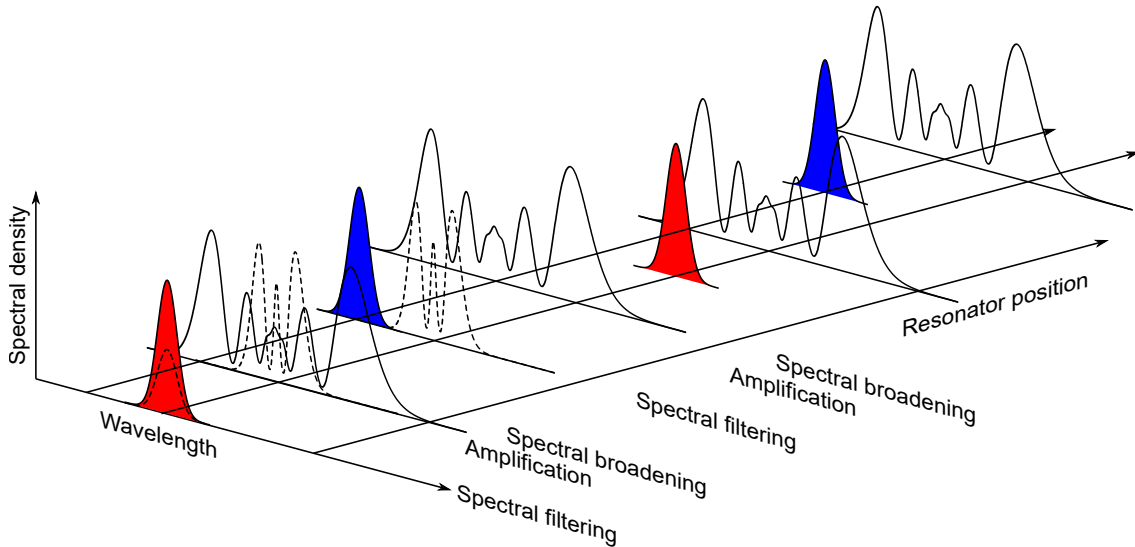


Figure 3.2.: Schematic illustration of the principle of the mode-locking mechanism in a Mamyshev oscillator. By alternating spectral filtering between spectral regeneration lines, low pulse peak powers (dashed lines) are strongly suppressed (due to weak SPM) and a lower loss for pulses that are strongly broadened by SPM.

The transmission intensity through the BPFs scales with the spectral density of the signal at the BPF transmission window. Independent of the intensity, the spectral shape and width are constant, only the seed energy in the succeeding arm scales with the increasing amplification. By this, the handling of high pulse energies without nonlinearly overturning the saturable absorption is possible.

Mamyshev oscillators can accumulate a high nonlinear phase in the range of 60π without showing signs of pulse breaking. This results from the pulse parabolic pulse evolution that tolerates a strong nonlinear phase. This amount of nonlinear phase can be compared to the pulse evolution in NPE-lasers (cf. Appendix A), which operate with nonlinearities not exceeding 10π [111].

Already in one of the first publications on alternating spectral filtering, in 1994, it was expected that the initiation of mode-locking would pose a difficulty [106]. An oscillator based on optical regeneration is, by definition, not self-starting. This means that pulses are spectrally and energetically regenerated, but not generated from noise [141]. In practice, the mode-locked state in the MO is bistable with operation of amplified spontaneous emission (ASE), as opposed to the cw-operation of NPE-lasers. ASE does not generate seed pulses with sufficient energy for the mode-locking. The spectral broadening by SPM requires sharp pulse edges rather than high pulse intensities, therefore, self-starting poses a difficulty in this design. Many MOs that were reported to date, contain an external pulse injection in order to regenerate the pulse train. Pulse injection can be done by an external laser source [80, 113, 108]. In a closed system, another possibility is the self-injection by using an additional cavity employing a semiconductor saturable absorber [121] or NPE [98]. These additional cavities generate pulses from the noise of one MO-arm, which are then injected into and regenerated by the MO. These cavities do not require a separate gain section. Another type of pulse self-injection is the pump modulation of a pump diode to form a gain switched pulse in one of the regeneration lines [117].

3. Fundamentals of Fiber-Based Amplification Schemes

Nevertheless, by exploring the range of the cavity parameters, it has been shown that modulation instability processes could generate pulse trains in oscillators sufficiently close to the definition of a MO [141]. The theoretical concept of this mode-locking mechanism is introduced in the following paragraph. Experimentally, the modulation instability is initiated by spectrally overlapping the BPFs so that a small amount of light can pass [114, 110, 149] and a subsequent increase in the spectral separation of the BPFs.

Mode-Locking Mode-locking in MOs depends on the periodic modulation of spectral losses, as opposed to the periodic amplitude modulation, as described in Appendix A. Still, the pattern formation of the light fields in the MO results from the periodic perturbation of the homogeneous state and can be described through instabilities [103]. The pattern in the MO is associated with the standing longitudinal waves in an oscillator in theoretical publications, like References [103] or [141]. The homogeneous state refers to a stable cw oscillation, the formation of the pattern describes the emergence of a pulse train. The instability that is used to trigger the pattern formation is experimentally realized by a saturable absorber, which is the alternating spectral filtering in the MO.

The Faraday instability was introduced by M. Faraday in 1831 [27] to describe the pattern formation in a vertically shaken fluid, i. e. the emergence of maxima and minima on the fluid surface. This Faraday instability in a more generalized form also occurs in other parts of physics, such as the nonlinear optics. Here, the instability results from the periodic temporal modulation of diffraction, dispersion or nonlinearity of a (laser) system. In the case of a dispersion-managed soliton laser for instance, the dispersion is periodically modulated, leading to the formation of pulses.

In order to describe the instability, i. e. the initiation of pulse formation, in a MO, Perego *et al.* introduced the *dissipative* Faraday instability (DFI) [103, 134]. This refers to the dissipative parameter that is periodically modulated in the MO, the spectral losses. Mathematically, the DFI is associated with the complex Ginzburg-Landau equation (CGLE) where a suitable parametric modulation results in pattern formation [103]. The CGLE in general describes a system near an oscillatory instability and has been used to model a wide variety of physical systems², including the mode-locking of a MO.

A stability analysis of the CGLE reveals an instability resulting from alternating spectral filtering around a central longitudinal mode. More detailed information on the theoretical analysis of the DFI can be found in References [103] and [134].

The experimental consequence of the DFI is the following: When losses are applied to a spectral region $+\Delta\omega$ of a central frequency ω_c , the damped spectral components experience a fast growth due to a four-wave mixing process involving the homogeneous mode and the symmetrically located longitudinal modes in the region $-\Delta\omega$. After the nonlinear pulse evolution and shaping in the fiber, the damping takes place for the spectral region around $-\Delta\omega$ and the process is repeated symmetrically, ultimately destabilizing the homogeneous state [134]. As the energy is injected from the undamped spectral side to the other, the newly generated longitudinal modes are locked, leading to a pattern in the temporal domain, i. e. a pulse train. The spectral coherence is maintained by the

²“Aronson Lectures”, Lecture Scriptum from the Institute of Theoretical Physics, Technische Universität Berlin, <https://www.itp.tu-berlin.de/fileadmin/a3233/grk/aronsonLectures2015/AronsonLecture2.pdf>, accessed: October 20, 2020. Further phenomena described by the CGLE include nonlinear waves, superconductivity or Bose-Einstein condensation.

coherent phase coupling from $\pm\Delta\omega$ to $\mp\Delta\omega$ [141]. The spectral coherence is a requirement for mode-locking.

Mode-locking in the MO can be initiated by the Faraday instability. After initiation, the repetition rate of the pulse train is usually a higher harmonic of the fundamental resonator repetition rate. The order of the higher harmonic can be decreased by increasing the spectral filter separation. The oscillating pulses then require a higher spectral bandwidth generation, when increasing the filter separation, which is achieved by a higher pulse energy. Maintaining the pump power leads to the merging of pulses in order to distribute the available energy to less pulses and, therefore, increase the pulse energy of the remaining pulses. Increasing the spectral filter separation ultimately decouples the oscillator arms and two (Mamyshev) regenerators are formed, thus improving the pulse parameters, while simultaneously preventing a restart in the case of lost mode-locking. This also shows that the stability of the DFI-induced pattern formation is significantly influenced by the frequency detuning of the filters [114, 141].

The dependence of the repetition rate on the pump power as mentioned above leads to the consideration that self-starting of the MO is only a question of available pump power, because theoretically, Gaussian shaped BPFs always overlap. In real systems however, as well the available pump power is too limited for a large detuning of the spectral filters as the power handling of the fiber components is limited. MOs should be more likely to self-start with spectral transmission shapes of the spectral filters with steep edges, i. e. a Supergaussian shape, compared to Gaussian shaped filters. If there is only a small overlap of the signal spectrum with the BPF spectrum, a steep-edged filter transmits a relatively larger part of the overlapping spectrum than a filter with a shallow edge. In the experiments, however, filters with a Gaussian transmission shape are applied for different reasons as explained in the Section 7.2.

4. Characterization of Ultrashort Pulses by Dispersion Scans

Ultrashort pulses are modified in temporal shape and spectrum during the propagation in fiber sections, as discussed in the preceding chapters. It is, therefore, necessary to analyze the pulse shape afterwards and several methods for the complete pulse characterization have been developed over the last 30 years [137]. The characterization is challenging, because ultrashort pulses belong to the shortest events that can be created artificially. Two commonly applied and well-established techniques are the autocorrelation (AC) [7] and the frequency-resolved optical gating (FROG) [58], schematically depicted in 4.1 (a) and (b). Those concepts are introduced in detail in Appendix C. In this chapter, the concept of the dispersion scans (d-scans) [89], which is a relatively recent development, will be addressed (Fig. 4.1 (c)). As the d-scan method was initially developed for and commonly used in few-cycle pulse laser systems, an analysis of relatively long pulses from a fiber amplifier, compressed in a grism compressor, faces several challenges. The d-scan concept will be introduced theoretically in Section 4.1 and the applicability will be demonstrated experimentally in Section 4.2.

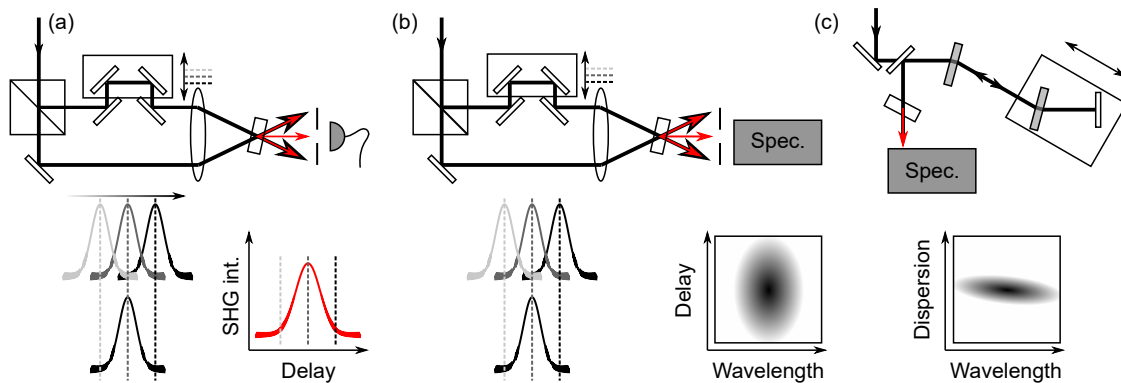


Figure 4.1.: Three different methods to retrieve information about the pulse duration: (a) autocorrelation, (b) frequency-resolved optical gating, (c) dispersion scans. On the top, a respective schematic setup is given, on the bottom a sketch of a typically resulting trace. SHG int.: Intensity of the second harmonic, Spec.: spectrometer.

4.1. Dispersion Scans

The d-scan method, first reported by Miranda *et al.* in 2011 [89], is a conceptually different method to the self-referenced methods of AC and FROG. Instead of comparing the ultrashort pulse with a delayed copy of itself, the technique consists of the measurement of the spectrum of the second harmonic generation (SHG) signal of a pulse, that underlies different and well-defined amounts of dispersion. Originally, this technique was used to

4. Characterization of Ultrashort Pulses by Dispersion Scans

measure few-cycle pulses with extremely broad optical spectra. In these cases, introducing a certain amount of glass into the optical path via a wedge pair provided a reliable way for a precise addition of dispersion.

The retrieval of the d-scan traces was carried out by an optimization algorithm that calculated the spectral phase of the pulse, expressed as a multi-parameter unknown value [89]. The quality of the retrieval is determined by a merit value which is the root mean square error between the measured and the simulated trace. The phase is iteratively updated in order to minimize the merit value. This is also the principle for FROG retrievals.

Due to the simultaneous use of the compression stage (which is required in most fiber laser systems) as pulse compressor and analysis device, this approach combines the measurement with a simultaneous compression of ultrashort pulses, as shown in Figure 4.2. The stability and precision requirements of an interferometric setup, such as for an AC, the beam splitting, delaying, and recombination can be avoided.

Multi-cycle pulses in the range of ≈ 100 fs – 200 fs pose the problem that adding glass does not induce sufficient dispersion for a reliable d-scan trace. However, the compressor from a chirped-pulse amplification (CPA) system, e. g. based on a grism compressor, provides sufficient amounts of dispersion. Furthermore, due to the simultaneous compression and measurement, the d-scan technique is highly interesting for the use in combination with grism compressors, in which multiple parameters must be adjusted to receive optimum compression.

The principle of applying the d-scan method to a grism compressor is schematically depicted in Figure 4.2. An introduction to grism compressors is given in Appendix B. Instead of adding glass with increasing thickness, the prism-to-prism separation is varied. This variation has a linear impact on the dispersion with an almost fixed relation of third to second order dispersion (β_3/β_2). At each scanning step, the spectrum of the second

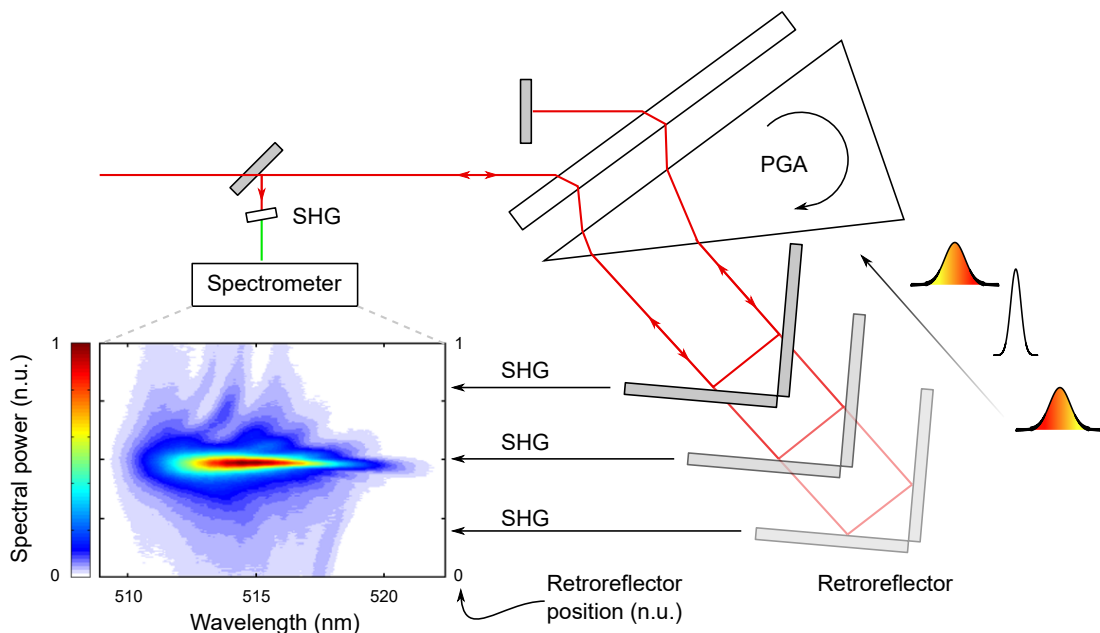


Figure 4.2.: Principle of the recording of d-scan traces from a laser system incorporating a four-pass grism configuration. PGA: Prism-grating angle, SHG: Second harmonic generation.

harmonic is recorded. Due to the different dispersion on the pulse, the intensity and the shape of the SHG-spectrum vary, so that a two dimensional trace is created. As the grism compressor can induce huge amounts of dispersion compared to a glass plate, also long pulses can be characterized.

A problematic aspect of the pulse characterization with the grism compressor via d-scans is that the amount of induced dispersion induced by the grism compressor can hardly be precisely determined, because it strongly depends on the exact adjustment. A small relative change of the prism grating angle (PGA) results in a distinct change of the dispersion induced by the grism. For the pulse compression, the exact value of dispersion is not a necessary requirement for operation, but for the retrieval algorithm, it is.

A solution was proposed by Alonso *et al.* with the “self-calibrating d-scan” [4] in 2018. The self-calibrating d-scan retrieval is based on a nonlinear optimization algorithm in which the pulse’s spectral phase is treated as a multi-parameter unknown variable and the unknown phase induced by the compressor is described by a theoretical model depending on the compressor position, in this case by a Taylor series to a given order. An initially random phase is iteratively modified by the use of the merit value, until the simulated and the measured trace coincide. As a consequence, the spectral phase of the pulse and the exact dispersion of the compressor up to the given order of the Taylor series can be determined synchronously. The Taylor series up to the third order is sufficient for most applications. With the help of this retrieval algorithm, the transition from the analysis of few-cycle pulses to relatively long pulses and the compression of the grism is straightforward.

A major advantage of the d-scan technique is that the unretrieved data of the d-scans are also quite informative, regarding residual dispersion on the compressed pulse or the corresponding misalignment of the compressor. The optimum compression is achieved, if all possible second harmonic frequency components are generated with the highest intensity at one single retroreflector position. In Figure 4.2, this would be the case in the middle position of the retroreflector. If there is residual higher order dispersion on the compressed pulse, the trace would look different. A tilted trace for instance is generated by third order dispersion, as shown in Figure 4.5 below.

4.2. Experimental Results

The experimental setup is depicted in Figure 4.3. The seed source was an Yb-doped fiber oscillator that was mode-locked via nonlinear polarization evolution with a repetition rate of 50 MHz. The pulses had a spectral width of approximately 15 nm, centered around

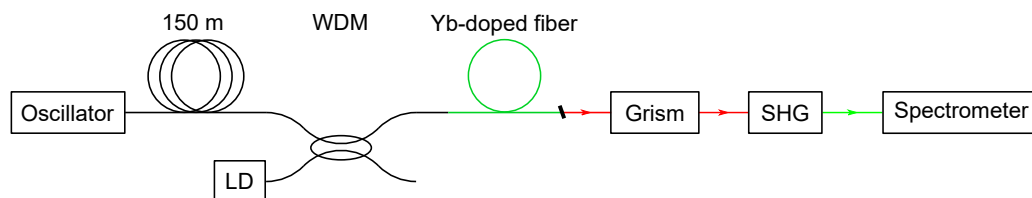


Figure 4.3.: Experimental setup for the analysis of pulses from a fiber-based chirped-pulse amplifier with the d-scan method. LD: Pump laser diode, SHG: second harmonic generation, WDM: wavelength division multiplexer.

4. Characterization of Ultrashort Pulses by Dispersion Scans

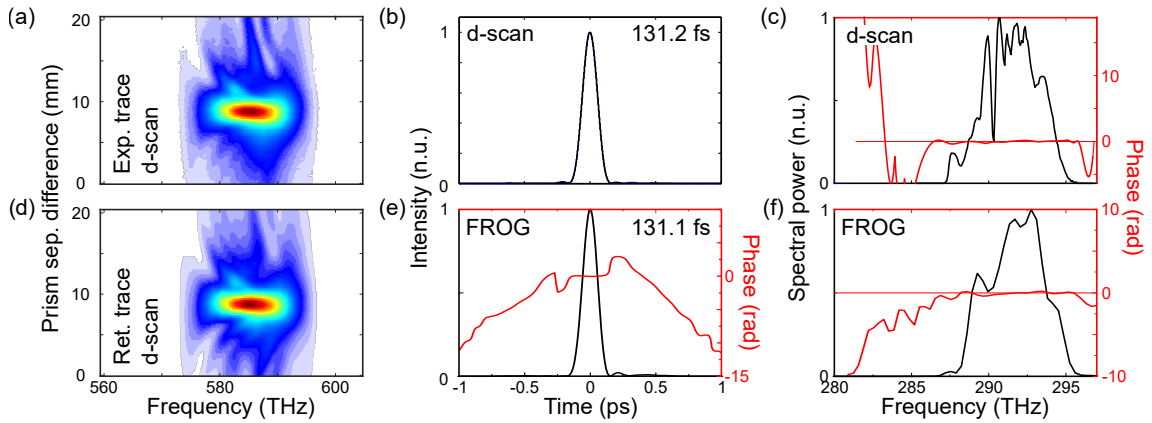


Figure 4.4.: Experimental (a) and retrieved (d) dispersion scan trace, retrieved pulse shape (b) and spectrum (c) from the d-scan trace, including the spectral phase, and the retrieved pulse shape (e) and spectrum (f) from a FROG trace of the same pulse for comparison.

1030 nm. After the outcoupling, the pulses were stretched to approximately 150 ps in a 150 m long standard, single-mode fiber and subsequently amplified to 150 mW in an Yb-doped fiber amplifier.

The grism was set to the optimum compression, as seen from the d-scan as well as a reference AC trace. With the use of the self-calibrating retrieval algorithm, the exact parameters of the grism were not required to be known. The retroreflector was automatically shifted over a distance of 5.08 mm in 100 steps. This resulted in a prism-to-prism distance variation of 10.16 mm. The result is shown in Figure 4.4. In Figure 4.4 (a) and (d), the experimental and the retrieved traces are shown, respectively. The retrieved pulse duration from the d-scan trace is shown in Figure 4.4 (b), the calculated FWHM-duration was 131.2 fs. Figure 4.4 (c) shows the measured fundamental spectrum with the spectral phase calculated by the d-scan retrieval. The phase is flat over the course of the spectrum which coincides to the pulse shape shown in Figure 4.4 (b), showing a duration very close to the Fourier-limited duration of 130 fs. The d-scan retrieval is compared to a FROG measurement, shown in Figures 4.4 (e) and (f). The retrieved pulse duration from the FROG measurement fits well to the d-scan measurement. The calculated fundamental spectrum from the FROG retrieval shows less details than the measured one, most likely due to a significantly lower number of data points. Still, the measured and the FROG-retrieved spectrum show similar features. The spectral phase determined by the FROG trace also coincides with the one retrieved from the d-scan trace. The flat spectral phases are a consequence of the almost Fourier-transformed pulse duration and were achieved by the compensation of TOD in the grism. The self-calibrating retrieval algorithm produced the same results as the FROG retrieval.

Optimization of the Grism Compressor Besides the full characterization of the pulses, the d-scan traces can be used to optimize the grism alignment. Initial hints on the uncompensated dispersion on the pulse can already be seen from the raw data in the two dimensional trace. With TOD on the pulse, the trace is tilted, as can be seen in Figure 4.5 (a)-(c). The FROG retrievals in Figure 4.5 (d)-(e) clearly show the same indication through the discontinuous steps in the temporal phase as well as the satellite pulses in the temporal

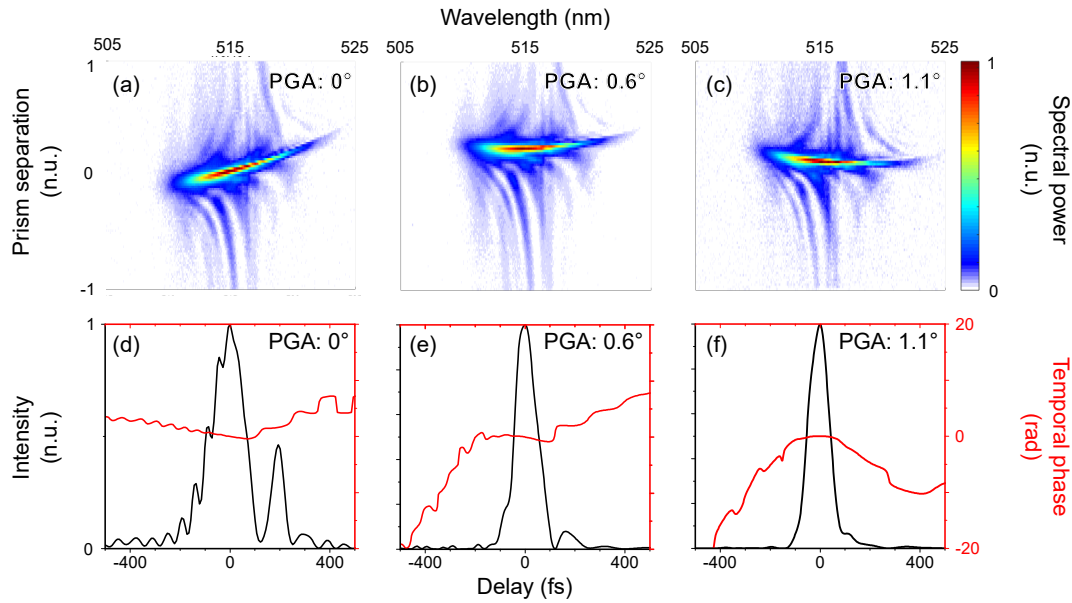


Figure 4.5.: (a)-(c) Experimental d-scan traces for different prism-grating angles (PGA), (d)-(f) temporal shape of the pulses, retrieved from a FROG trace for the specified PGA.

intensity. Due to this indication, the prism can be turned into the optimum position. The time for a retrieval algorithm to converge is saved by this procedure. It can be seen that also rather marginal changes of the PGA of 0.6° from Figure 4.5 (a) to (b) drastically changes the β_3/β_2 -relation. Here, this is expressed by the amount of uncompensated TOD.

The recording-speed of a d-scan trace depends on the speed of the translation of the retroreflector, the integration time of the spectrometer and the number of dispersion steps taken. For a faster recording of the traces in order to optimize the grism alignment, the number of traces can be reduced and the step size enhanced. In the experiments the recording lasted roughly 10 s or less. This was sufficiently short to have a frequent feedback on the residual higher order dispersion on the pulse while aligning the grism compressor.

4.3. Conclusion

The d-scan method has become an established technique for the analysis of pulses shorter than 30 fs [49, 132, 95]. The transfer to longer pulses is rarely reported. The reason for this is at least partly the consequence the good availability of commercial pulse analysis devices which work well for the analysis of pulses with durations of more than 50 fs.

The applicability was, however, successfully shown for longer pulse durations and for the use in combination with a grism compressor. The d-scan trace was retrieved by a self-calibrating retrieval algorithm which treated each point of the phase as an independent variable and the dispersion induced by the grism as a Taylor series up to the third order [4]. The retrieved data coincided well with a corresponding FROG-trace.

4. Characterization of Ultrashort Pulses by Dispersion Scans

Parallel to the work presented in Section 4.2, other groups carried out research for the d-scan retrieval algorithms. The d-scan method was applied to a chirped-pulse amplification system based on a Titanium:Sapphire laser in combination with a grating compressor and with pulse durations of 20 fs [90]. Here, a block of reference glass could be inserted into the beamline in order to have a precisely known amount of additional dispersion in a reference d-scan trace. This concept was not possible in the experiments above. The research for a solution for the problem of the unknown dispersion was carried out within this thesis, but became redundant with the development of the self-calibrated d-scan [4]. This method was published on the ArXiv in September 2017¹. A low-cost retrieval method for pulses in the range of 470 fs and the compression in a grating compressor was reported in July 2018 [28].

The use of the grism compressor for the recording of d-scans is enabled by the linearly variable dispersion compensation with a fixed β_3/β_2 -relation through the delay of the retroreflector. Residual dispersion of higher orders can be identified by the shape of raw trace and the phase on the pulse can be linearized by accordingly optimizing the grism compressor, even without an explicit retrieval of the trace. The retrieval is, however, required for the exact characterization and is enabled by a sophisticated algorithm. A grism and d-scan-based standalone pulse analyzer does not seem feasible, but the information retrieved by the raw trace is sufficient to allow for an automatization of the compression for alignment and diagnostic purposes in a turn-key laser amplifier system. The demand for a variable compressor in a commercial system can e. g. result from a varying pulse repetition rate that is emitted from the laser system, which causes a different pulse evolution in a fiber-based power amplifier.

The self-calibrating d-scan retrieval algorithm was still on research level during the experiments with this method. For this reason and the fact that the compressors were frequently altered, the pulses were characterized using AC or FROG traces in the further course of this thesis, although the complete pulse characterization was possible in principle via d-scans. Besides the already mentioned availability of adequate pulse analyzing devices, in Chapters 6–8, grating compressors were used with a very small grating separation for which an automatized shift for the variation of the dispersion was impractical.

¹ArXiv ID: 1709.05207

5. Linear Amplification of Ultrashort Pulses in Glass Fibers

The use of high-energy femtosecond laser pulses allows for precise and thermal-damage-free material processing [16]. The high complexity and low processing speed in combination with unwanted effects from heat accumulation in the workpiece at higher laser powers of femtosecond pulse amplifiers [11] has hindered the common use in industrial facilities [63]. This can be circumvented by the use of pulse bursts, i. e. low repetition rate-groups of pulses with a high intra-burst repetition rate [64]. For the generation of these pulse bursts, high repetition rate lasers are utilized, which are picked, e. g. by acousto-optic modulators (AOMs), to pulse bursts with durations in the nanosecond regime. An amplification system was planned for the increase of the pulse energy of a pulse train with a high repetition rate that could be used for material processing by cold ablation.

High-energy pulses are usually generated in a master-oscillator power-amplifier system. Low-energy seed pulses from the master-oscillator can be easily and more simply modified to the specific needs of the laser system, e. g. the emission of pulse bursts. The seed pulse energy is then boosted in a power-amplifier to receive the required pulse energy for the application.

The posterior amplification of the ultrashort pulses in glass fibers poses the problem of a pulse distortion by nonlinear effects, mainly self-phase modulation (SPM). In general, there are two ways to handle SPM: the first is to mitigate it as far as possible by a local reduction of the intensity in order to have a linear amplification, the other is to embrace the nonlinearity in order to exploit its advantages. The linear amplification regime will be discussed in this chapter, the nonlinear amplification will be discussed in Chapter 6. In Section 5.1, the state of the art of fiber-based chirped-pulse amplifiers with compressed pulse durations of less than 1 ps will be outlined. In Section 5.2 the experimental setup and the results of the linear amplification will be discussed. Afterwards, fundamental limitations of the linear amplification will be addressed in Section 5.3.

5.1. State of the Art

The amplification of chirped pulses is well-established and widely used for fiber amplifiers [150]. Since the first report of chirped-pulse amplification (CPA), the compression of the chirped pulses became more and more sophisticated. As D. Strickland *et al.* used a grating compressor, the residual TOD was soon limiting the pulse duration. In 1997, Kane *et al.* introduced the concept of combining gratings with prisms [59]; the amplification of pulses to the energy level of 1 mJ with 30 fs duration was discussed. For high power CPA systems, grating stretchers and compressors were soon established [22], as the dispersion could be better matched. In the laboratory, this approach poses no problem as mechanical

5. Linear Amplification of Ultrashort Pulses in Glass Fibers

Table 5.1.: Parameters of the fiber-integrated, single-channel, Yb-doped chirped-pulse amplification system generating the highest pulse energy, highest average power and shortest pulse duration, respectively. The value for the shortest pulse duration is given with respect to the high average power. In the publication, the pulse was further compressed in a nonlinear stage.

Publication	Pulse duration	Average power	Pulse energy	Peak power	Repetition rate
Eidam <i>et al.</i> [24]	480 fs	11 W	2.2 mJ	3.8 GW	5 kHz
Eidam <i>et al.</i> [23]	650 fs	830 W	10.6 μ J	12 MW	78 MHz
Jocher <i>et al.</i> [53]	265 fs	250 W	0.9 μ J	3.2 MW	250 MHz

disturbances can be efficiently reduced. The compression of amplified chirped pulses to significantly less than 100 fs requires nonlinear compression, because of the limited gain bandwidth of the amplifiers.

The exclusive linear amplification of pulses in fibers is still limited by the strong confinement, and therethrough the nonlinear effects, and the distortion of the pulse by higher order dispersion of the fibers. Chirped-pulse amplifiers can be optimized for the generation of high pulse energies, high average powers or short pulse durations. The highest values for single-channel, linear fiber chirped-pulse amplification based on Yb-doped gain fibers and with sub-ps pulse duration have been set by the group of J. Limpert in Jena¹, almost ten years ago. The respective parameters are collected in Table 5.1. Values for the pulse duration are difficult to compare, because they often increase with increasing signal power; stronger amplification leads to longer pulses. The pulse duration is limited by the gain cross-section of the laser material on the one hand [70] and (linearly) uncompressible spectral phase resulting from higher order dispersion and nonlinear effects on the other hand. Further fiber-based scaling of the pulse energy and the average power is usually achieved by the coherent combination of multiple amplification lines [36, 94]; the pulse duration can be decreased by nonlinear stages that increase the spectral width [53].

Some basic correlations can be seen from the parameters in Table 5.1, such that a high pulse energy usually corresponds to a low repetition rate. A lower repetition rate leaves more time to build up inversion in the gain fiber between two pulses, thus allowing for a stronger pulse amplification. Furthermore, the average power is lower for lower repetition rates, despite a higher pulse energy. Another correlation can be seen for pulse duration and the power handling of the amplifier. Usually a higher output power corresponds to a longer pulse duration. The pulse duration is increased by a nonlinear phase in the case of high powers. When aiming at short pulse durations from a CPA system, a nonlinear postcompression stage is often implemented. In Reference [53], the nonlinear postcompression stage was based on a short piece of a large-pitch photonic crystal fiber, in which the spectrum of the precompressed pulse was broadened by SPM. This allowed for the postcompression to 23 fs pulse duration in a standard compressor.

Reaching extremely high parameters in fiber-based amplifiers requires elaborate designs. The power amplifier system for the high pulse energies from Table 5.1, included to pulse stretchers and a pulse shaper based on a spatial light modulator [24]. The different ampli-

¹“Institute of Applied Physics”, https://www.iap.uni-jena.de/fiber_waveguide+lasers.html, accessed: September 21, 2020.

fier stages consist of photonic crystal fibers with extremely large mode-field diameters and are free-space coupled in order to reduce fiber paths.

Apart from reaching record pulse parameters, there are other optimization targets, as for example the all-fiber setup. Present publications on fiber-based CPA-systems include a report on a fiber-integrated CPA-system, generating $27 \mu\text{J}$ pulses at 500 kHz repetition rate, limited by stimulated Raman scattering [14] (which could theoretically be suppressed by the use of a larger mode-field diameter). Here, chirped fiber Bragg-gratings were used for stretching and pre-shaping of the pulses, which were amplified in five amplification stages in total. Another optimization target is a low noise. A frequency comb was generated for 180 fs, 130 W, 250 MHz pulses [81]. The amplifier consisted of three stages of which the two last amplifiers were made from PCFs and are thus free-space coupled.

Fiber-based CPA has inherently lower limitations regarding the pulse power, energy and higher pulse duration, compared to free-space chirped-pulse amplifiers. Free-space chirped-pulse amplifiers routinely generate hundreds of terawatt peak powers with few femtoseconds (compressed) pulse duration [42]. The highest limitation threshold of the amplification in fibers that cannot be handled to date is the onset of transverse mode instabilities [150].

5.2. Experimental Results

Within the scope of this thesis, the amplification of chirped pulses with high repetition rates was realized. The high repetition rate was required due to the high intra-burst repetition

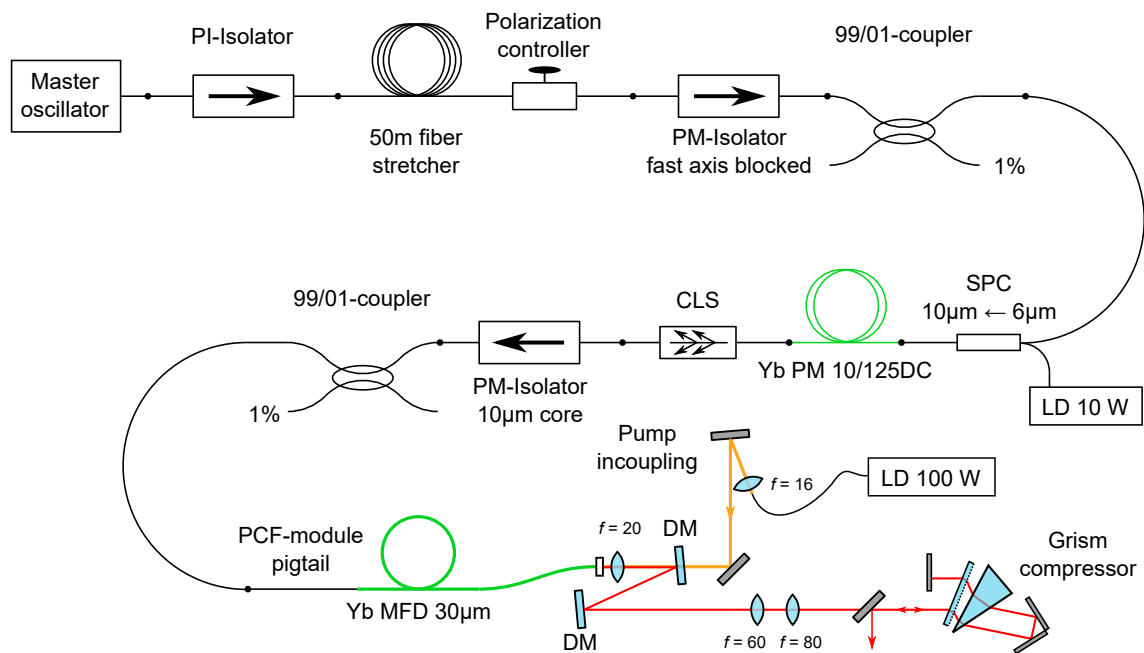


Figure 5.1.: Layout of the master-oscillator power-amplifier based on chirped-pulse amplification. CLS: cladding-light stripper, DC: double-clad fiber, DM: dichroic mirror, f : focal length in mm, LD: pump laser diode, MFD: mode-field diameter, PCF: photonic crystal fiber, PI: polarization-insensitive, PM: polarization-maintaining, SPC: signal-pump combiner

5. Linear Amplification of Ultrashort Pulses in Glass Fibers

rate of the pulse bursts that should be used for material processing. In order to evaluate the linear amplification, a master-oscillator power-amplifier as schematically presented in Figure 5.1 was set up and characterized. A fiber-based layout for mechanical robustness and a fiber stretcher-grism compressor combination were chosen. The amplification of ultrashort pulses up to μJ pulse energy and the compressed pulse duration in the range of 150 fs were defined as target output parameters, in order to conduct successive experiments on the cold ablation.

The amplifier is fiber-integrated from the seed oscillator up to the output of the power amplifier. By this design, a high environmental stability and reduced adjustment efforts are intended. The amplification in two stages was chosen in order to ensure a saturated seed in the power amplifier. Unsaturated seed pulse energy increases the risk for the emergence of ASE. Multiple 1%-couplers were included for monitoring purposes. The setup will be discussed more precisely below.

Seed Oscillator The master-oscillator was an Yb-doped all-fiber laser, mode-locked by nonlinear polarization evolution (cf. App. A). The master-oscillator emitted pulses with a repetition rate of 66.7 MHz and a spectral full-width at half-maximum (FWHM) bandwidth of 10 nm, corresponding to a Fourier-limited pulse duration of 225 fs. The output parameters are shown in Figure 5.2. The average output power of the oscillator was 43.5 mW, resulting in an output pulse energy of 0.65 nJ.

The optical spectrum, as seen in Figure 5.2 (a), is characteristic for an all-normal dispersion ultrafast laser, also called dissipative soliton laser. The two peaks at the sides of the spectrum result from the spectral broadening by SPM for positively chirped pulses [2]. The radio-frequency (RF) spectrum (Fig. 5.2) around the fundamental beat-node of the laser shows a signal-to-noise ratio of 82 dB, which indicates stable mode-locking. The pedestal that can be seen around the main peak, might result from small pulse amplitude fluctuations. Fluctuations of the pulse amplitude result in an amplitude modulation of the pulse train [75]. The RF trace shows symmetric side maxima around the main signal maximum at ± 2 kHz. This kind of amplitude modulation is difficult to verify in the oscilloscope trace, due to the limited sampling rate of the oscilloscope over large time intervals.

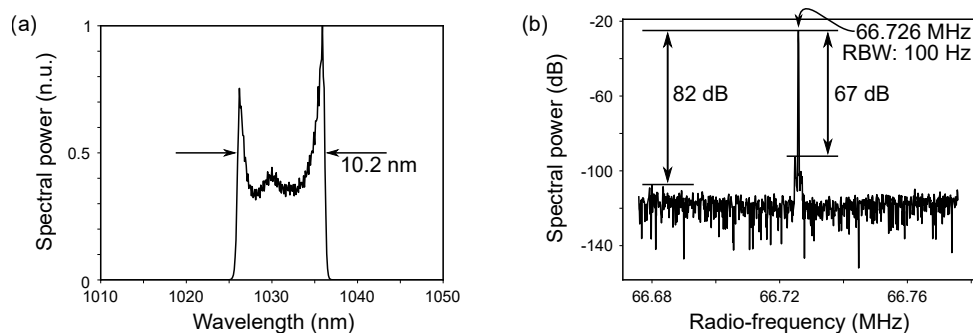


Figure 5.2.: Output parameters of the seed oscillator: (a) optical spectrum, linear scale and (b) the radio-frequency spectrum, showing the fundamental beat node at 66.72 MHz. RBW: resolution bandwidth.

Pulse Stretcher Master-oscillator and stretcher were separated by a fiber-coupled isolator, which attenuated possible backreflections from splicing points by 30 dB. The stretcher consisted of 50 m of polarization-insensitive (PI) fiber. A PI fiber was chosen for the stretcher for availability reasons. The pulse duration was increased to 33 ps in the stretcher (cf. Fig. 5.3 (b), inset). The short fiber stretcher reduced the accumulation of TOD and the relatively short stretched pulse duration prevented overlapping of the pulses when using high intra-burst repetition rates in the GHz-range.

In order to compensate the TOD, a grism was used as pulse compressor (cf. App. B). The second and third order dispersion of the stretcher fiber was matched by the grism, which consisted of a grating with 600 lines/mm, a fused silica prism with an apex angle of 45° and a prism-grating angle of roughly 10° , according to the Configuration 1 from Table B.1. The grism was set up in the simplified configuration with one grating and one prism, as shown in Figure B.2.

Following the fiber stretcher, the pulses were coupled into a polarization-maintaining (PM) fiber in order to increase the environmental stability. The polarization of the pulses was adjusted by a polarization controller. This component induces birefringence to the PI fiber by mechanical stress. According to the applied pressure and twist, the polarization controller can act as a fiber-integrated quarter- and half-wave plate combination. Afterwards, a PM fiber-coupled isolator only transmitted pulses in the slow polarization axis. This prevented polarization mode dispersion and double pulsing. Besides the polarization filtering, the PM isolator increased the overall isolation of the seed-laser, preventing interaction of backreflected light from successive components of the amplifier chain with the master-oscillator. The 1%-port of the succeeding fiber coupler was used for monitoring.

Preamplifier Fiber amplifiers allow for very high gain values. The limitation is excessive amount of ASE, which can be built up in the time between two pulses and when the signal power is too weak to deplete all the available excited atoms. ASE can cause self-lasing in the amplifier. Spiking during the onset of self-lasing generates high energy burst pulses, which can cause catastrophic destruction of the fibers and fiber components. Preamplification of the seed pulses reduces excessive ASE in the main amplifier by effective seed saturation. It should be noted that the small-signal gain along with the high available pump power at low pulse energies can increase the noise of the amplified pulses in each (linear) amplification stage.

The preamplifier was based on an Yb-doped fiber with a $10\ \mu\text{m}$ core-diameter. These fibers have V numbers of around 2.5, varying to some extent across the suppliers. Exceeding the critical value of V_c for only a small amount, these fibers are usually considered as single-mode fibers (cf. Sec. 2.1). Owing to the larger core-diameter compared to standard single-mode fibers, these fibers show a reduced amount of nonlinearities. The active fiber is pumped by a 10 W, fiber-coupled laser diode at a wavelength of 976 nm. The unabsorbed pump light is stripped from the fiber in a cladding light stripper (CLS). In the CLS, the pump light is removed from the outer cladding by the use of a high-index gel that influences the total internal reflection condition for the pump light in the outer cladding. The output characteristics of the preamplifier are shown in Figure 5.3.

In Figure 5.3 (a), the signal power characteristics are shown. The maximum average power from the preamplifier was 2.5 W, corresponding to a pulse energy of 38 nJ. The optical-to-optical efficiency of the amplification was 27%. The overall linear increase in

5. Linear Amplification of Ultrashort Pulses in Glass Fibers

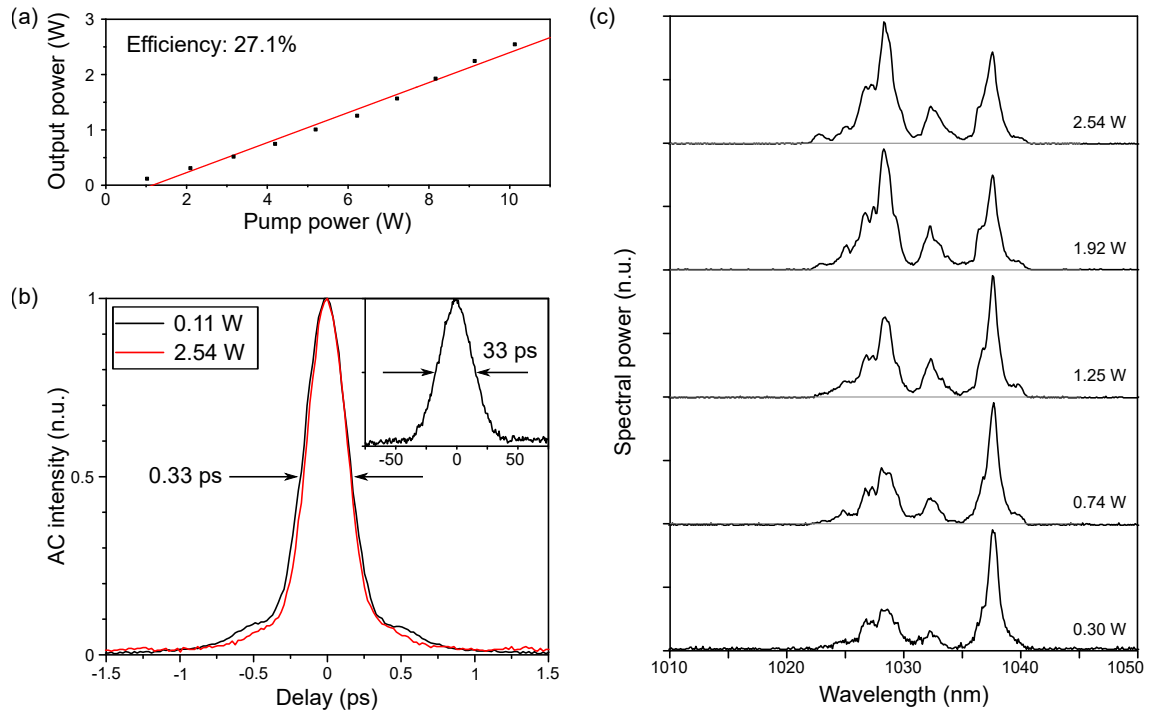


Figure 5.3.: Performance of the preamplifier, measured behind the isolator: (a) the pump-signal characteristic line, the linear fit (red) indicated an efficiency of 27%, (b) the AC traces of the compressed pulses at minimum and maximum output power and the uncompressed AC trace in the inset, (c) the optical output spectra for different output powers in linear scale. The performance indicates an overall linear amplification.

the signal output power shows that the amplification is not saturated, but pump power limited. The AC traces of the compressed pulses have a duration of 0.33 ps, shown in Figure 5.3 (b), and show no dependency on the pulse energy. This indicates a very low influence of nonlinear effects, resulting from the chirp and the increased mode-field diameter. Furthermore, the spectral shape of the preamplification pulses was not altered by nonlinear effects, such as SPM (cf. Fig. 5.3 (c)). The spectral maximum on the blue side of the spectrum is amplified stronger than the maximum on the red side, as a result of the gain cross-section of the Yb-doped fiber (cf. Sec. 2.1). Further amplification was not possible due to the limited amount of available pump power, but the available signal power was sufficient to seed the main amplifier.

Behind the preamplifier, the pulse energy is boosted in the power amplifier. The two amplifier stages are separated by a fiber-coupled isolator. This isolator is necessary because of potential back-propagating ASE-light from the power amplifier. A 1%-port of a fiber coupler is used for monitoring purposes.

In order to keep the further amplification in the linear regime, a fiber with a larger core-diameter is used in the power amplifier. As larger core-diameters allow the propagation of multiple modes, the beam quality can degrade. The use of photonic crystal fibers (PCFs) pose a solution to this problem. Owing to a different principle of light confinement in this special fiber as compared to the wave guiding described in Section 2.1, larger mode-field diameters without the loss of the single-mode properties can be achieved.

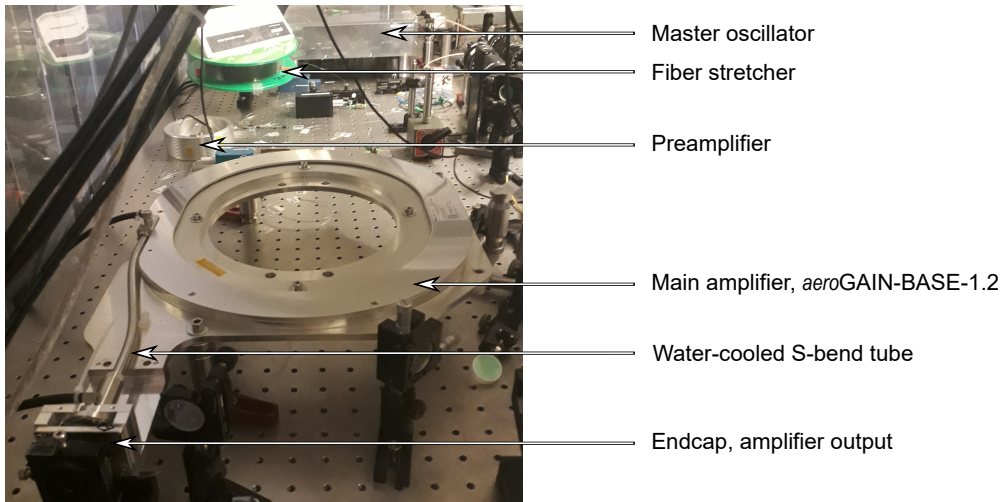


Figure 5.4.: Photograph of the CPA-system.

Main Amplifier The main amplifier was based on the *aeroGAIN-BASE-1.2*-module from NKT photonics², as shown in Figure 5.4. This amplification module consists of a 1.8 m Yb-doped double-clad PM PCF that is spliced to a passive PM-fiber with a 10 μm -core diameter for the seed incoupling. A cladding light stripper is included to remove residual pump light and an endcap on the outcoupling side to protect the fiber end facet. The fiber is covered in a protective metal housing and the outcoupling side is water-cooled. The parameters of the gain fiber are collected in the following Table 5.2.

Table 5.2.: Parameters of the gain photonic crystal fiber.

Properties	Unit	Value
Mode field diameter	μm	31 ± 2
Mode field area	μm^2	700 ± 100
Signal core diameter	μm	40 ± 2
Signal core numerical aperture		0.03
Pump cladding diameter	μm	200 ± 2
Pump cladding numerical aperture		0.55 ± 0.05
Pump absorption at 976 nm	dB/m	10
Fiber length	m	1.8
Birefringence		$1 \cdot 10^{-4}$

In this module, a fiber-integrated pumping scheme was not possible. The pump light was delivered free-space through the end facet, as shown in Figure 5.1, resulting in a backward pumping scheme in the main amplifier. In general, a forward pumping scheme is advantageous regarding the noise from the amplifier, as there is a saturated amplification in the end section of the gain fiber. In terms of gain however, a backward pumping scheme is advantageous because in the end section of the amplifier, where the signal power is higher, the available pump power is also higher than in the beginning of the gain fiber.

²“aeroGAIN-BASE high power ytterbium fiber gain modules”, <https://www.nktphotonics.com/lasers-fibers/product/aerogain-base-high-power-ytterbium-fiber-gain-modules/>, accessed: May 25, 2020

5. Linear Amplification of Ultrashort Pulses in Glass Fibers

Furthermore, the emergence of ASE is less likely, because there is less undepleted inversion due to excessive pump power in the amplifier.

Several precautions had to be taken in order to handle the high optical power that was targeted by the amplifier system, as high optical power can cause a strong thermal impact on the material. Misalignment of the pump radiation at the input stresses the fiber material. Therefore, the pump incoupling side of the PCF was covered in an S-bend tube and was cooled by a water flow. Misalignment of the pump radiation furthermore affects the residual pump light absorption at the seed input of the PCF, in which unabsorbed pump light is stripped from the system. As misaligned pump light only has a small overlap with the Yb-doped core of the fiber, only a small amount is absorbed. Consequently, a high power must be removed at the cladding light stripper. High optical powers may cause thermal damages in the component. Another problem may arise from insufficient seed power: An unseeded amplifier generates ASE, which can cause self-lasing and spiking during its build-up, leading to a destruction of the fiber, the end facets or fiber components. This should be prevented by careful splicing, alignment and a fast interlock that switches off the pump power as soon as the seed oscillator's average output power falls below a certain threshold. Furthermore, back-reflections into the seed oscillator are suppressed by the multiple isolation stages, in order to prevent the loss of mode-locking in the oscillator.

The PCF-supplier specified the maximum input pump power to 100 W. A laser diode from BWT Beijing, coupled to a fiber with a 135 μm cladding and a NA of 0.22 was used as pump source. The laser diode had a maximum output power of 100 W at a wavelength of 976 nm. The temperature (and the wavelength) was actively stabilized by Peltier elements on a water-cooled heat sink. The fiber tip was angle cleaved in order to prevent back reflections into the diode. Two dichroic mirrors, which were highly reflective for the pump light and highly transmissive for the signal light, were used for the pump alignment and simultaneously for separation of pump and signal light. The imaging was done by a lens with a focal length of 20 mm behind the PCF for incoupling of pump light and outcoupling of signal light and a 16 mm-lens for the collimation of the pump light from the laser diode.

Alignment of the pump was achieved in three steps: First, the collimation lens behind the PCF was adjusted with the help of the seed light only and optimized for the propagation of the seed light. The seed light has a longer wavelength and is guided in a core with a smaller diameter, therefore, the coupling of pump light must be further improved. In the second step, the pump light was aligned at low power by beam walking of the two dichroic mirrors in order to receive an optimal amplification of the seed light. This could be verified by a (fast) powermeter when blocking the cladding light with an aperture. Finally, also the position of the lenses is readjusted to receive the maximum output power. It should be noted that the 16 mm-collimation lens behind the PCF was optimized for the pump light. In order to correct the chromatic aberrations and focussing differences due to the different wavelength and core diameters, respectively, for signal and pump light, a telescope with a 60 mm-lens and a 80 mm-lens was used.

The results of the pulse amplification in the power amplifier are shown in Figure 5.5. In Figure 5.5 (a), two traces of the amplification process are shown, depending on the seed input power of the preamplifier. It can be seen that the traces follow a linear trend in both cases and difference between the two slopes stays almost linear, in accordance to the seed power difference of 1.25 W in the first case and 1.92 W in the second case. The invariance of the difference indicates saturated amplification in the amplifier, i. e. sufficient seed power is available. High seed power is furthermore advantageous for the performance, as

the threshold for ASE and parasitic self-lasing is increased. Furthermore, it shows that the total output power only has a low dependence on the input power. Small fluctuations of the seed input signal are not amplified in an exponential matter, but stay small, especially as the seed power is relatively small compared to the amplified output power. This is an indication for seed saturation, i. e. a sufficient seed signal for the amplification. The supplier specified a minimum input of 500 mW for a safe operation, which is exceeded in this case. The maximum output power of the amplifier system is limited by the available pump in the gain fiber. A nonlinear limitation cannot be seen from the spectral evolution.

The output spectra for different amplification values are shown in Figure 5.5 (b). It can be seen that the shape of the spectrum strongly differs from the spectrum of the master-oscillator as presented in Figure 5.2 (a). This results, most likely, from the gain dynamics in the main amplifier. These gain dynamics cause prominent features of the optical spectrum to be amplified stronger than weaker features. It is, however, interesting that the spectrum of the main amplifier spans over a larger range than the master-oscillator spectrum. The spectral broadening is attributed to SPM-induced broadening in the beginning of the stretcher fiber. Spectral broadening in the main amplifier can be excluded, because the width does not change with increasing pulse energy. The combination of the increasing spectral peak around 1027 nm and the decreasing spectral peak at 1042 nm are noteworthy. The wavelength of 1027 nm is at the maximum of the gain cross-section of Yb. For low amplification values, the amplifier appears to be unsaturated, resulting in self-absorption on the blue side of the spectrum and a shift to the red side. For increasing pump power, the amplifier is more and more saturated and the red-shift reduces. The spectral peak at 1027 nm can already be seen in the spectrum of the master-oscillator and the preamplifier.

The corresponding AC traces of the amplified pulses are presented in Figure 5.5 (c) and (d) for a seed power of 0.87 W and 1.25 W, respectively. After the amplification in the PCF, the pulses were compressed in a grism compressor to AC durations of 0.41 ps to 0.70 ps, depending on the preamplifier power. A shorter pulse duration is achieved at less seed power and the same output power. The grism consisted of a transmission grating with a line density of 600/mm and a prism with an apex angle of 45°. The prism-grating angle was 0°, instead of the 10°, which were calculated to be the optimum (cf. Tab. B.1), in order to compensate for a residual nonlinear phase. The grism needed to be readjusted for each amplification step and the compressibility of the pulses was reduced for higher powers of the preamplifier. Both are indications for a nonlinear phase that has a stronger impact at higher pulse energies. This nonlinear phase is accumulated as a result of the high pulse peak power due to insufficient pulse chirping. Another noteworthy feature in the AC traces are the satellite pulses with a distance of 1.2 ps to the main pulse. One possible origin of these satellite pulses could be polarization mode dispersion resulting from the splice in front of the PCF. The distance between main pulse and satellite pulse would then correspond to the runtime difference Δt in the two polarization axes (refractive indices n_x and n_y) which would exactly match the length l_{PCF} of the PCF (cf. Table 5.2):

$$\begin{aligned} \Delta t &= \frac{s}{v_1} - \frac{s}{v_2} = \frac{l_{\text{PCF}}}{c/n_x} - \frac{l_{\text{PCF}}}{c/n_y} \\ &= \frac{1.8 \text{ m}}{c/1.5002} - \frac{1.8 \text{ m}}{c/1.5} = 1.2 \text{ ps}, \end{aligned} \quad (5.1)$$

with the speed of light c . The significant amount of energy in the satellite pulses however, would require a strong mismatch in the alignment of the polarization axes. Another reason

5. Linear Amplification of Ultrashort Pulses in Glass Fibers

could be an unexpected and uncompensated phase on the pulses. This phase can result from nonlinear effects or from an unexpected relation of second to third order dispersion. A nonlinear phase is suggested because of the dependency of the satellite pulses on the preamplifier power. A nonlinear phase can be approximated by the Taylor series and, therefore, partly compensated along with the second and third order dispersion. For this, the prism was rotated as mentioned above, which reduced the intensity of the satellite pulses to 15% relative to the main pulse in the AC trace.

The rather low pump-signal conversion efficiency of roughly 30% can be caused by multiple effects. The free-space coupling is prone to significant losses. Firstly, there is the multimode beam of the laser diode fiber: Due to the necessity of various dichroic filters to separate pump and signal light and the optical components for the alignment of the pump, the path of the pump light was about 40 cm. Because of the low beam quality, the beam cannot be well collimated or reliably focussed into the PCF. Secondly, there were losses resulting from lens aberrations. The lens in front of the PCF end cap is a critical component because signal and pump light with different wavelengths need to propagate through it. Lastly, the optical spectrum of the pump light is rather broad, resulting in an inefficient overlap of the pump wavelength with the optimum gain cross-section of Yb. The low overlap of pump cladding to Yb-doped core and the (relatively) low doping concentration of the core only have a minor impact on the low efficiency. The cladding

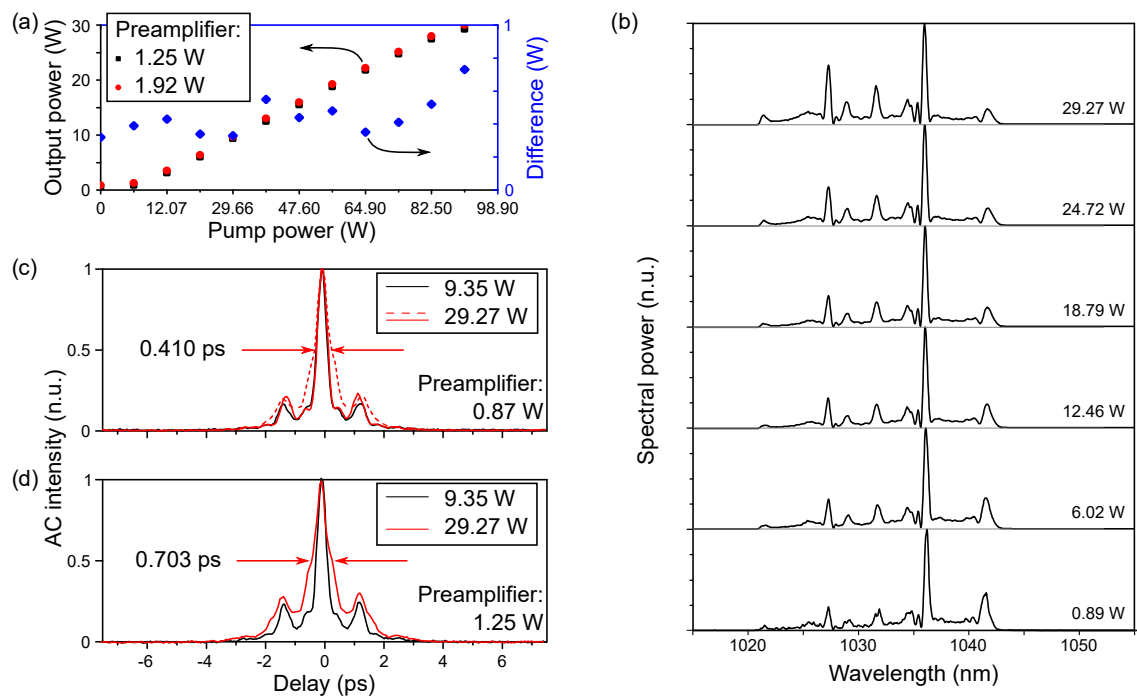


Figure 5.5.: Results from the main amplifier: (a) the characteristic output power curve of the main amplifier output, depending on the driving current of the pump diode for two output settings of the preamplifier. The signal output spectra from the main amplifier at different output power values are shown in (b). AC traces at the output of the main amplifier for a preamplifier signal power of (c) 0.87 W and (d) 1.25 W, at two different main amplification points each. The course of the AC trace from the power amplifier in (d) is mirrored in (c) by the dashed line.

absorption of ≈ 10 dB over 1.8 m should be sufficient. Due to the low efficiency, the pump power would have to be increased to reach the targeted output pulse energies. As this was not possible due to the suppliers restrictions, the design of the amplification system must be altered.

In order to further analyze the pulse shape and thereby the nonlinear influence on the pulse, a FROG trace was recorded. The results are presented in Figure 5.6. The FROG trace was taken at an output power of 21.84 W ensuring stable operation and in order to reduce the laser fluence on the PCF endcap. The FROG trace was retrieved with an error of 0.52% which represents a reliable value [69]. The retrieval algorithm generated a pulse shape as shown in Figure 5.6 (a). According to the FROG trace, the pulse has a FWHM duration of 293 fs. A Fourier transform of the optical spectrum (Fig. 5.6 (b)) at the given output power yields a minimum pulse duration of 155 fs, the Fourier-transformed pulse duration of the master-oscillator was 225 fs, as mentioned above. The deviation of retrieved to calculated minimum pulse duration can be caused by the nonlinear phase coming from the seed oscillator or from a misalignment of the grism compressor. With the given pulse duration τ_p , the peak power P_p can be determined:

$$P_p = \frac{L_{avg}/R}{\tau_p} \cdot 0.94 = \frac{21.84 \text{ W}/66.7 \text{ MHz}}{293 \text{ fs}} \cdot 0.94 = 1.05 \text{ MW} \quad (5.2)$$

with the average power L_{avg} and the repetition rate R . The factor 0.94 accounts for the approximated Gaussian shape of the main pulse peak. The pulse shape shown in Figure 5.6 (a) includes the satellite pulse at a distance of 1.2 ps to the main pulse that was anticipated from the AC traces from Figure 5.5. The remaining phase shown in Figure 5.6 (a) reveals a nonlinear trend and cannot be compensated by the grism compressor. The nonlinear phase most probably results from SPM in the beginning of the stretcher fiber, at which point the seed pulse is still relatively short and the fiber core diameter small.

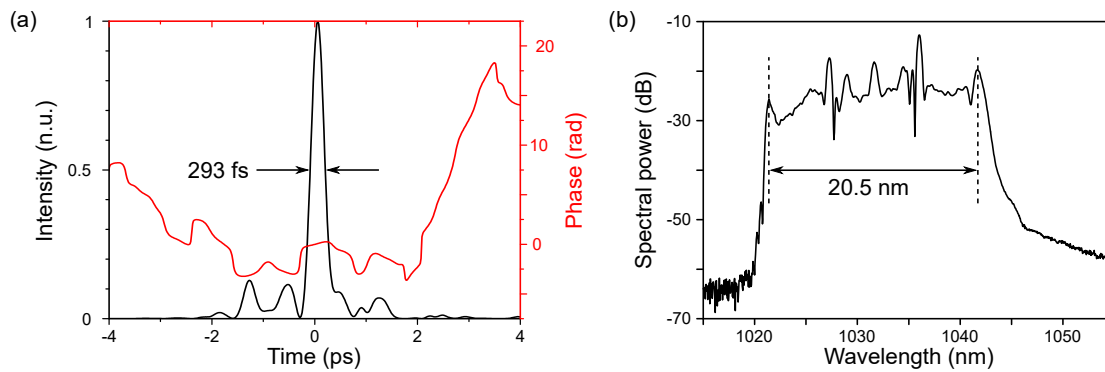


Figure 5.6.: (a) Pulse shape and duration and temporal phase of the pulses from the main amplifier at an average output power of 21.84 W, retrieved from a FROG trace; (b) the corresponding optical spectrum.

5.3. Conceptual Limitations

Nonlinear effects are a frequently reported limitation of a CPA system. Besides the deformation of the pulse shape by SPM, the onset of stimulated Ramans scattering, or,

5. Linear Amplification of Ultrashort Pulses in Glass Fibers

more general, an excessively accumulated nonlinear phase, the pulse quality in CPA systems is limited by the seed pulse parameters. A post-compression to durations below the transform-limit of the initial pulse is not linearly possible.

Gain Narrowing Ultrashort pulses require a broad spectrum. Opposed to this, many laser transitions are narrow-band, such as in Nd:YAG or Yb:YAG. But also the laser materials that are relatively well suited for the amplification of ultrashort pulses such as Yb- or Tm-doped glass fibers have a finite gain bandwidth (cf. Fig. 2.3). Strong amplification in these fibers result in a stronger amplification of those wavelength components that overlap with the gain maximum. This reshapes the spectrum of the pulse and causes an effective narrowing of the FWHM of the optical spectrum [51]. Strong gain narrowing limits the Fourier-limited pulse duration to roughly 120 fs [70] in power amplifiers based on Yb-doped fibers. As the shape of chirped pulses follows the spectral intensity distribution, another effect of gain narrowing in CPA systems is the effective shortening of the chirped pulse duration. This results in a faster emergence of nonlinear effects.

The gain narrowing effect can, however, be diminished. A broad optical spectrum can be preshaped, i. e. filtered, before amplification such that the part overlapping with the gain maximum has a lower spectral intensity than the spectral sides. During amplification, a higher gain is necessary to first compensate the filtered wavelength components and afterwards narrowing the spectrum. Another way of reducing the effect of gain narrowing is the precompensation of the optical spectrum, i. e. using an extremely broad input spectrum in the first hand that can be narrowed to some extent, but still supports ultrashort pulses with the targeted duration. The spectrum can also be compensated by nonlinear effects like SPM during amplification at the price of a strong nonlinear phase.

Nonlinear Phase The pulse quality in the CPA system described above is mainly degraded by SPM. In general, significant amounts of energy are transferred from the pulse peak to the pedestal, even for a low value of accumulated nonlinear phase of $\approx \pi$ [104]. The use of a matched stretcher and compressor does not suffice in this case, because the compressor induces a fixed phase that can hardly compensate phases resulting from nonlinear effects.

The accumulation of nonlinear phase contributions is reduced by strong chirping of the pulse in order to decrease the pulse peak intensity. The pulse chirping is limited at some point by the repetition rate of the laser system. A pulse must not overlap with a successive pulse, since the interaction can cause unwanted effects like cross-phase modulation or the generation of satellite pulses by interferences. Alternatively, the mode-field diameter of the gain fiber can be increased, e. g. by the use of PCFs, in order to distribute the intensity to a larger area, which is also limited at some extent.

5.4. Conclusion

The chirped-pulse amplification (CPA) system presented in this chapter achieved an average output power of almost 30 W at a repetition rate of 66.7 MHz, resulting in a maximum pulse energy of 450 nJ. The amplification was limited by the available pump power. The pulses could be recompressed to a duration of 293 fs at an overall gain of

28.4 dB. The system presented in this chapter did not achieve the target parameters of $1 \mu\text{J}$ and 150 fs, respectively.

In research-grade CPA systems, the fiber-integrated setup is rarely chosen, because the degrees of freedom are limited in an all-fiber approach. Amplified pulses targeting high-end parameters regarding pulse duration require a chirp precompensation in a free-space stretcher or pulse shaper. Strong gain values ultimately require the pulse amplification in several stages of rod-type fibers that cannot be connected in a fiber-integrated way due to the lack of matching fiber components. CPA systems that are fiber-integrated usually focus on high pulse energies corresponding to low repetition rates as for example in References [55, 31, 14]. Besides the different target parameters, the power handling in these systems is comparable to the experimental system presented above. In those publications, pulse energies of several μJ and pulse durations of < 180 fs are reported at repetition rates of 1 MHz and less. Furthermore, the systems have in common, that the pulse spectrum is distinctly less modified than that shown in Figure 5.6 (b), but also have a spectral bandwidth in the range of 20 nm. The pulse duration of < 180 fs is achieved by counterbalancing third order dispersion by self-phase modulation [55], respectively a pre-compensation of higher order dispersion in the stretcher [31, 14].

It can be seen that an improved seed pulse is required for achieving the targeted pulse parameters. The other opportunities would be a more sophisticated stretcher or an improvement of the pulse parameters by nonlinear effects in the amplifier.

The explicit design of a CPA system always follows a trade-off between final pulse duration, pulse energy and average power, as also mentioned in Section 5.1. A stronger chirping requires a more sophisticated compressor, and, at some point, a lower repetition rate, in order to prevent an overlap of the successive pulses. Increasing the fiber core-diameter may result in the reduction of the beam quality. Alternative fiber designs, like photonic crystal fibers, circumvent the loss of beam quality with simultaneously increasing the mode-field diameter at the price of strongly increased costs.

In combination with the advantages of the nonlinear effects like the spectral broadening by SPM, the accumulation of the nonlinear phase can also be intended and enforced. This requires a different approach in the amplification and will be the subject of the following chapter.

6. Nonlinear Amplification of Ultrashort Pulses in Glass Fibers

The motivation for a linear amplification in a chirped-pulse amplification (CPA)-system is that linear changes of pulse parameters, as for instance the spectral phase, can be well controlled and reversed. Nonlinear effects on the other side are more demanding to anticipate. Small fluctuations in the pulse peak power can have drastical effects on the output parameters and nonlinear parts of the phase cannot necessarily be compensated by linear compressors.

In contrast, nonlinear effects can be exploited in order to improve the pulse parameters. In fact, ultrafast oscillators handle huge accumulations of nonlinear phase, as well as significant spectral and temporal changes during one roundtrip, and still show excellent pulse qualities [102]. These pulse dynamics along with the nonlinear effects can also be exploited in an amplification stage. The prospect of generating high-energy pulses, which are compressible towards their Fourier-limit, comes at the expense of a fixed working point.

In this chapter, first, the state of the art of nonlinear amplification systems is presented in Section 6.1. Afterwards, experimental results of a nonlinear amplification system are discussed in Section 6.2.

6.1. State of the Art

Nonlinear effects can be implemented into an amplification stage in various ways. In CPA-systems for instance, self-phase modulation (SPM) can be used to compensate third order dispersion (TOD), by balancing the nonlinear phase with the dispersive phase [151]. This is also possible the other way round. Intentionally induced TOD by a mismatched grating compressor was used by Zaouter *et al.* to cancel the nonlinear phase in a chirped-pulse amplifier and subsequently generate 270 fs, 30 W, 100 μ J pulses [147].

The use of a self-similar pulse shape enables the improvement of the input pulse parameters along with the amplification (cf. Sec. 3.3). The first experimental demonstration of parabolic pulse propagation was reported by Fermann *et al.* in 2000 [30]. Here, the wave-breaking free propagation was verified by analyzing the pulse before and after amplification and after further propagation in a passive fiber. In this demonstration, pulse parameters were improved by SPM-induced spectral broadening such that an initial 200 fs-pulse could be compressed to 68 fs.

Since then, pulses with energies in the range of 1 μ J and with durations of less than 100 fs based on self-similar amplification were frequently reported. For amplification, usually large mode area fibers such as rod-type fibers were used in order to reduce the nonlinear influence and enable higher pulse energies. In 2008, Zaouter *et al.* reported pulses with 10 W average power, 64 fs duration and energies of 1 μ J from a rod-type

nonlinear amplifier stage [148]. Further developments include the use of a pre-chirper in front of the amplification in order to manage the TOD in the amplifier, which otherwise limited the parabolic pulse propagation. Liu *et al.* reported 100 W, 60 fs, 1.3 μJ pulses by the use of a pre-chirper and a single-stage large-pitch fiber amplifier in 2015 [77]. In 2016, Liu *et al.* produced 93.5 W, 33 fs, 1.7 μJ pulses by using a three-stage amplifier with a grism-based pre-chirper in front of the final amplifier [79]. Preserving a stable pulse shape in the amplifier is a paramount requirement for the high-pulse energy generation. Besides the pre-chirping, the pre-shaping of a Gaussian pulse into a parabolic pulse in a piece of normal dispersive passive fiber is a well-established method [32]. A Gaussian pulse shape can be generated by a spectral filtering of a broadband spectrum. By the spectral filtering prior to the amplification stage, narrowband picosecond pulses can be amplified to end up with broadband femtosecond pulses. Song *et al.* generated 6.1 W, 66 fs, 203 nJ pulses with this technique [126]. Fu *et al.* also showed that not even mode-locked seed sources are necessary to improve the pulses towards femtosecond duration [39]. They demonstrated the generation of 140 fs, μJ -level pulses from a gain-switched diode, which was achieved by spectral broadening, offset filtering and spectral broadening again. This concept allows for a reliable pulse-on-demand application. The applied amplification scheme is also employed in Mamyshev regenerators, discussed in Chapter 7.

In general, the most significant distinction of these self-similar nonlinear amplifiers to CPA-systems is the severely reduced pulse duration of the amplified pulse. A tendency can further be noted to use the nonlinear amplification preferably in combination with a high repetition rate in contrast to the amplification in CPA-systems. In CPA-systems, the repetition rate can be reduced in order to increase the pulse energy. This is not possible in self-similar amplifiers, because the pulse energies are limited to $\approx 1 \mu\text{J}$ [39].

The amplification of the pulse energy in a self-similar nonlinear amplifier is limited by Raman scattering and the resulting Stokes wave. As Raman scattering is most likely to occur at the pulse peak, the Raman scattering induced loss is most significant at that point. At this point, also the parabolic profile is most critical for the self-similar evolution. For output pulse durations of less than 100 fs, the Raman scattering limits the amplification to pulse energies of 1 – 2 μJ [37]. Increasing the seed pulse duration leads to a lower impact of nonlinear effects and, therefore, to less spectral broadening and longer output pulse durations, but also to a higher threshold for Raman scattering. Self-similar amplification of seed pulses with transform-limited durations of 27 ps were reported to be amplified to pulse energies of 60 μJ with compressed durations of 780 fs [107].

6.2. Experimental Realization

In this section a nonlinear amplifier is described that continues the work to reach the target parameters, introduced in Section 5.2: pulse energies in the μJ -regime and pulse durations below 150 fs for the potential use in material processing. In order to overcome the dependence of the amplified pulses from the seed pulse parameters, a nonlinear amplifier was set up, according to the scheme presented in Figure 6.1, in which the pulses were amplified self-similarly.

An ultrafast oscillator delivered the seed pulses for the nonlinear amplifier. The seed pulses had a repetition rate of 11 MHz, pulse energies of 31 nJ, a very broadband optical spectrum ranging from 1000 nm to 1080 nm and a slight chirp due to the normal dispersion

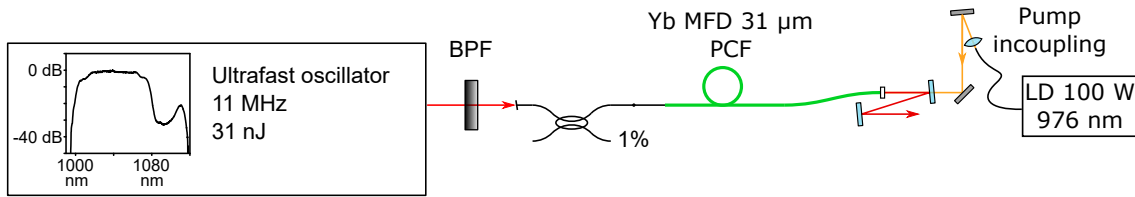


Figure 6.1.: Setup of the self-similar amplification stage: The ultrafast oscillator with the indicated parameters is used as seed source for the fiber amplifier based on the PCF gain module from the preceding chapter. BPF: Band-pass filter, LD: laser diode, MFD: mode-field diameter, PCF: photonic crystal fiber.

in the glass fibers, leading to a duration of 3 ps in the autocorrelation (AC). An improvement of the pulse parameters is expected due to the self-similar amplification. At the same time, different input pulse shapes are compared in order to evaluate the output pulse parameters. First, the seed pulses were coupled into the amplifier without any manipulation. Afterwards, two different band-pass filter (BPF) designs were compared to the case in which no prior filtering was applied. Interference BPFs (IBPFs) were implemented due to a fairly simple adjustment. Diffraction gratings in combination with the fiber incoupling were used, which cause a Gaussian shape that was expected to be advantageous.

Due to the broadband signal of the seed, the spectrum after the BPF could be adjusted in width, central wavelength, and shape, allowing for the investigation of the effect of the nonlinear amplification on different input parameters, as the temporal shape influences the SPM. Because of the broadband seed pulse, the spectral filtering resulted in a power loss of roughly 90%. Owing to the chirp of the seed pulses, the spectral shape of the filtered pulses had a similar temporal shape.

Amplification without Prior Filtering The power amplifier from the preceding chapter was used for the amplification. The gain fiber was an Yb-doped photonic crystal fiber (PCF) with a mode-field diameter of 31 μm and a length of 1.8 m. The large core diameter reduced the influence of the nonlinear effects, allowing for a stronger amplification and a higher pulse energy limitation resulting from nonlinear effects. The amplifier was pumped at a maximum of 100 W with a laser diode centered at 976 nm, as depicted in Figure 6.1. In this case, the BPF was replaced by a silver mirror that transmitted the complete seed pulse spectrum.

Coupling into the fiber via a silver mirror, i. e. using the full spectrum and full pulse energy from the seed laser quickly resulted in strong stimulated Raman scattering. The results of the amplification are presented in Figure 6.2. The optical spectra of the seed, the amplifier input at specific amplification values are shown in Figure 6.2 (a), the corresponding AC traces of the amplified pulses in Figure 6.2 (b). At a low gain, the spectrum shifted to the red. The red-shift is a result of the self-absorption in the unpumped parts of the gain fiber. For increasing amplification values, the signal shifted further to the blue. The peak at the blue edge of the spectrum is mitigated as an increasing amount of energy is shifted into the broad Raman peak on the red edge of the spectrum. The modulation on the Raman peak resulted from a systematic error: a neutral density filter was used in front of the spectrometer in order to reduce the fluence on the detector and this component generated double pulses.

6. Nonlinear Amplification of Ultrashort Pulses in Glass Fibers

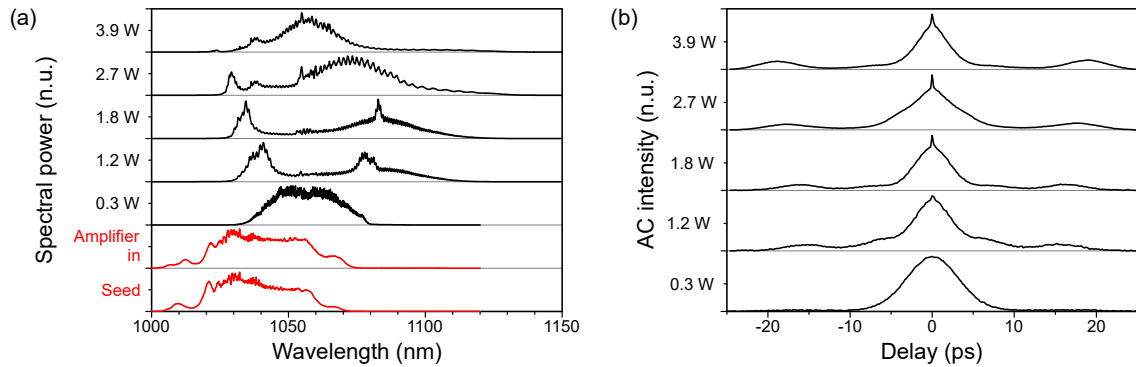


Figure 6.2.: Results from the nonlinear amplifier without filtering of the seed. The optical spectra are shown in (a), the corresponding AC durations in (b) for the respectively indicated average output powers. The modulations on the spectra for the output powers of 1.8 W, 2.7 W and 3.9 W result from reflections from the neutral density filter in front of the spectrometer.

The pulses turned out to be hardly compressible (cf. Fig. 6.2 (b)). Besides the broad main peak in the AC traces, side maxima shifting from a delay of 15 ps to 20 ps for increasing signal power emerged and optical wave breaking occurred. As the broad input spectrum allows a very short pulse, a limitation of the pulse quality by Raman scattering would be expected at low pulse energies [39]. This indicates that the amplification of pulses with narrowband spectra allows for the generation of higher pulse energies and broader spectra.

Filtering with Interference Band-Pass Filters In order to reduce the spectral width, first, an IBPF was used that transmitted a spectrum with a Supergaussian shape. Three different filtered bandwidths at full-width half-maxima (FWHM) of 3 nm, 5 nm, and 10 nm were applied instead of the silver mirror from the previous case.

The input spectra and the spectra of the pulses after amplification are shown in Figure 6.3 (a)-(c). In particular, the input spectrum, measured at the 1%-port (cf. Fig. 6.1), and the output spectrum for the maximum amplification before the onset of nonlinear limitations are presented. The corresponding AC traces are depicted in Figure 6.3 (d)-(f). The IBPFs are designed for the central wavelength 1064 nm and can be spectrally tuned to lower wavelengths by changing the angle of incidence. As an unintentional side effect, this also causes peaks in the transmitted spectral shape (Fig. 6.3 (a), (b)).

The maximum pulse energy was comparable for the filters with the 3 nm and 5 nm bandwidth (cf. Fig. 6.3 (a), (b), (d), (e)). In order to avoid self-lasing, the central input wavelength was set to 1040 nm. At the powers of 5.2 W and 5.8 W for the 3 nm-filter and the 5 nm-filter, respectively, the output power was limited by optical wave breaking. This can be seen in the AC traces, in which a strong pedestal was formed and the pulse quality was severely degraded for higher pump powers.

The pulses that were filtered by the 10 nm-IBPF could be amplified to an average power of 4.1 W at the central wavelength of 1030 nm (cf. Fig. 6.3 (c)), when optical wave breaking occurred. Due to the slight chirp on the pulses, the pulses were longer than the narrowband-pulses with the FWHM of 3 nm or 5 nm. Firstly, longer pulses generate less new frequency components, which can also be seen in Figure 6.3 (c). Secondly, this pulse requires a longer

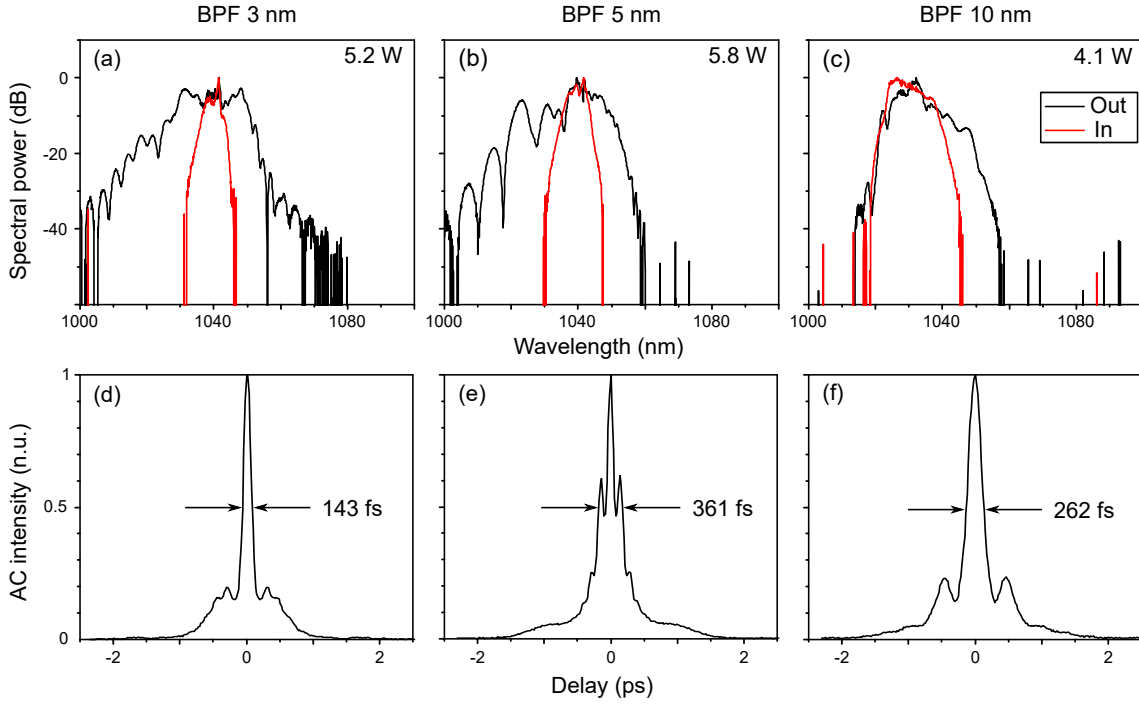


Figure 6.3.: (a)-(c) Input and output spectra of the pulses from the nonlinear amplifier behind band-pass filtering with an interference BPF, for different input bandwidths. The maximum possible average output power before the onset of the respective limitation is indicated in the graphs. (d)-(f) AC traces of the compressed pulses at the maximum output power with the full-width half-maximum duration as indicated in the respective graphs.

fiber line to evolve into a parabolic pulse shape (cf. Eq. (3.6)). Therefore, the pulse shape is destabilized sooner and optical pulse breaking occurs at lower pulse energies.

The pedestal in the AC traces may result from the Supergaussian temporal input pulse shapes. The pulses have steep edges and a plateau in the center. Due to the steep edges, the spectral broadening was strong at these pulse parts. Owing to the plateau, however, which did not generate SPM, the pulse phase was strongly nonlinear (cf. Fig. 2.4 (b)). This prevented a sufficient compression of the pulses by the (linear) grating compressor, as depicted in Figure 6.3 (d)-(f). A strongly nonlinear phase is also an indication that the amplification is not self-similar. Apparently, the Supergaussian shape does not evolve into a parabolic shape in the fiber section of this amplifier.

Filtering with Diffraction Gratings Using a diffraction grating as BPF yielded an optical spectrum with a Gaussian shape. The Gaussian shape is expected to evolve faster into a parabolic shape than the Supergaussian. Therefore, higher pulse energies were expected, before the onset of nonlinear limitations. The results of the amplification with this filter type are presented in Figure 6.6. A 300 lines/mm-grating (Fig. 6.5) and a 600 lines/mm-grating (Fig. 6.6) were used at center wavelengths of 1040 nm and 1060 nm, each.

The amplifier for the experiments was modified. In order to reduce the effects of self-lasing and the cost of damages through spiking from excessive ASE, a standard fiber was implemented as gain fiber, as shown in Figure 6.4. In the mode-field adapter (MFA), the single-mode fiber was matched to a few-mode fiber with a core-diameter of 20 μm . The

6. Nonlinear Amplification of Ultrashort Pulses in Glass Fibers

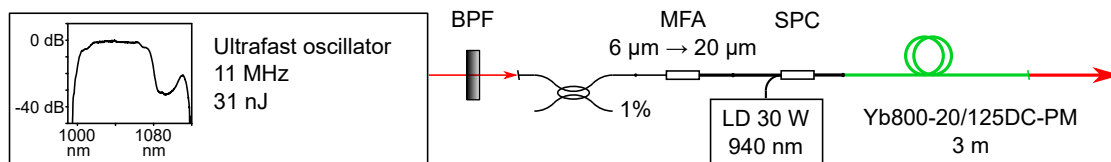


Figure 6.4.: Setup of the self-similar amplification stage: An ultrafast oscillator is used as seed source for the fiber amplifier based on a standard step-index gain fiber. BPF: Band-pass filter, LD: laser diode, MFA: mode-field adapter, SPC: signal-pump combiner.

maximum pump light of 30 W at 940 nm was delivered by a fiber-coupled laser diode and coupled into the amplifier by a signal pump combiner (SPC), obtaining a higher stability for the pump coupling. The wavelength 940 nm provided a homogeneously distributed gain along the active fiber. Behind the SPC, the pulses were amplified in a low Yb-doped fiber (nlight, Yb800-20/125DC-PM) with a length of 3 m. The low doping of the active fiber in combination with the relatively long length and the “off-peak”-pumping at the wavelength of 940 nm were applied to support a self-similar evolution of the pulse in the amplifier. The pulses were coupled out directly behind the active fiber. The residual pump light was blocked by a dichroic mirror. A fiber-based stripping of the residual pump light was not realized in order to keep the fiber length short at the points of high pulse energies. This is necessary because the pulse energy is ultimately limited by nonlinear effects which scale with the fiber length.

Using a 300 lines/mm-grating as BPF, caused spectral widths of 4.0 nm and 5.3 nm for the central wavelength of 1042 nm and 1060 nm, respectively. The results of the amplification are shown in Figure 6.5. For the central seed wavelength of 1042 nm, the pulses could be amplified to an average power of 4.9 W before the onset of optical wave breaking. At this power level, the spectrum ranged from roughly 1010 – 1120 nm. The corresponding pulse duration could be decreased to 77 fs in the AC trace. For the central seed wavelength of 1060 nm, the limitation due to optical wave breaking occurred at the average power of 3.8 W. At that point, the pulse parameters in terms of optical bandwidth and compressed pulse duration were comparable to the previous case.

The limitation to lower pulse energies for the input wavelength of 1060 nm (Fig. 6.5 (b)) can be explained by the gain cross-section of Yb-doped fibers. During amplification, new wavelength components were generated preferably at the blue edge of the spectrum, where the gain cross-section of Yb-doped fibers is higher. This quickly led to a very broad spectrum that only had a relatively small overlap with the spectral gain. This is a limitation to the self-similar propagation as explained in Section 3.3. Still, in this setup, nonlinear effects, like excessive SPM with a nonlinear spectral phase, did not distort the pulse and compressed pulse durations of less than 100 fs were possible.

The limitation of the average output power was comparable to the results of the narrow-band IBPFs, while the compressed pulse duration was much shorter, despite the smaller mode-field diameter in this amplifier. This indicates a linear chirp from the self-similar amplification.

The grating with the 600 lines/mm caused a smaller spectral width of 1.3 nm at the central wavelength of 1040 nm. The results for this case are presented in Figure 6.6 (a) and (c). With these parameters, the pulse energy could be increased to more than 1 μJ, corresponding to 11.2 W average power at a repetition rate of 11 MHz. The spec-

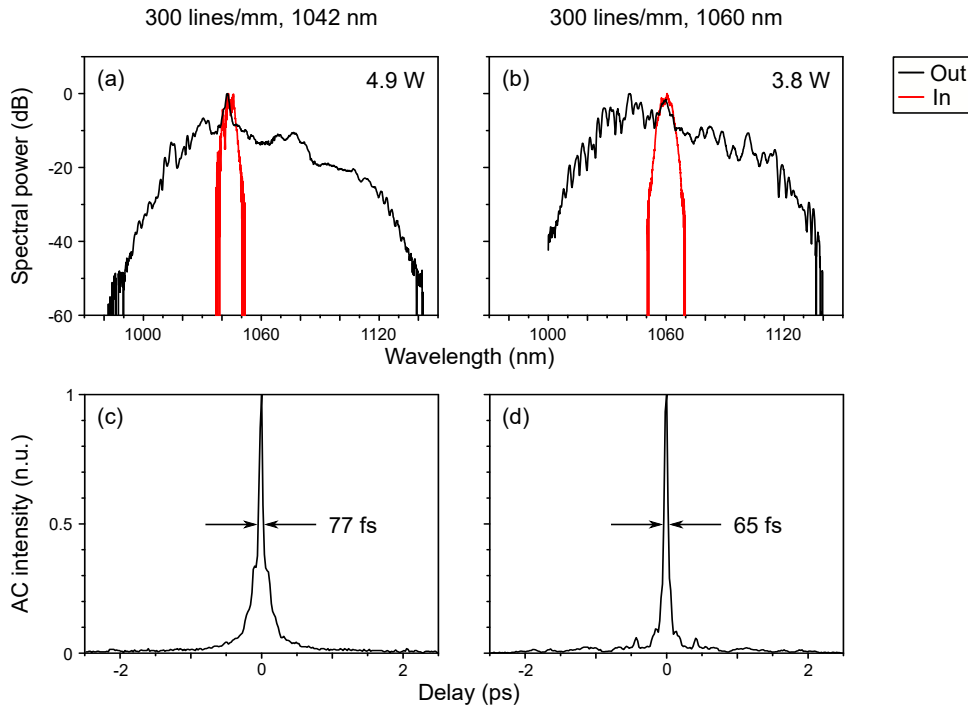


Figure 6.5.: (a), (b) Input and output spectra at the maximum gain value and (c), (d) AC traces after compression from the amplification of pulses in the nonlinear amplifier after band-pass filtering with a 300 lines/mm-grating. The indicated power values correspond to the maximum average output power before the onset of optical wave breaking. The indicated durations are the durations of the AC trace.

tral width increased monotonically for increasing pump power, as expected from the parabolic pulse evolution. At the highest pulse energy, the spectrum roughly ranged over 120 nm without any significant modulations, except for a prominent maximum around 1042 nm. This spectral maximum has a large overlap with the input wavelength. The peak's spectral width is too broad to result from parasitic self-lasing, and in combination with the radio-frequency traces of the amplified signal, which did not show any degradation, self-lasing was excluded. The Fourier-limited pulse duration was 39 fs, despite of the rather prominent maximum at the wavelength 1040 nm. The corresponding Fourier-limited AC duration of 55 fs is close to the measured AC duration of 63 fs (Fig. 6.6 (c)). Nonlinear distortions of the pulse in this amplifier setup were not observed.

For higher output power than 11.2 W, the signal power slowly decreased with increasing pump power. As this effect was reversible (by decreasing the pump power) and reproducible, it could be a sign of transverse mode instability. This instability results from the interference of the fundamental mode in the amplifier and the higher order modes. In the case of high powers (≈ 100 W–kW average power), this interference can be caused by a thermo-optic effect. In the case of lower powers (like in the case of this thesis), the interference can be caused by refractive index changes due to strong differences in the inversion in the high gain amplifier [118]. The maximum possible output pulse energy of more than 1 μ J in combination with 50 fs pulse duration could not be reached with the other filter parameters of the BPF that were investigated.

6. Nonlinear Amplification of Ultrashort Pulses in Glass Fibers

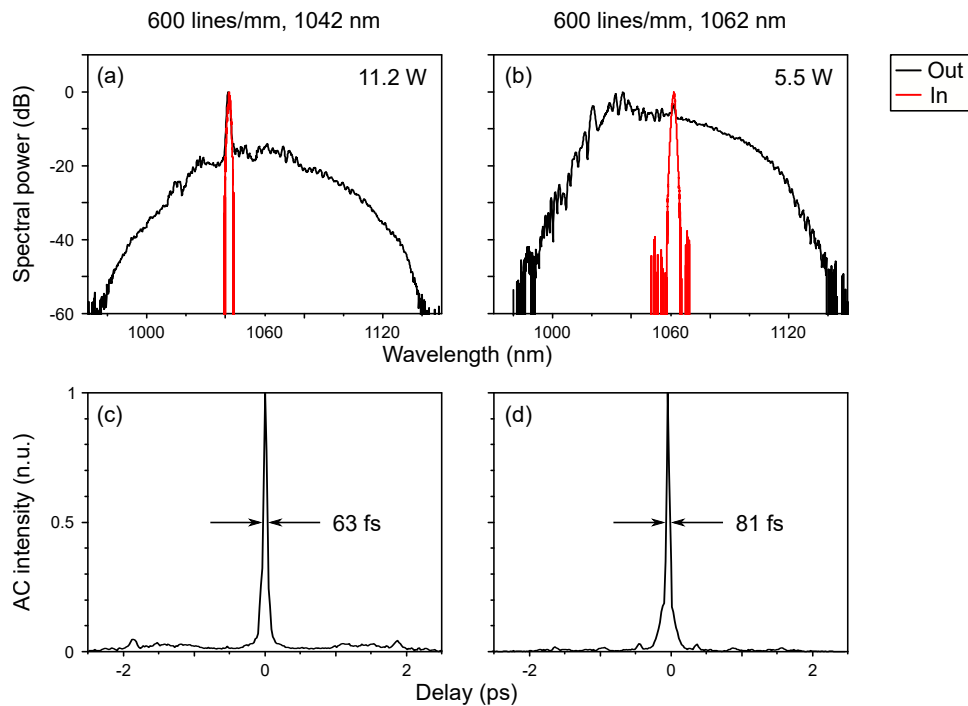


Figure 6.6.: (a), (b) Input and output spectra at the maximum gain value and (c), (d) AC traces after compression from the amplification of pulses in the nonlinear amplifier after band-pass filtering with a 600 lines/mm-grating. The indicated power values correspond to the maximum average output power before the onset of optical wave breaking. The indicated durations are the durations of the AC trace.

At the input wavelength around 1060 nm (Fig. 6.6 (b), (d)) and a spectral width of 1.5 nm, the onset of the limitation, most likely nonlinear optical pulse breaking, occurred above a pulse energy of 507 nJ, corresponding to 5.5 W average power. In the output spectrum, dominant wavelength components can be noted on the blue side of the seed spectrum. The preferred generation of new wavelength components around 1030 nm is attributed to the gain cross-section of Yb-doped fibers, as explained above. The occurrence of pulse breaking at lower pulse energies are also attributed to this effect. The spectrum allows for the generation of pulses with a Fourier-limited duration of 39 fs and a Fourier-limited AC duration of 57 fs. The measured AC duration was 81 fs. Aside from uncompressible features due to the deviation from ideal parabolic pulse shape, the phase of the amplified pulse was mostly linear.

Gain-Managed Nonlinear Amplification The amplifier design showing the most promising results with the 600 lines/mm-grating as BPF and the central input wavelength of 1042 nm (Fig. 6.6 (a), (c)) was more closely analyzed. Although a strong dependence of the pulse quality on the pulse energy would be expected from nonlinear amplification, the performance appeared to be stable over a wide range of pulse energies, as shown in Figure 6.7. Figure 6.7 (a) shows the spectral evolution of the pulses from the amplifier for different gain values. The spectrum was quickly broadened and remained stable for higher pulse energies. The spectra showed a slight modulation at the blue side of the newly generated

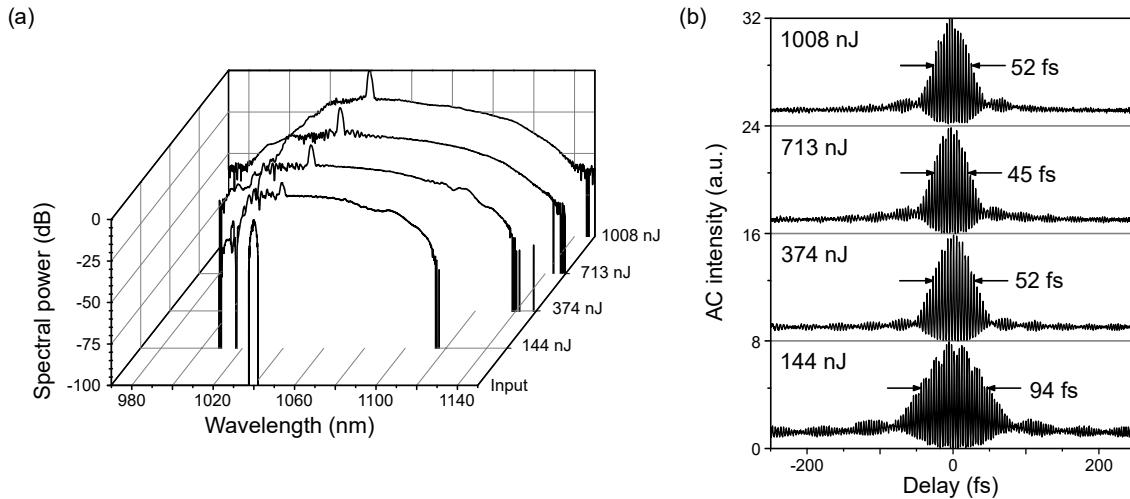


Figure 6.7.: Results from the nonlinear amplifier for the combination of band-pass filtering with a grating with a narrow bandwidth at a central input wavelength of 1040 nm.

wavelength components and a very smooth course on the red side. At the maximum pulse energy of 1 μJ , the spectrum ranged from 980 nm to 1140 nm. A noteworthy feature is the narrow peak around 1040 nm that could be seen in all amplification values. This peak resulted from the seed signal. As it increased when inducing a lower seed pulse energy, it is probably caused by a small-signal gain in the beginning of the amplifier. The prominent peak hardly degraded the temporal pulse quality, as can be seen from the AC traces in Figure 6.7 (b).

The AC traces from Figure 6.7 (b) show the same evolution of the pulse quality as the optical spectra: The quality stays stable over a large amplification range. The compressed pulse duration relates to the spectral width and ranges around 50 fs for high pulse energies (and broad spectra). The pulses were analyzed by using fringe-resolved autocorrelation (cf. App. C), the ratio of 1:8 from baseline to peak verified that the prominent peak at 1040 nm had a low impact on the pulse quality and the traces did not show a coherence spike above a very broad pedestal. The low significance of side maxima in the AC traces indicate a linear phase, that was generated by the nonlinear amplification, and hence a high compressibility by a standard (linear) grating compressor.

In 2019, Sidorenko *et al.* proposed a new nonlinear attractor besides the self-similar propagation, which they called “gain-managed nonlinear amplification” [120]. Gain-managed nonlinear amplification describes the strong amplification of a spectrally narrow pulse. During the amplification in an Yb-doped fiber, the gain cross-section shifts to the red, because of self-absorption and the strong inversion. The results include an extremely broad spectrum while maintaining a good compressibility of the pulse. The results presented in Figure 6.7 fit to the new regime: A long gain fiber was employed, the input bandwidth was narrow, the output bandwidth very broad and the output spectra were relatively smooth. Finally, the central wavelength was shifted to the red for increasing output pulse energy. The first two points, i. e. the long fiber and the narrow but increasing input spectral bandwidth, were employed and expected for the parabolic pulse evolution. The specific shape of the spectrum, however, is consistent with the amplification model proposed by Sidorenko *et al.*. The gain-managed nonlinear amplification model depends on solving

the rate equations for the inversion simultaneously with the pulse evolution. This is another indication that the pulse evolution is in the gain-managed nonlinear amplification-regime, as the experimental data presented in Figure 6.7 could not be reproduced by a simulation with the Fiberdesk software¹. The Fiberdesk simulation was based on a fixed gain amplification model.

6.3. Conclusion

The nonlinear amplification in a single-stage amplifier with strong filtering beforehand allowed for excellent pulse qualities. The pulse parameters were improved following the self-similar pulse propagation, resulting in broad optical spectra and short durations along with high pulse energies. Best results were achieved by the use of a narrow, Gaussian-shaped band-pass filter in front of the amplification stage. In the amplification stage, the focus was on self-similar pulse evolution, which included a low Yb-doped fiber and an off-peak amplification scheme. With the given parameters, at the repetition rate of 11 MHz, the pulses could be amplified to 1 μ J and compressed to pulse durations of 50 fs, leading to an estimated maximum pulse peak power of 18.8 MW. By this, the initial targets for pulse amplification were accomplished.

Compared to the laser systems mentioned in Section 6.1, the design described above is based on a strongly simplified setup. The amplification was carried out in a standard fiber instead of a rod-type or photonic crystal fiber. Furthermore, a single-stage amplification was sufficient to reach the pulse energy of 1 μ J and the manipulation of the seed pulse only included a simple filtering instead of pre-chirping or pre-shaping in a spatial light modulator. The pulse energy could be further increased by the implementation of a larger fiber core diameter, as reported by Sidorenko *et al.* in 2020 [122].

While the amplification to the desired pulse energy of 1 μ J was achieved to not a small part as a result of the lower repetition rate, the pulse duration of 50 fs could have not been reached in a linear amplifier from the (filtered) seed pulse. Although the nonlinear amplification cannot be used for a distinct further amplification, the advantage to decouple the pulse quality from the parameters of the master oscillator can be seen.

As already mentioned in Section 6.1, it was not possible to generate pulse energies that are considerably higher than 1 μ J, because of a nonlinear limit. The grade of the pulse parameter improvement is, however, interesting. The amplification stage can act as a pulse (Mamyshev) regenerator. Feeding back a small portion of the output as a seed to itself can produce a self-preserving pulsed output with pulse energies distinctly above those of common fiber-based ultrashort pulse sources. Using two concatenated nonlinear amplifiers in a ring to establish a stable pulse train will be the topic of the following chapters.

¹“Fiberdesk”, www.fiberdesk.com/, accessed: August 31, 2020

7. Nonlinear Amplification with Feedback in Normal Dispersion Fibers

A feedback of the output as a seed signal back into the nonlinear amplifier can lead to a reproduction of the pulse. This principle is realized in the Mamyshev oscillator (MO), which generates high energy and optically broadband pulses. In contrast to common laser oscillators, MOs do not start from noise, i. e. they “merely” reproduce and regenerate the injected seed pulses. As stable, mode-locked pulse trains are emitted, these pulse generators can be compared to other fiber-based oscillators. Many new mode-locking concepts have already been reported since the publication of the soliton laser [92]. The MO was the latest step in the line of laser performance breakthroughs [38] and will be addressed in this chapter.

A brief overview on the development of different mode-locking mechanisms and an introduction to the state of the art, will be given in Section 7.1. Afterwards, the experimental results of the MO based on normal dispersive fibers will be presented in Section 7.2.

7.1. Ultrafast Oscillators Based on Ytterbium-Doped Fibers

Ultrafast fiber lasers promise low costs, high environmental stability and simplicity, and, therefore, stand as an alternative to crystal-based solid-state lasers which, as of now, allow for higher pulse peak powers and shorter pulse durations. Hence, much effort is put into the improvement of the output parameters of ultrafast fiber oscillators.

Ultrafast oscillators can be categorized in two ways, either from the point of pulse evolution mechanisms or from the type of saturable absorber they employ. The first classification refers to the pulse shaping mechanism in the oscillator, e. g. soliton [91], dispersion-managed soliton [97] or dissipative soliton [17]. The specific saturable absorber for passive mode-locking serves as the second categorization method and is more suitable here. The demands to saturable absorbers for femtosecond pulse generation are high. They need to be fast in switching and regeneration, i. e. blocking after the transmission of a pulse, they need to suppress continuous wave (cw)-light efficiently, to show a high modulation depth [111], and a high damage threshold.

Frequently incorporated mode-locking mechanisms include real saturable absorbers, e. g. semiconductor saturable absorber mirrors (SESAMs) [62]. SESAMs absorb light until a certain threshold is achieved. Above the threshold, the absorption is reduced. Therefore, a lower loss is induced for high intensities than low intensities. Laser systems based on SESAMs offer a simple setup, because the modulation is reliably induced by a single component without the need of an elaborate resonator design. Modulation speed and depth can be individually tailored in the manufacturing process, corresponding to the requirements of the laser application [139]. However, these saturable absorbers must be

7. Nonlinear Amplification with Feedback in Normal Dispersion Fibers

operated close to the damage threshold, which limits the maximum possible emitted pulse energy and decreases the longterm reliability.

Other mode-locking mechanisms depend on artificial absorbers which are usually faster in switching of the modulation. Artificial saturable absorbers are for example nonlinear-optical loop mirrors (NOLMs) [20], or nonlinear amplifying loop mirrors (NALMs) [29], NOLMs and NALMs are based on nonlinear Sagnac interferometers. Due to a phase shift of high intensities, a pulse is transmitted, while the low intensity radiation is rejected. Nonlinear loop mirrors allow for the design of environmentally robust oscillators, owing to the possibility of an all-fiber and all-polarization maintaining (PM)-fiber setup with the reduced risk of damaging the saturable absorber [26, 3, 130]. The output pulse parameters depend on the power splitting ratio at the coupler to the fiber loop mirror, the fiber lengths in main loop and loop mirror, the pump power in the loops and a band-pass filter that is used to reset the pulses every roundtrip. The transmission-intensity curve of the saturable absorption is nonlinear, excessive or insufficient pump power leads to a pulse destabilization and rogue wave emission, respectively.

Another mode-locking mechanism based on an artificial saturable absorption is the nonlinear polarization evolution (NPE, cf. App. A). Mode-locking by nonlinear polarization rotation of pulses with high peak powers and filtering via a polarization dependent component is described in detail in Appendix A. It offers the highest modulation depths of the aforementioned saturable absorbers ($> 70\%$) [38], which is necessary for the generation of high-energy pulses [111]. The drawback of this concept is the periodicity of the transmission-intensity curve. High pump powers can lead to multipulsing and a cw-breakthrough. Although NPE has also been reported in an all-PM-fiber setup [131], most NPE-lasers incorporate non-PM fibers and are, therefore, more sensitive to environmental disturbances.

A relatively new method for artificial saturable absorption is the alternating spectral filtering [106] that is discussed in detail below. The concept of alternating spectral filtering as a mode-locking mechanism was introduced in the early 1990s [62, 106], but did not attain much attention. The first operating MO in the Yb-regime at $1\ \mu\text{m}$ wavelength was reported in 2015 by K. Regelskis *et al.* [110]. Their setup consisted of a linear cavity based on Yb-doped fibers with offset fiber Bragg gratings as resonator mirrors that could be wavelength tuned by a temperature variation. The mode-locking mechanism was investigated at $1.5\ \mu\text{m}$ wavelength in the Er-regime by N. Tarasov *et al.* [134] with a focus on the theoretical description of the pulse formation in MOs by the dissipative Faraday instability (cf. Sec. 3.4). The breakthrough of this design came with the generation of outstanding pulse energies around $50\ \text{nJ}$ and durations of $40\ \text{fs}$ from a ring oscillator in the Yb-regime, published by Z. Liu *et al.* in 2017 [80], that was externally injection seeded. The spectral separation of the BPFs in this MO was $10\ \text{nm}$ with a transmission bandwidth of $2\ \text{nm}$ full-width at half-maximum (FWHM).

The spectral separation of the BPFs allows for different operation modes. By reducing the filter separation, a stable emission of pulses with higher orders of the repetition rate instead of single pulse-emission can be triggered [108]. The larger the separation, the more nonlinear phase must be accumulated to pass both filters. Using large-mode area photonic crystal fibers (PCFs), the threshold for pulse breaking is further increased (cf. Sec. 3.2). This led to pulse energies of more than $1\ \mu\text{J}$, which have been reported directly from the oscillator [78]. Spectral broadening can be supported by employing a highly nonlinear fiber, by the use of which spectra ranging from $900\ \text{nm} - 1300\ \text{nm}$ were reported [83].

7.2. Experimental Results

The resonator design of a MO can be optimized to study several properties of the MO. Research can be focussed on the self-starting behavior of the oscillator, on the emission of broad spectra in combination with short pulses, the variation of the repetition rate, or others.

The pulse generation in MOs differs significantly from the pulse generation in ultrashort pulse lasers based on nonlinear polarization evolution. In MOs the nonlinear discrimination does not aim at high intensities (cf. App. A) but on short pulse durations, i. e. sharp pulse edges, at which the spectrum is broadened by SPM. This exacerbates the initiation of mode-locking through noise. As furthermore described in Section 3.4, self-starting in MOs is possible by the dissipative Faraday instability. Dissipative Faraday instability has been realized in long cavities in order to have a long interaction between light and material. This is a distinct requirement to the cavity design and, therefore, not a priority.

Self-injection of pulses is an alternative to initiate mode-locking. On the one hand, this option offers the stand-alone operation of the system. On the other hand, self-injection usually requires an already adjusted setup with the correct filter separation and gain values. In order to have more freedom in the investigation and optimization of the MO adjustment parameters, in the scope of this work, initiating pulses were injected by an external laser source.

MOs have been realized in linear cavities and in ring setups. In general, ring designs with free-space sections between the two arms showed refined output parameters [121, 78, 82] compared to linear designs [110, 134] which, on the other side, tend to be advantageous for the starting process. As in this thesis, the focus was on the generation of high pulse energies and broad output parameters, the ring oscillator design was chosen. Compared to a previous setup that was already published [113] and according to the results shown in Chapter 6, the design was further optimized for higher pulse energies by the use of a few mode fiber in the second arm of the MO, as described below. The MO in general is designed more like two cascaded amplifiers with feedback than the precisely adjusted resonator of a common ultrafast laser.

Setup The setup of the MO is schematically presented in Figure 7.1. It consisted of a ring cavity with two arms, each with amplifier sections of Yb-doped fibers. The active fiber in arm 1 with a length of 1 m and a core-diameter of 6 μm was cladding pumped through a signal-pump combiner (SPC) by a multi-mode pump diode with a maximum pump power of 25 W at the wavelength of 976 nm. The residual pump light was stripped from the system by a cladding-light stripper (CLS). A fiber-based isolator stabilized the mode-locked operation and prevented catastrophic damages by backreflections in the active fiber in arm 1 during the high-power ASE emission operation mode. The passive fiber line behind the amplification supported the pulse evolution by SPM, to allow for a low-power operation. The whole arm 1 supported only the fundamental mode. In the following free-space section, a diffraction grating with 600 lines/mm was used as a tunable BPF with a Gaussian transmission spectrum centered at 1028 nm and a full-width at half-maximum (FWHM) spectral bandwidth of 1.6 nm. The grating spatially expands the beam by diffraction, the limited aperture of the fiber only allows the transmission of a specified wavelength range. A grating with 600 lines/mm was used in order to

7. Nonlinear Amplification with Feedback in Normal Dispersion Fibers

reduce the transmission bandwidth, in accordance with the results described in Section 6.2. In general, a narrower spectral bandwidth enables the generation of shorter pulse after the amplification on the one hand [37]. On the other hand, the narrower spectral bandwidth results in a reduced seed pulse energy in the subsequent arm which can cause an unsaturated amplification. The interference BPF (IBPF) was used to support the suppression of the blocking bandwidth and reduce the fluence on the reflection gratings.

In arm 2, the signal was coupled into a passive single-mode fiber to ensure the excitation of the fundamental mode in the following large-mode area fiber. The amplifier fiber was a low-doped step-index double-clad Yb-fiber with a core diameter of 20 μm and a length of 3 m (nLIGHT, Yb800-20/125DC-PM). The mode-field of the single-mode and the amplifier fiber were matched by using a mode-field adapter (MFA) which was included in the SPC. The amplifier was co-propagating pumped by a multi-mode laser diode, emitting at 940 nm with an output power of up to 70 W. Pumping at this wavelength reduced the gain in the active fiber and allowed for the evolution of parabolic pulses. In addition, due to the lower absorption cross-section at 940 nm, the threshold for ASE was higher. The active fiber was coiled with a diameter of 10 cm to suppress the excitation of higher-order modes. Cooling of the coiled fiber in a water bath increased the threshold for transverse mode instabilities and removed the higher heat load due to the increased quantum defect compared to the pumping scheme at the wavelength 976 nm. Problems owing to ASE were not observed in this amplifier. In the second free-space section, an optical isolator ensured a unidirectional operation. The output coupler was based on a polarizing beam splitter cube (PBS) in combination with a half-wave plate (HWP) and coupled out roughly 95% of the pulse energy. A diffraction grating with 600 lines/mm was implemented as the other BPF, with a central transmission wavelength of 1050 nm and a FWHM of 1.5 nm. Several fiber-based 99/01-couplers inside the cavity were used for monitoring issues. All fibers and fiber components were PM.

A pulse train from an external, mode-locked Yb-fiber oscillator was picked from the repetition rate of 66.7 MHz down to 278 kHz in an acousto-optic modulator and injected into arm 1 via the 0th order of the 600 lines/mm diffraction grating to initiate the pulse circulation. The repetition rate of the injection pulses had to be distinctly below the

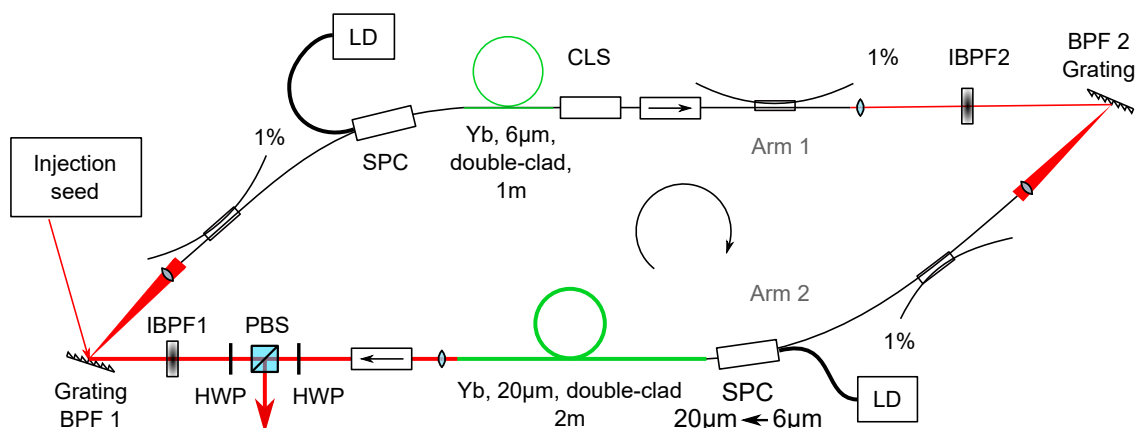


Figure 7.1.: Setup of the MO. BPF: Band-pass filter, CLS: cladding-light stripper, HWP: half-wave plate, IBPF: interference band-pass filter, LD: pump laser diode, PBS: polarizing beam splitter cube, SPC: signal-pump combiner.

fundamental repetition rate of the MO. By this, the preferred amplification of the signal pulses could be ensured [113]. The injection pulses had a pulse energy of 3 pJ and a pulse duration of approximately 7 ps, which was sufficient for starting the MO. The spectral width of the injection pulses was 10 nm, centered around 1031 nm. The injected pulses were amplified in arm 1, spectrally broadened by SPM, and filtered at the BPF2. The transmitted part was then amplified, spectrally broadened in arm 2, and filtered again at the 600 lines/mm-grating (BPF1). If all the boundary conditions matched, the pulses were reproduced after one roundtrip. This mode-locked operation could be verified by the immediate broadening of the optical spectrum at the output and a stable pulse train with the repetition rate of the MO as seen on the oscilloscope. After the initiation of the mode-locking, the injection could be blocked or switched off. Leaving the injection unblocked had a minor effect on the performance of the MO in terms of stability and spectral width; the mode-locked operation of the MO was more efficient than the amplification of the injection pulses.

Different mode-locked operation states of the MO are possible. The different operation states are set by varying the pump power in both arms and the spectral separation of the two BPFs. Two exemplary states are presented in the following; first a state with a broadband output spectrum, afterwards the state that produced the highest pulse energies.

Broadband Spectrum State The broadband output spectrum from the first operation state, that is discussed here, and the transmission spectra of the BPFs are shown in Figure 7.2. For the spectral separation of 22 nm of the two BPFs, an average output power of 5.1 W was achieved. With the fundamental repetition rate of 12.9 MHz (cf. Fig. 7.3 (b)), this corresponds to 395 nJ pulse energy. At this output power, the output spectrum ranged roughly from 1010 nm – 1110 nm. The spectral shape was expected from the results in Section 6.2, shown in Figure 6.7. The expansion was increased more strongly on the red side of the seed wavelength, the overall course was smooth and some oscillations could be seen on the blue side. Furthermore, the significant spectral peak overlaying

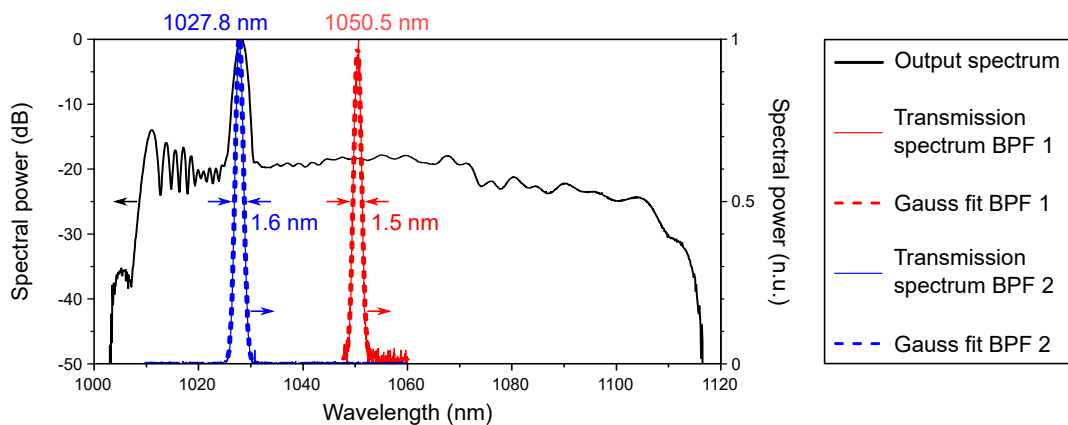


Figure 7.2.: Optical output spectrum (black) of the MO and transmission spectra of the BPFs (red, blue). The transmission spectra were fitted to a Gaussian curve, with the indicated central wavelength and the full-width at half-maximum for the filters, respectively. The output spectrum is given at a logarithmic scale while the transmission filters are given at a linear scale.

the input wavelength of arm 2 could be seen as well. The spectral shape coincides with the criteria given in Reference [122] for the amplification regime called “gain-managed amplification”. This regime describes a recently defined amplification regime in which nonlinear spectral broadening is balanced by strong, longitudinally evolving gain-shaping. In contrast to conventional amplification regimes, in which the gain is static, in the gain-managed amplification regime, the gain spectrum is red-shifted over the course of the gain fiber [120]. The theoretical criteria from this amplification regime work well for the description of the pulse evolution in arm 2, as can be seen at the output spectrum in Figure 7.2. In correspondence with the theoretical predictions [122], oscillations occur on the blue side of the spectrum. Furthermore, the central wavelength shifts (from 1027.8 nm, Fig. 7.2, blue line) into the red. Another indication for the amplification according to the gain-managed amplification regime is that the spectral course of the output spectrum cannot be reconstructed by a standard numerical simulation based on the flat gain model.

The stability of the mode-locking mechanism was analyzed by the use of the radio-frequency (RF) spectra, as shown in Figure 7.3. Figure 7.3 (a) presents the RF spectrum from 1 MHz to 5 GHz. The smoothly declining slope of the maxima was expected and proves the absence of double pulses within the response of the photodiode, which had a rise-time of 18.5 ps. The close-up of the first beat-note shows the fundamental repetition rate of the MO of 12.908 MHz and a signal to noise ratio of 77 dB, proving a stable, mode-locked operation. In Figure 7.3 (c), a comparison of the fundamental beat-note (blue) to the 100th (red) and the 1000th harmonic (blue) is shown. According to the von der Linde-method, fluctuations of pulse amplitude and repetition rate are reflected more strongly with increasing order of the harmonic [75]. The hardly increased noise floor beneath the 1000th harmonic and the hardly increased width of the 1000th peak showed a high short-term stability of the laser system, regarding the repetition rate and pulse peak modulations.

The analysis of the relative intensity noise (RIN) supports these findings (cf. Fig. 7.3 (d)). The RIN measures fluctuations of the intensity depending on the respective frequency. Measurements can be taken up to the half of the repetition rate to be sure to exclude the (intended) pulsed operation of the laser from the noise measurement. In Figure 7.3 (d), the measurement of the RIN of the MO at the state of the average output power of 5.1 W is depicted. The noise was measured from 1 Hz to 100 kHz, because the most significant noise features will be displayed in this range, such as mechanical vibrations, thermal impacts or electrical disturbances. It can be seen that the noise curve has the most significant impact at low frequencies and decreases for higher frequencies. This behavior is common for mode-locked fiber lasers [119, 13, 81]. The noise in the regime from 1 Hz to 100 Hz is likely to be caused by slow mechanical and fast thermal impacts. The electric temperature control of the pump diodes for example acts in this regime, as can also be seen in the power variation, shown in Figure 7.3 (e). Especially the pump diode for arm 1 at the wavelength range of 976 nm has a critical temperature response resulting from the absorption cross-section in Yb (cf. Fig. 2.3). Important features in the technical noise include distinct peaks around 50 Hz and its harmonics. Those result from the alternating current in the electricity grid. The short-term noise of the MO sums up to 1%rms from 1 Hz to 100 kHz, which is relatively high. The high output power is at least partly responsible for the high noise, as a high output coupling ratio has a detrimental effect on the noise performance [13]. Another reason is influence of the thermal management of the pump diodes which can also be seen in the power measurement over 15 min, shown in Figure

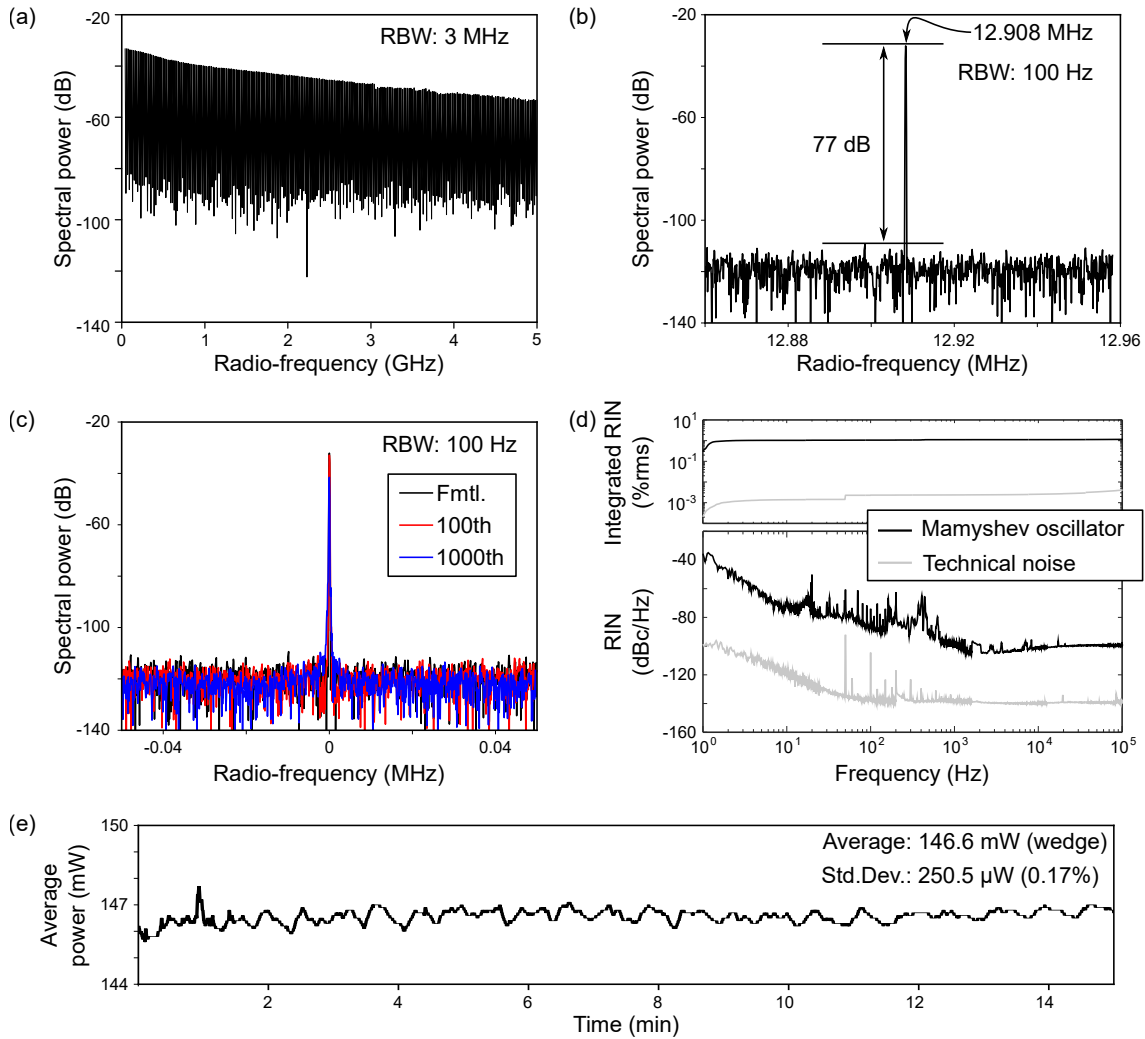


Figure 7.3.: Stability analyses of the oscillator at 5.1 W output power: Radio-frequency spectra (a) in the range from 1 MHz to 5 GHz, (b) the fundamental beat note of the repetition rate with a window of 100 kHz, (c) comparison of the fundamental peak (blue) to the 100th (orange) and the 1000th harmonic, (d) measurement of the relative intensity noise from 1 Hz to 100 kHz (bottom) and the integrated noise (top), and (e) power measurement over 15 min at a wedge behind the output. Fmtl.: fundamental, RBW: resolution bandwidth, RIN: relative intensity noise, Std.Dev.: standard deviation.

7.3 (e). The temperature control of the pump diodes varied over $\pm 0.5^\circ\text{C}$ with a period of $\approx 30\text{ s}$ due to a systematic error in the stabilization device. For the determination of the technical noise (Fig.7.3 (d), gray), the signal beam was blocked and the measurement repeated. The technical noise from 1 Hz to 100 kHz summed up to $4 \cdot 10^{-3}\%$ rms. The power measurement shown in Figure 7.3 (e) was taken at a wedge right behind the output of the MO. The reflection ratio was 2.9%. Taking this reflection ratio into account, the measured average power of 146.6 mW (Fig. 7.3 (e)) corresponded to 5.1 W with a standard deviation of 8.6 mW.

The pulses emitted by the MO were slightly chirped, resulting from the positive group velocity dispersion (GVD) of the fibers. The full-width half-maximum (FWHM) duration

7. Nonlinear Amplification with Feedback in Normal Dispersion Fibers

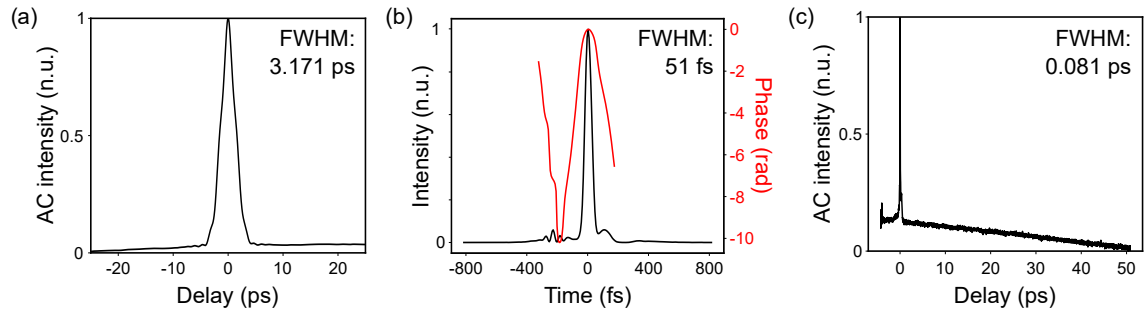


Figure 7.4.: Pulse duration measurements: (a) autocorrelation measurement of the uncompressed pulse, (b) frequency-resolved optical gating measurement of the compressed pulse and (c) longrange autocorrelation measurement of the compressed pulse in order to exclude double pulsing. FWHM: Full-width at half-maximum.

of the output pulse was roughly 3.2 ps in the autocorrelation (AC) measurement, as shown in Figure 7.4 (a). The AC trace shows an almost triangular pulse shape. This corresponds to a rectangular temporal pulse shape, which results from the optical spectrum, that is also relatively rectangular (Fig. 7.2), and the fiber dispersion. The pulses were compressed in a standard grating compressor with 1000 lines/mm and an overall power efficiency of 79%. The compressed pulses were analyzed with a frequency-resolved optical gating (FROG) device. The result is shown in Figure 7.4 (b). The compressed pulse duration was 51 fs with a flat spectral phase over the main peak of the pulse. Satellite pulses can be seen as well as steps in the temporal phase over the satellite pulses, which is a typical result of uncompensated third order dispersion (TOD). The Fourier-limited pulse duration calculated from the optical spectrum given in Figure 7.2 is 36 fs, despite the prominent spectral peak at 1028 nm. The difference of the measured and the Fourier-transformed pulse duration results from uncompensated TOD, which has a significant impact for pulse durations below 100 fs. The possibility to reduce the pulse duration to almost 50 fs demonstrates the advantages of the self-similar amplification, that was incorporated in the MO. The linearly chirped pulse (Fig. 7.4 (a)) can be well compressed (Fig. 7.4 (b)). In Figure 7.4 (c) a longrange AC measurement of the compressed pulse is shown. The FWHM duration corresponds to the measurement from the FROG. More importantly, the rather long AC trace (Fig. 7.4 (c)) does not show any additional pulses besides the main pulse. In combination with the unmodulated optical spectrum (Fig. 7.2) and the smooth decline in the longrange RF trace (Fig. 7.3 (a)), double pulsing at the pulse energy of 395 nJ can be excluded. The decreasing background was attributed to a misalignment of the beam into the AC device.

Assuming a Gaussian shape for the measured pulse (factor 0.94) and regarding the transmission of the grating compressor (79%), the peak power of the pulses can be estimated to be as high as 5.7 MW at 395 nJ output pulse energy.

High-Pulse Energy State By the repeated increase of pump power and adjustment of the spectral BPF separation as soon as double pulses can be seen on the oscilloscope, output pulses with a higher energy than in the previously discussed state can be generated by the MO. The output parameters for the state with the highest output power are depicted in Figure 7.5. In this state, the average output power was 8.1 W. With the repetition rate

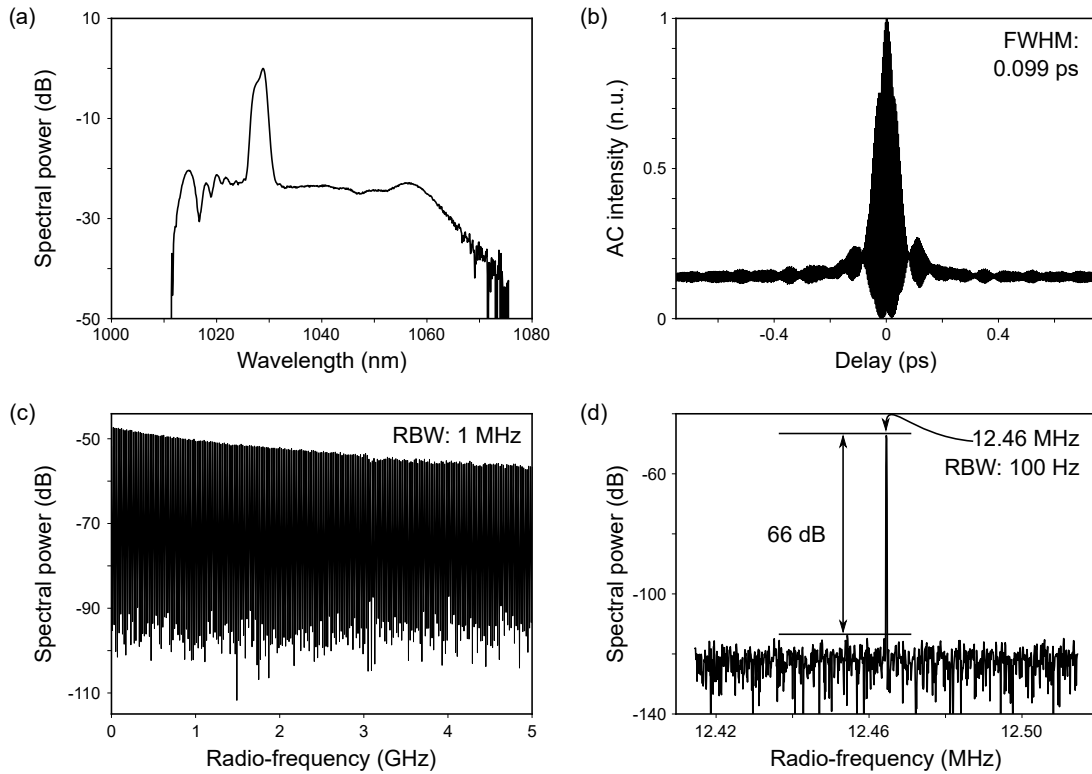


Figure 7.5.: Output parameters at a operation state with pulse energies of 650 nJ: (a) Optical output spectrum, (b) AC trace of the compressed pulse, (c) longrange radio-frequency trace, and (d) fundamental beat-note of the radio-frequency trace. FWHM: Full-width at half-maximum, RBW: Resolution bandwidth.

of 12.46 MHz, this corresponds to a pulse energy of 650 nJ. The repetition rate in this measurement is a little different compared to the previous state due to some splices that were improved and re-cleaved fiber end facets. The optical spectrum, shown in Figure 7.5 (a), was not as broadband as in the state above (Fig. 7.2). This is unexpected as a higher pulse energy should correspond to a higher impact of nonlinear effects. Furthermore, the spectral peak around the wavelength of 1030 nm in this case had a higher contrast compared to the case above (Fig. 7.2). This indicates a lower seed pulse energy in arm 2. The spectral separation of the BPFs was 21 nm, the BPF in front of arm 1 was at 1049 nm, the BPF in front of arm 2 at 1028 nm, which was almost the same as in the upper case.

The relatively narrow optical spectrum may result from a longer pulse duration in arm 2. A longer pulse corresponds to more shallow edges, leading to less spectral broadening from SPM. Another possibility is the presence of a rather intense cw-signal at a wavelength of around 1030 nm. The resolution of the optical spectrum shown in Figure 7.5 (a) was 0.5 nm. With this spectral resolution, the cw-signal cannot be verified. However, due to the signal-to-noise ratio in the RF traces that is in the same range as in literature [121, 78], and the interferometric AC trace with the peak-to-background ratio of 1:8, a cw-signal was assumed to be unlikely.

The Fourier-transformed pulse duration of the spectrum shown in Figure 7.5 (a) is 75 fs. This corresponds well to the AC trace shown in Figure 7.5 (b) with the AC duration of

7. Nonlinear Amplification with Feedback in Normal Dispersion Fibers

99 fs. Due to the relatively narrow spectrum, a shorter pulse duration would have not been expected. Assuming the actual pulse duration to be 80 fs, the pulse peak power is estimated to be 7.6 MW.

The long-range RF trace and the more detailed trace of the fundamental beat-note, shown in Figure 7.5 (c) and (d), respectively, indicate the operation at a stable single pulse state. In the long-range RF trace, no modulations can be seen in the range between 0 GHz and 5 GHz. The more detailed trace over the range of 100 kHz in Figure 7.5 (d) gives a signal-to-noise ratio of 66 dB and does not show any side maxima. The signal-to-noise ratio is lower than in the case described above, shown in Figure 7.3. This may result from the larger output coupling ratio, which has a detrimental effect on the noise performance [13]. Still, the value of 66 dB, along with the range of 100 kHz and a resolution of 100 Hz was expected as an indication for stable mode-locking at the high-power output [78]. Lower output powers often result in a higher signal-to-noise ratio.

Amplification in a Few-Mode Fiber The amplification in the second arm of the MO was carried out in a few-mode fiber (cf. Fig. 7.1). The mode-locked operation in the MO requires a single-mode beam: Due to modal dispersion that occurs when multiple modes co-propagate, multiple pulses emerge in the temporal domain. Multiple pulses have a reduced peak power on the one hand and several rising and descending flanks on the other, both weakening the SPM-induced spectral broadening and thereby destabilizing the oscillation.

The prevalent guidance of the fundamental mode in a few-mode fiber is initiated by the mode-field adapter in the SPC that coupled most of light from the single-mode fiber into the fundamental mode of the few-mode fiber. Furthermore, the few-mode fiber was coiled to a diameter of less than 10 cm in order to filter out higher-order modes. As it can be seen in the analysis of the output beam profile, shown in Figure 7.6, the coiled few-mode gain fiber behaves like a single-mode fiber. The data were recorded behind several deflectors, still the beam profile in Figure 7.6 (a) is quite round, indicating a high content of the fundamental mode. This is verified by an M^2 -measurement. The M^2 -measurement, shown in Figure 7.6 (b), is measured at the intensity threshold of $1/e^2$. Only the central part of the beam is therefore taken into account for the measurement. This is, however, acceptable,

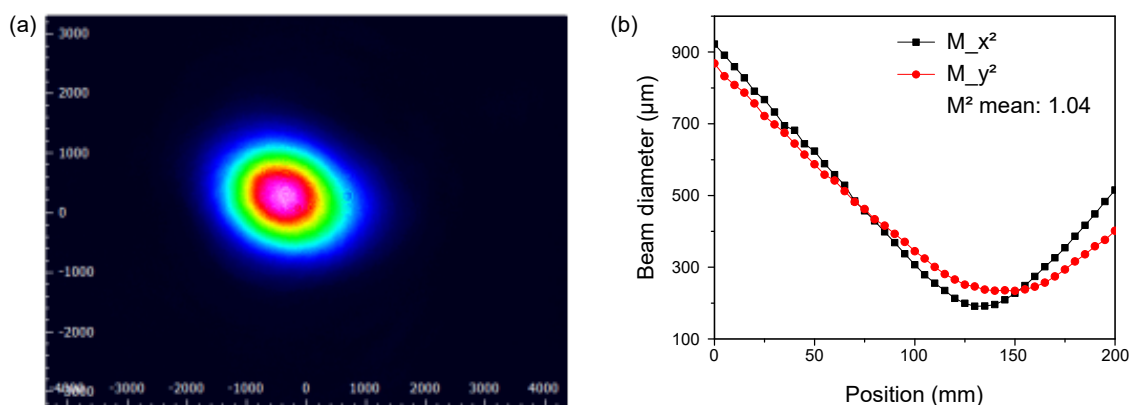


Figure 7.6.: Analysis of the output beam profile: (a) intensity distribution as false-color image, (b) M^2 -measurement to the intensity threshold of $1/e^2$.

because only the central part of the beam can be coupled into the single-mode input of arm 1. The determined value of $M^2 = 1.04$ is close to the theoretical limit of a Gaussian beam of $M^2 = 1$. As higher-order modes have a higher relative intensity at the edge of the beam, the mode-locking in the MO is not disturbed by higher-order modes as can be seen from the results shown above.

7.3. Conclusion and Prospects

The concept of the Mamyshev oscillator (MO) has drawn much attention recently. By the analysis of the nonlinear amplification in a fiber section that is designed as one arm of a MO (cf. Chapter 6), parameters for the improvement of the output pulse energy can be found. Those parameters include a few-mode gain fiber in arm 2, a narrow transmission spectrum of the band-pass filters and a focus on self-similar pulse amplification or gain-managed amplification. A high-power MO was developed, capable of a stable pulse reproduction with output energies of 395 nJ that could be compressed to 51 fs. The estimated peak power of the compressed pulses was 5.7 MW. In another operation state, the output pulse energy could be increased to 650 nJ, along with a slightly increased pulse duration of still < 100 fs. In this case, the peak power of the compressed pulse was estimated to be 7.6 MW. Despite the amplification in a large-mode area fiber, the output had a large content of the fundamental mode.

The output pulse energy of the MO presented here (650 nJ) fits well to the previously reported results of a MO with a 10 μm fiber core diameter in arm 2 (190 nJ) [121] and a MO containing a photonic crystal fiber with a single-mode diameter of 29 μm (1 μm) [78]. These results can be well compared due to the similar design of these MOs and the comparable repetition rate. The spectrum from Reference [78], furthermore, is quite similar to the spectrum shown in Figure 7.2, including the significant peak at the wavelength 1030 nm.

The MO has shown to be capable of generating outstanding pulse parameters in terms of pulse energy and spectral width. The further optimization to specific applications is nevertheless possible.

The *chirally-coupled core* (CCC) fiber is a recently emerged fiber design [76], promising further improvements. In this design, the higher-order modes are immediately coupled to side cores that are chirally wrapped around the central core. As a consequence, the core diameter can be greatly enlarged while maintaining the single-mode quality of the beam in the core. This fiber type is an alternative to PCFs with the advantage of easier manipulation in order to manufacture fiber components. Core-diameters of 35 μm or even 55 μm [84] could potentially allow the output pulse energy to exceed 1 μJ . Compared to the use of PCFs, by which similar output pulse energies can be achieved, the implementation of CCC fibers allows for a higher integrability. For the fabrication of fiber components, the CCC fiber can be handled as a standard fiber [48], as opposed to PCFs.

Pulses that are further amplified by chirped-pulse amplification (CPA), require durations of $\approx 50 - 100$ ps. Generation of such strongly chirped pulses can be achieved by the *giant-chirp oscillator* (GCO) concept [26]. A GCO has a rather long fiber cavity of several tens of meters in order to generate pulse trains with a repetition rate in the low MHz-regime and a strong chirp. These pulses can be further amplified without the need for a separate stretcher. The simultaneously reduced fundamental repetition rate is interesting for microscopic applications [40]. A GCO based on a MO should be feasible by increasing

7. Nonlinear Amplification with Feedback in Normal Dispersion Fibers

the cavity length [38]. The increased cavity length might be beneficial for the self starting capabilities of the MO, owing to the longer interaction length of pulse and material [134]. By the same process, a higher-order repetition rate-operation should be possible, taking into account that, in general, giant-chirp pulses require a longer pulse-to-pulse spacing than short pulses in order to avoid overlapping. The output pulse energy will not be as high as in the results of Section 7.2, but resulting from the pulse shaping process, broad spectra can be emitted, which is important as a precompensation of gain narrowing in the CPA.

Another interesting concept is the conjunction of all wavelength windows of the rare earth-doped fibers [38]. The most important lasing windows of rare earth-doped fibers are 1 μm (Ytterbium), 1.5 μm (Erbium), 1.9 μm (Thulium) and 2.05 μm (Holmium). A connection of these windows in a single MO, e. g. one arm based on an active fiber doped with Erbium, the other one based on Thulium-doped fibers seems possible and could generate very broad spectra. The coherently combined spectra could ultimately support single- or sub-cycle pulses directly from the oscillator. Another target could be the covering of wavelength regimes lying between two laser regimes, like the wavelength 1750 nm, which is interesting for the microscopic analysis of biological samples [50].

Thulium and Holmium exhibit a sufficiently broad spectral overlap regarding their gain cross-sections. Among the other rare earth-doped fibers, they are the most promising candidates to realize the broadband spectrum generation. First of all of course, the MO must be feasible in all of these wavelength ranges. Most MOs reported to date were based on Ytterbium-doped fibers, but well performing MOs have also been reported in the Erbium wavelength-range [98, 144]. The realization of Thulium and Holmium-based MOs is challenging because of the lacking availability of commercial normal dispersive gain fibers. The setup of a MO based on anomalous dispersive Thulium-doped fibers will be presented in the following Chapter 8.

8. Nonlinear Amplification with Feedback in Anomalous Dispersive Fibers

Ultrafast oscillators in the Thulium (Tm) wavelength range are often bound to the emission of solitons because of the anomalous dispersion in standard silica-based fibers in this range. The solitonic pulse energy is limited by the dependence on the balance of anomalous dispersion and nonlinear effects. Due to the high pulse energy it offers, the transfer of the Mamyshev oscillator (MO) concept to the 2 μm wavelength range is interesting. The main challenge for the transfer is the anomalous dispersion in standard silica-based gain fibers in this wavelength region, since this prevents the parabolic pulse evolution. This is the most important pulse shaping effect in MOs the 1 μm wavelength range.

In this chapter, first a brief overview about Tm-doped fiber ultrashort pulse oscillators is given (Sec. 8.1). Afterwards, the setup and the experimental results of the developed MO based on Tm-doped fibers is presented in Section 8.2, followed by a numerical validation of the results in Section 8.3. The chapter concludes with a summary and future prospects.

8.1. Ultrafast Oscillators Based on Thulium-Doped Fibers

Lasers in the short-wave mid-infrared can be used in applications different from Ytterbium (Yb)-lasers. Owing to the high absorption in water, cutting of biological tissue is more efficient [35]. Another example is the parametric conversion of light to the mid-infrared, without the need for a specific laser transition in this range [47]. The parametric process in this case can be pumped at the wavelength of 2 μm . The recent development of novel highly nonlinear non-oxide crystals with transparency windows reaching far into the mid-infrared (up to $> 10 \mu\text{m}$) has established nonlinear frequency down-conversion schemes based on parametric processes, which are able to exploit the mid- and far-infrared radiation and their numerous applications. Ultrashort 2 μm -laser sources are well suited to pump such schemes, because these crystals suffer from two-photon absorption when pumped at wavelengths below 1.9 μm [46].

On the one hand, the longer wavelength offers some advantages considering the various nonlinear effects in optical fibers. The nonlinear coefficient γ is reduced (cf. Eq. (2.11)), and the mode-field diameter of single-mode fibers can be increased (cf. Eq. (2.4)). This enables light propagation with higher pulse energies than in the Yb-wavelength range; chirped-pulse amplification systems based on Tm-doped fibers up to pulse energies of 13.2 μJ and 1 kW average power have been demonstrated [41].

On the other hand, ultrafast oscillators often operate in the soliton regime in the 2 μm wavelength range, owing to the anomalous dispersion of the active fibers. This usually limits the output pulse energy to the pJ-regime [65, 72, 125] as described by the soliton area theorem [2]. Nevertheless, oscillators with higher pulse energies based on other pulse evolution concepts have been built. Dispersion-managed solitons reaching output

pulse energies of 2 nJ [15] or even 10 nJ [146] have been reported. The pulse energy is then usually limited by multi-pulsing or the tolerance to nonlinear phase in the cavity [133].

In order to reach higher output energies from the oscillators, the concept of the MO is interesting, as already discussed in Chapter 7. Pulse energies in the range of 1 μ J were, however, not expected because of the lack of the parabolic pulse evolution, as mentioned above.

8.2. Experimental Results

The design of MOs in the 1 μ m wavelength range with Yb-doped fibers is quite prominent [110, 134], because of the normal dispersion of the standard glass fibers that supports the spectral broadening by self-phase modulation (SPM) (cf. Chapter 7). For longer wavelengths, e.g. in the well-established Erbium-regime at a wavelength of 1.5 μ m, the setup of MOs is more demanding, because of the anomalous dispersion in standard glass fibers. MOs based on Er-doped fibers have been reported by North *et al.* with pulse durations of less than 0.5 ps, in which the spectral width is generated in a highly nonlinear fiber [96]. Pulse durations in the fs-regime and high pulse energies of up to 31 nJ were generated by Olivier *et al.* by the use of normal dispersive Er-fibers [98]. In the wavelength range of Thulium-doped fibers (TDFs), MOs are even more difficult to realize, as normal dispersive gain fibers (for the parabolic pulse evolution) are not commercially available. The theoretical description of mode-locking in MOs with TDFs, which have anomalous dispersion, has recently been reported [141].

The MO based on TDFs is designed to operate with the same principle as the MO based on Yb-doped fibers, as introduced in Section 3.4: offset alternating band-pass filtering between sections of spectral regeneration. As spectral broadening by self-phase modulation (SPM) requires an up-chirp of the pulse, a dispersion management becomes necessary. The experimentally set up MO is schematically shown in Figure 8.1. The design is a ring cavity with passive normal dispersive fibers (NDFs) to overcompensate the anomalous dispersion of the active and passive fibers that are used for the fiber couplers.

Cavity Design The MO (cf. Fig. 8.1) consisted of two amplification stages based on TDFs (OFS, TmDF200), separated by two band-pass filters (BPFs). An inhouse-built 1550/1950 nm-wavelength division multiplexer (WDM) was used in the beginning of arm 1 to couple in signal light and merge it with the pump light. The WDM consisted of an anomalous dispersive single-mode (SM) fiber (Corning, SMF28e) with a length of 0.5 m. The dispersion values of all used fiber types are listed in Table 8.1. The rather large core-diameter of the SMF28e-fiber simplified the free-space coupling of the signal light into arm 1. The WDM was followed by a 2.8 m-long normal dispersive fiber (Nufern, UHNA4), referred to as NDF, which was necessary to ensure the positive chirp of the pulse and to receive a normal net cavity dispersion of 0.623 ps². The TDF in arm 1 had a length of 1.4 m with a group velocity dispersion of -0.0182 ps²/m. Behind the TDF, a 1 m section of NDF was inserted to support the spectral broadening by SPM. The signal light was coupled out through a 10 cm piece of SMF28e with a FC/APC-connector. The polarization could be adjusted by a fiber polarization controller (PC) and a quarter-wave plate (QWP). By squeezing and twisting, stress was induced in the fiber, which caused a specific amount of birefringence. Therefore, the PC acted as a fiber-integrated, combined half- and quarter-

Table 8.1.: Fiber parameters for the simulation of the Mamyshev oscillator. The group delay dispersion (GDD) is calculated by multiplying β_2 with the respective fiber length. The dispersion values are given for the central wavelength of 1960 nm. MFD: mode-field diameter, NA: numerical aperture, β_2 : group velocity dispersion, β_3 : third order dispersion.

Fiber type	SMF28e	TmDF200	UHNA4
MFD (μm)	13.1	6.2	5.7
Core NA	0.14	0.26	0.35
Total length (m)	1.30	2.65	8.00
β_2 ($\frac{\text{ps}^2}{\text{m}}$)	-0.0748	-0.0182	+0.0959
GDD in cavity (ps^2)	-0.097	-0.048	+0.768
β_3 ($\frac{\text{ps}^3}{\text{m}}$)	$+3.52 \cdot 10^{-5}$	$+1.09 \cdot 10^{-5}$	$+5.38 \cdot 10^{-5}$

wave plate. In order to enable a polarization manipulation of 2π , the additional QWP was used. A glass wedge was used as a monitoring port. The signal was band-pass filtered by a reflective diffraction grating with 600 lines/mm. The diffraction efficiency was optimized by the polarization controller. The filtered spectrum had a Gaussian shape with a full-width half-maximum (FWHM) bandwidth of 2 nm at a central wavelength of 1960 nm. The second arm was set up similar to the first, except for slightly different fiber lengths, as indicated in Figure 8.1. Unidirectional circulation through the two arms was ensured by a free-space isolator between arm 2 and arm 1. The pulses were coupled out right behind the isolator via a polarizing beam splitter cube (PBS). Thereby, the isolator also prevented the loss of mode-locking due to backreflections from outcoupled light. The coupling ratio could be adjusted by a half-wave plate (HWP). For coupling back into arm 1, spectral filtering was applied by using a second diffraction grating with a line spacing of 600 lines/mm. The BPF reset the pulse to a spectral FWHM of 2 nm with a Gaussian shape at a central wavelength of 1967 nm.

The pump light for the two MO arms was provided by a SM seed diode, operating at a wavelength of 1550 nm that was amplified in two separate fiber stages (for the two oscillator arms) in Yb:Er-co-doped double-cladding fibers. This allowed for a maximum available output power of 2 W in each arm. During operation, arm 1 was pumped with a power of 700 mW, arm 2 with a power of 830 mW. The core-pumping scheme was chosen in order to have a high overlap between pump light and doped fiber. Thereby the anomalous TDF could be kept as short as possible.

Normal dispersion in the NDF is achieved by a relatively small core. This causes a large portion of the light to be guided in the cladding, leading to a higher waveguide dispersion and a total normal dispersion. The numerical aperture (NA) depends on the difference of the refractive index, and is relatively high for the NDF (cf. Tab. 8.1). Fiber components in this setup are based on SMF28e, which has a larger core than the NDF. The larger core also simplifies the adjustment for the coupling into the arms. Splicing of the different fiber types is challenging and needs to be carried out very carefully. The splices with large differences of the mode-field diameters (MFDs) and NAs are prone to significant losses [145].

In order to initiate mode-locking in the MO, an injected pulse was necessary. The injection pulse from a stretched-pulse fiber laser, as presented in Ref. [143], had a spectral FWHM of 26 nm around a center wavelength of 1977 nm. The pulses had an energy of

130 pJ and a pulse duration of 190 fs. The unpicked pulse train from the injection laser (at the repetition rate of 62 MHz) would cause a strong depletion of the inversion in arm 1 and prevent the MO from starting. Therefore, a Pockels cell was used to reduce the repetition rate of the injection pulse train to 5 kHz. In order to start the MO, the injected pulse was coupled in via the 0th diffraction order of the grating of BPF1. The BPF2 had to transmit the injected pulse and was hence set to a center wavelength covered by the spectrum of the injection laser. During operation, BPF2 could be tuned to a proper wavelength in order to achieve the optimum performance.

The whole setup consisted of non-polarization maintaining (non-PM) fibers owing to availability and handling issues of the fibers and fiber components. In order to avoid splicing losses between different fiber types, fiber-based monitoring ports were not installed.

Experimental Results After initiating the mode-locked operation by injecting a pulse, the spectral separation of the BPFs in front of arm 1 and arm 2 as well as the pump power can be increased iteratively. After each iteration, the output can be optimized by adjusting the polarization in the oscillator. The injection pulse can be blocked, when a pulse oscillation is seen on the oscilloscope and a spectral broadening is seen in the spectrometer.

The output spectrum at a pulse energy of 6.4 nJ is shown in Figure 8.2. It ranged over a FWHM of 58 nm, from 1938 nm to 1996 nm, supporting Fourier-limited pulse durations of 137 fs. The spectral filter separation was 7 nm. The BPF2 in front of the second amplifier needed to have a sufficient overlap with the spectrum of the injection seed in order to initiate mode-locking. The BPF1 in front of the first arm was tuned to shorter wavelengths because of the gain cross-section in Tm-doped fibers, which is higher at shorter wavelengths (cf. Fig. 2.3). The output spectrum showed oscillations, which were expected for the spectral broadening of almost unchirped Gaussian pulses by SPM [2] with minor deviations.

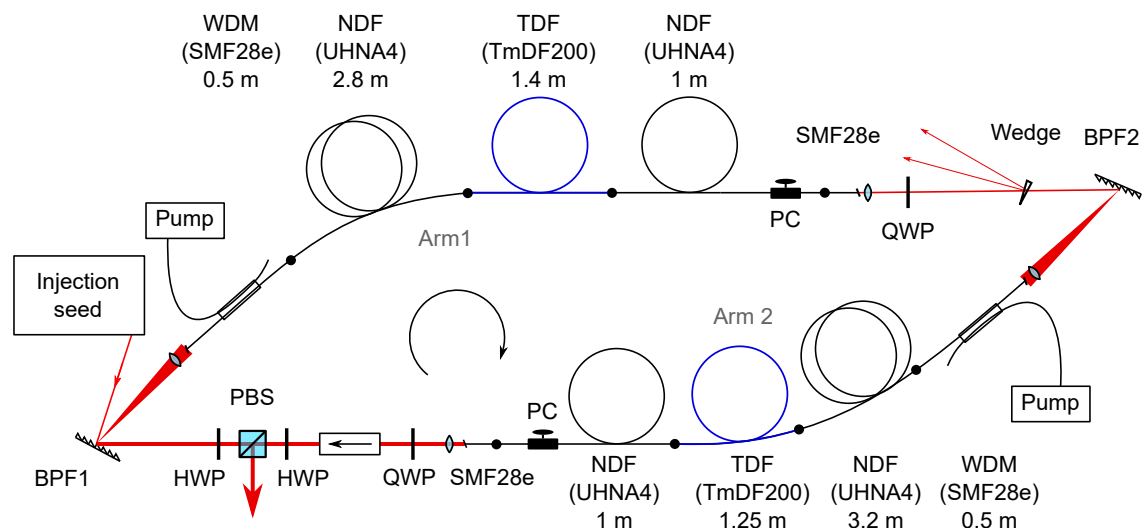


Figure 8.1.: Setup of the Mamyshev oscillator based on Tm-doped fibers. BPF: band-pass filter, HWP: half-wave plate, NDF: normal dispersive fiber, PBS: polarizing beam splitter cube, PC: polarization controller, QWP: quarter-wave plate, SMF28: anomalous dispersive single-mode fiber, TDF: Tm-doped fiber, WDM: wavelength-division multiplexer.

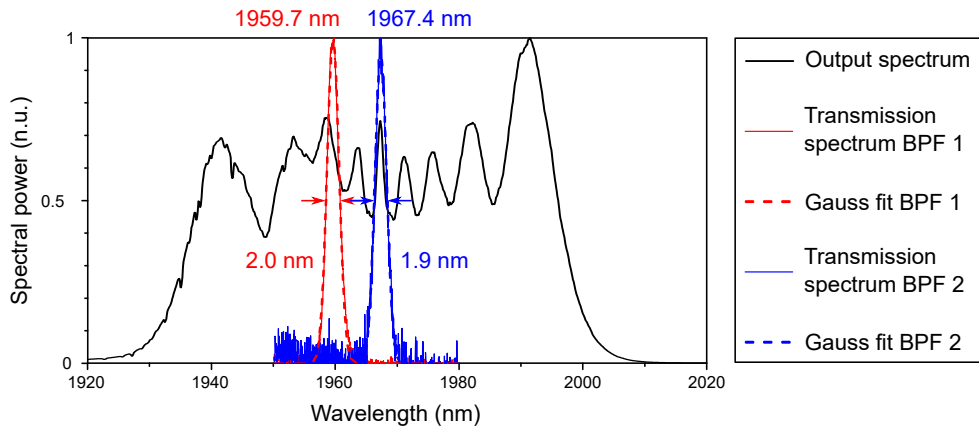


Figure 8.2.: Optical spectrum at the output of the Mamyshev oscillator (black), and the position and bandwidth of the band-pass filters 1 (red) and 2 (blue).

The optical spectrum was measured at the output of the MO. It was distorted by water absorption lines which become significant for wavelengths shorter than ≈ 1950 nm, as shown in Figure 8.3. The blue side of the spectrum is reduced in intensity, relative to the red side, due to water absorptions. Although the water absorption lines result in a significantly reshaped output spectrum, they appear to have no effect on the pulse circulation. In the fiber sections, the water absorption does not pose a problem. Similar absorption lines can result from OH^- -vibrations in the glass. However, these impurities are usually removed before the drawing of the fiber [142]. Therefore, spectral losses mainly occur in the free-space sections and can be seen in the output spectrum. The fed back part (into arm 1) is spectrally filtered at a wavelength on the red side of the water absorption lines and is, therefore, not affected at this filter separation setting.

Photons with energies corresponding to the wavelength range of 1950 nm excite different specific vibration states of the water molecules. This excitation requires the exact amount

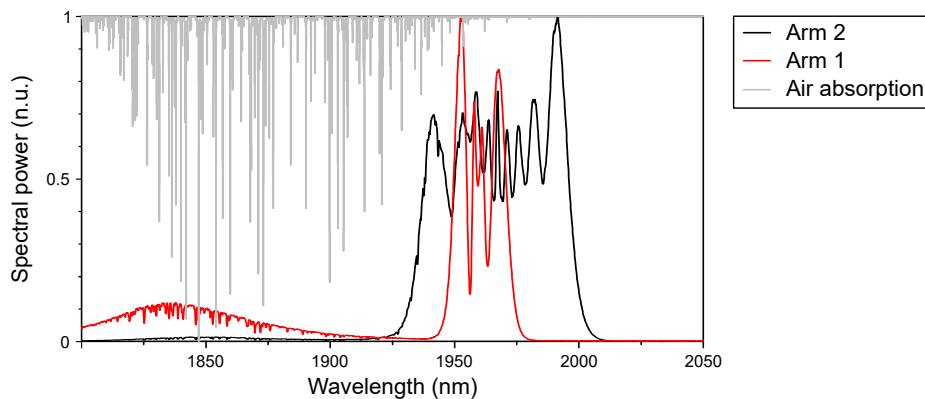


Figure 8.3.: Spectra from arm 1 (red) and arm 2 (black) with the overlaid air absorption (gray). The absorption in air results from the water vapor in air, air absorption is congruent with the water absorption lines. The broad maximum around 1850 nm is a result of amplified spontaneous emission in the gain fiber.

8. Nonlinear Amplification with Feedback in Anomalous Dispersive Fibers

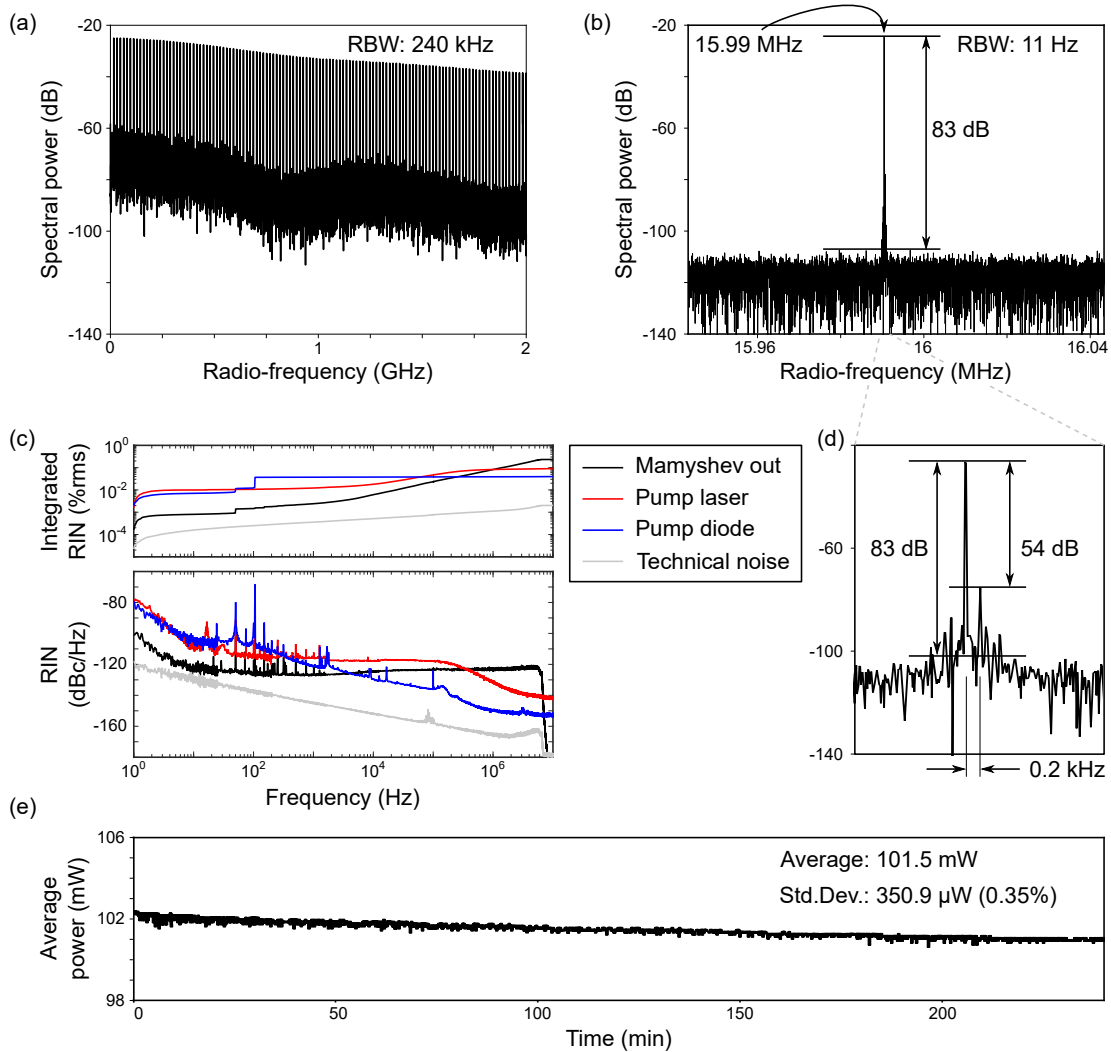


Figure 8.4.: Stability analysis of the Mamyshev oscillator at the output pulse energy of 6.4 nJ: Radio-frequency spectra (a) from 1 MHz to 2 GHz and (b) 100 kHz around the fundamental beat note at 15.99 MHz with a close-up in (d), (c) measurement of the relative intensity noise and integrated relative intensity noise, (e) power measurement over 4 hours. RBW: Resolution bandwidth, RIN: Relative intensity noise, Std.Dev.: Standard deviation.

of energy of the photon, which is consequently absorbed. The absorption lines are an important tool for spectroscopic analyses and are publicly available¹.

The stability analysis is shown in Figure 8.4. Figures 8.4 (a) and (b) show the radio-frequency (RF) traces at the output power of 6.4 nJ from 1 MHz to 2 GHz and for 100 kHz around the fundamental repetition rate, respectively. Up to 2 GHz (Fig. 8.4 (a)), the RF trace shows an expected course, i. e. smoothly declining maxima. Oscillations which would point to double-pulsing are not visible. The close-up of the fundamental repetition rate in Figure 8.4 (b) shows a very high signal-to-noise ratio of 83 dB. The repetition rate was 15.99 MHz. Some side peaks can be seen more clearly around the central peak in

¹"HITRAN on the web", <http://hitran.iao.ru/>, accessed: August 10, 2020.

Figure 8.4 (d). These are reduced by 54 dB compared to the signal. These side peaks correspond to an amplitude modulation of the pulse train [75].

The stability of the MO was further analyzed by the measurement of the relative intensity noise (RIN). The results are depicted in Figure 8.4 (c). The RIN-measurement method can be used to specify the short-term stability of the laser. The noise was recorded in a frequency-resolved manner for the frequency components between 1 Hz and 5 MHz. Larger radio-frequencies of the signal were blocked by electronic filters in order to suppress systematic errors from the signal. The range up to roughly 100 kHz is particularly interesting. In this range, the mechanical and electrical noise dominate. The MO was set up from non-PM fibers and is, therefore, susceptible to mechanical disturbances. But as the integrated RIN shows, the fluctuations in this regime add up to only 0.02% in this range, indicating low pulse-to-pulse fluctuations and good noise characteristics. Higher frequency noise resulting from the electronics and the high power cause a significant amount of noise up to 0.2%, as also seen in the RF trace from Figure 8.4 (b).

The long-term measurement of the output power was conducted with a thermal powermeter head (Fig. 8.4 (e)). The average output power over the 4 h of measurement was 101.5 mW with a standard deviation of 0.35 mW or 0.35%. This corresponds to a pulse energy of 6.4 nJ. The pulse energy in this experiment was limited by the generation of amplified spontaneous emission (ASE) in the gain fibers. ASE is the result of the low seed pulse energy that is fed back into the respective arms. Furthermore, generation of ASE at the blue side of the signal is caused by the higher gain cross-section in Tm-doped fibers. For self-lasing of ASE, a gain competition between self-lasing and mode-locked operation emerges, which reduces the stability of the output and the mode-locking.

The temporal pulse shape was analyzed with autocorrelation (AC) traces. The AC traces of the chirped and the compressed pulses are shown in Figure 8.5 (a) and (b), respectively. The uncompressed pulse, emitted from the MO, has a FWHM AC-duration of 5 ps. The AC trace is almost triangular, which can correspond to a rectangular pulse shape. The rectangular shape can be derived from the optical spectrum (cf. Fig. 8.2) and the dominating normal GVD.

The pulses were compressed by a standard diffraction grating compressor with grating line densities of 600 lines/mm and an incidence angle of 62° to an AC duration of 0.2 ps. The total transmission efficiency was 23%. The AC trace of the compressed pulse showed a

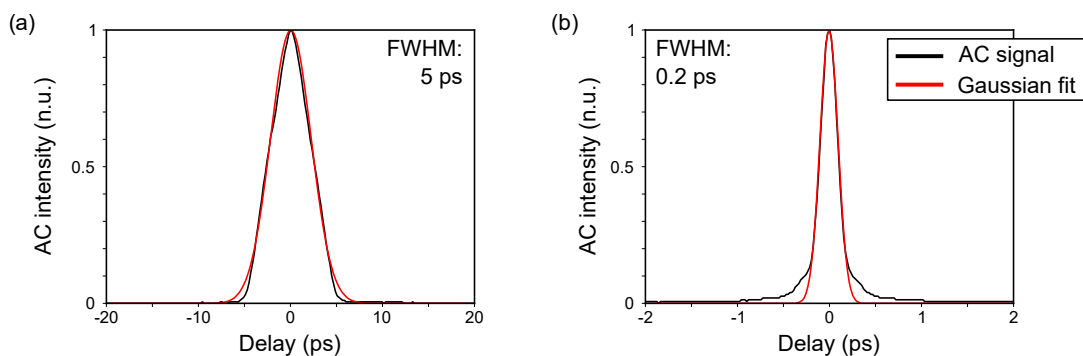


Figure 8.5.: Pulse duration measurement via the autocorrelation trace of (a) the dechirped pulse and (b) the pulse at the oscillator output. AC: Autocorrelation, FWHM: Full-width at half-maximum (the given value corresponds to the signal trace).

good overlap to the Gaussian fit. Deconvoluting the AC trace with the Gaussian correction factor of 1.41 leads to a pulse duration of 138 fs, which is very close to the Fourier-limit of 135 fs. The experimental AC trace shows a deviation from the Gaussian shape in the pulse flanks. These deviations are most likely a result from the rectangular spectral shape, which does not correspond precisely to a Gaussian pulse shape. The flanks can also be seen in the simulated AC trace, shown in Figure 8.7 (d). Assuming the Gaussian shape and the pulse energy of 6.4 nJ, the pulse peak power is 44 kW. The overall transmission efficiency of the pulse compression can be enhanced by optimized diffraction gratings, which will also increase the pulse peak power.

In order to validate the pulse evolution by SPM and simultaneously the alternating spectral filtering as mode-locking mechanism (instead of NPE), the oscillator was modeled in a simulation.

8.3. Numerical Analysis

In this section, first the experimental results are reproduced in order to analyze the pulse evolution in the MO. Afterwards, the theoretical scaling potential of the experimental setup is evaluated. In the experiments, the amplification was limited by self-lasing of the ASE in the gain fibers. This is not displayed in the simulations, it is, therefore, easy to surpass this limitation in order to find the energy at which a nonlinear limitation like optical wave breaking occurs. In a third simulation in the end of this section, the combination of Thulium- and Holmium-doped fibers in a MO is investigated.

Numerical Reproduction The numerical analysis was done by using the commercially available software Fiberdesk². This software is based on solving the extended nonlinear Schrödinger equation by using the split-step Fourier method, taking into account SPM, self-steepening, Raman response, fiber mode-field diameter (MFD) and dispersion up to the third order. A flat saturated gain model was used for the simulation of the gain cross-section of the TDF. The (calculated) fiber parameters for the simulation are collected in Table 8.1. More detailed information on the numerical model are given in Appendix D.

The simulation was started with a single pulse with the parameters from the injection laser that was also used in the experiment. The pulse converged to the output pulses in less than 5 roundtrips. In Figure 8.6, the pulse propagation of the 25th roundtrip is depicted, regarding the evolution of spectral width (a), pulse duration (b), and pulse energy (c).

The spectral width, as shown in Figure 8.6 (a), evolved as expected. In the first NDF-sections of both arms, no change of the spectral width can be noted due to the low pulse energy. As a result of the dispersion pre-compensation in these fiber sections with increasing pulse energy, the spectral width was, however, increased by SPM in the succeeding gain fibers and NDF-sections. The pulse duration evolution is shown in Figure 8.6 (b). It can be seen that the pulse duration in the TDF decreased to the level of the input of the respective arm. The normal dispersion of the first NDF sections was completely compensated by the anomalous dispersion in the TDF. In the second NDF-sections of

²"Fiberdesk", www.fiberdesk.com/, accessed: August 31, 2020

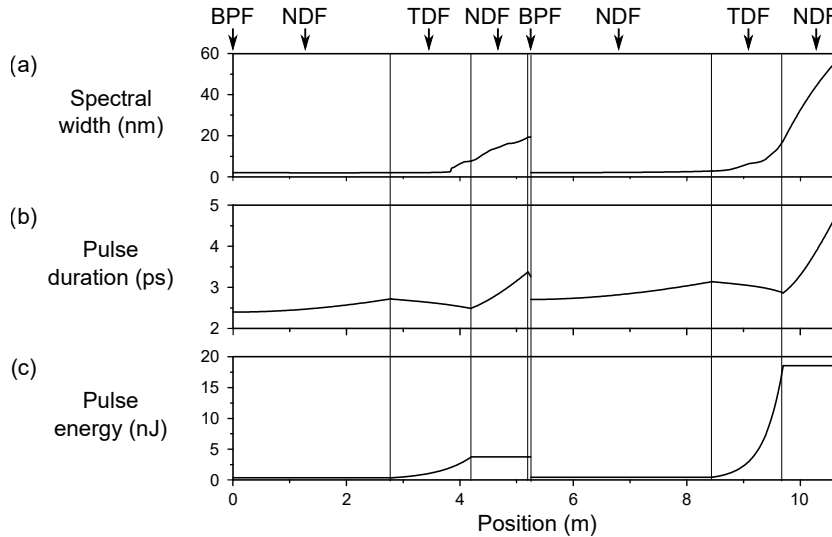


Figure 8.6.: Pulse evolution along the fiber line of the Mamyshev oscillator: (a) Spectral width, (b) pulse duration and (c) pulse energy.

each arm, the pulse duration increased as expected. The pulse energy (Fig. 8.6 (c)) only changed in the gain fibers and at the BPFs.

The pulse evolution in the TDF MO can be compared to the pulse evolution in Yb-doped fiber MOs, as for example presented by Liu *et al.* [80]. The most prominent difference was the reduction in the pulse duration in the anomalous active fiber (Fig. 8.6 (b)). This pulse duration reduction prevents the exploitation of parabolic pulse evolution in the TDF MO. As the anomalous dispersion of the TDF could be sufficiently overcompensated by NDF, spectral broadening remained however possible. The reduction of the pulse duration in the active fiber can also be an advantage as the increased peak power supports the influence of nonlinear effects.

The intra-cavity pulse energy at the end of arm 2 was 18.5 nJ in the simulation. The pulse energy that was coupled out in the experiments was 6.4 nJ. Assuming the same intra-cavity pulse energy in simulation and experiment, the experimental output coupling ratio would be roughly one third. At this point the B-integral was 10.7π , which is a common nonlinear limit for a dissipative soliton laser [80]. Instabilities might occur at this point due to the absence of self-similar propagation. As a comparison, in MOs based on Yb-doped fibers (based on self-similar spectral broadening), the B-integral can reach more than 60π [80].

The simulated pulse parameters at the end of the arms can be directly compared to the experimental results, as shown in Figure 8.7. In Figure 8.7 (a) and (c), the experimental and simulated spectra from arm 1 and arm 2 are shown, respectively. The spectral width and shape from both arms can be reproduced by the simulation model. The asymmetry between the peaks at the edges of the spectra that can be well-seen in the output of arm 1, resulted from the self-steepening effect and TOD. The output of arm 2 showed the same asymmetry, as reported in Ref. [112]. Here, the dominating mismatch of simulation and experiment in arm 2 resulted from the water absorption that was not considered in the simulation.

In Figure 8.7 (b) and (d), the AC trace of the pulse from arm 2 is shown in uncompressed and compressed state, respectively. In the uncompressed state, the AC shows the triangular

8. Nonlinear Amplification with Feedback in Anomalous Dispersive Fibers

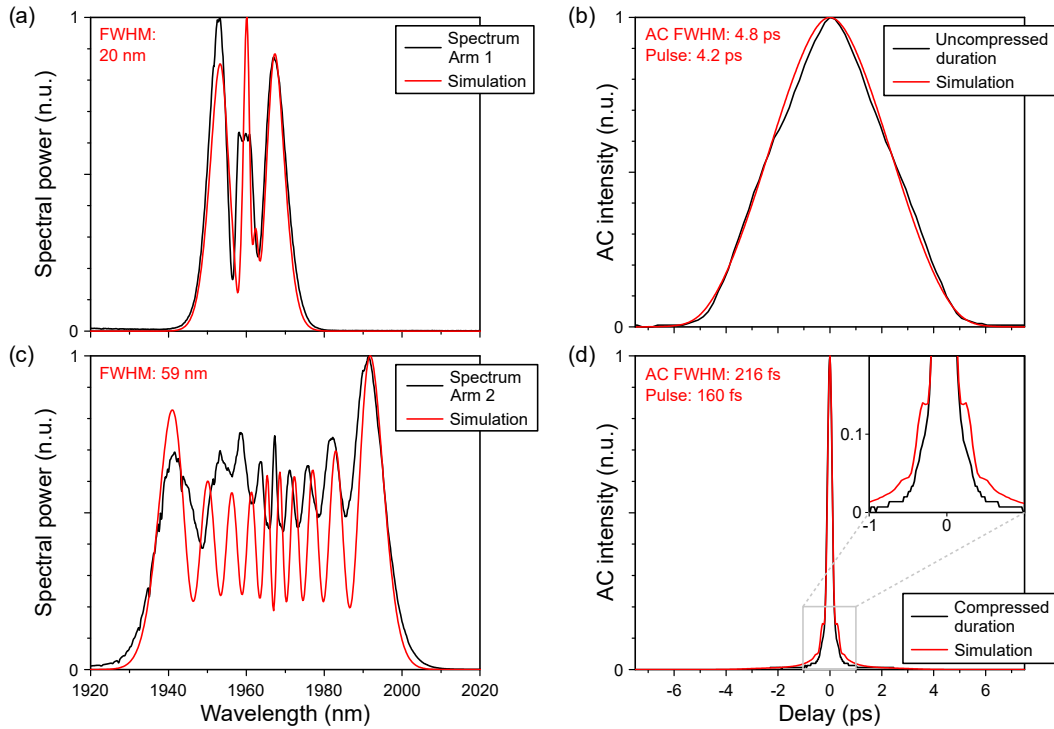


Figure 8.7.: Numerical reproduction (red) of the experimental data (black): (a), (c) Optical spectra at the output of arm 1 and arm 2, respectively, (b) autocorrelation traces of the uncompressed pulses at the laser output and (d) autocorrelation traces of the compressed pulses. The inset with the spectral full-width half-maximum (FWHM) in (a) and (c), as well as the temporal autocorrelation FWHM in (b) and (d) relates to the simulated data. The indicated pulse duration in (b) and (d) refers to the duration of the deconvoluted pulse.

shape that was also noted in the preceding Section 8.2. This can be derived from the rectangular pulse shape that is adopted from the spectrum (Fig. 8.7 (b)) influenced by GVD. The pulse was then compressed with the dispersion values corresponding to a grating compressor with gratings with 600 lines/mm and an incidence angle of 62° . Again, the correlation of simulation and experiment is very high, leading to the estimation that also the experimental pulse duration after compression is distinctly below 200 fs (cf. Fig. 8.7 (d)).

Scaling Potential As mentioned above, the experimental pulse energy was limited to 6.4 nJ owing to self-lasing of the ASE. The impact of ASE can be omitted in the simulations. Therefore, a numerical investigation of the scaling potential of this specific design is discussed in the following, in order to investigate the pulse energy that is limited by optical wave breaking.

The fiber lengths and the spectral separation of the BPFs are the same as above. Only the gain in both arms was strongly increased. The highest possible intra-cavity pulse energy was 164.5 nJ. Assuming the output-coupling ratio of one third as discussed in the preceding paragraph, the output pulse energy in this case would be almost 55 nJ. For that operation state, the output parameters are shown in Figure 8.8. At the output of arm 2 (Fig. 8.8 (a)), the spectral FWHM was increased to 231 nm. At the same time, the spectrum still

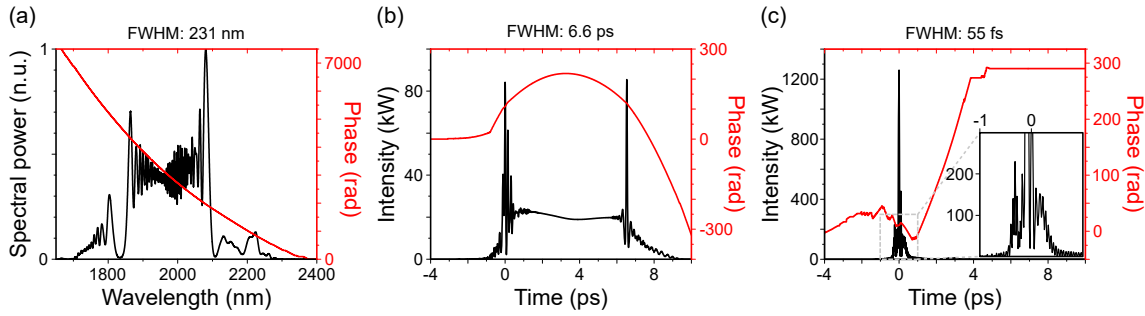


Figure 8.8.: Output parameters at the circulation of very high pulse energies: (a) Optical spectrum (black) and spectral phase (red) at the output of arm 2, (b) uncompressed pulse envelope (black) and temporal phase (red) at the output of arm 2, (c) pulse shape (black) and temporal phase (red) after compression in a grating compressor with the parameters from the experiments.

shows the typical oscillations of a spectrally broadened unchirped Gaussian pulse. In the temporal domain, the pulses had a duration of 6.6 ps, which is only slightly longer than the duration from the experiments. Due to the spectral width, that is much larger than in the experiments, a longer duration could have been expected. In the simulation, the impact of the broad spectrum is not as significant due to the relatively short fiber lengths. The uncompressed temporal pulse shape features two distinct peaks that evolve only in the last 15 cm of propagation in the anomalous dispersive fiber. Although the pulse can be recompressed to a FWHM duration of 55 fs in the above mentioned grating compressor, as depicted in Figure 8.8 (c), it can be seen that a pedestal consisting of multiple pulses emerges (Fig. 8.8 (c) inset). The pulse breaking occurs not until the last piece of anomalous dispersive fiber, and could be prevented by omitting the last piece of anomalous dispersive fiber.

Broadband Spectra In order to further increase the spectral width and subsequently reduce the possible pulse duration, amplification can be carried out in different laser gain media in the different MO arms. Here, the case of amplification in Tm-doped fibers, around 1980 nm, and Holmium (Ho)-doped fibers, around 2050 nm, is investigated in further simulations. The spectral broadening in each arm must be strong enough to cover severely increased the spectral gap between the two filters. The coherent combination of the output of the two arms is expected to generate an extremely broad spectrum.

The results for the filtering of BPF 1 at 1980 nm and of BPF 2 at 2050 nm are shown in Figure 8.9. Considering a flat gain in both arms, a stable circulation of pulses is possible with this setup. The BPF-bandwidth was kept at 2 nm with a Gaussian spectrum, the intracavity pulse energy at the end of arm 2 was 121 nJ. The spectral broadening in both arms exceeds the filter separation, as shown in Figure 8.9 (a) and (b). Consequently, a stronger gain also required in arm 1. The phase is relatively flat at the positions of the BPFs, which is a necessary requirement for the mode-locking mechanism. The spectral width of the output of the individual arms is in the range of 200 nm, i. e. similar to the spectral width of the state of highest pulse energy. The linear superposition of the (partly overlapping) spectra, shown in Figure 8.9 (c), sums up to 289 nm, leading to a Fourier-transformed pulse duration of 33 fs (Fig. 8.9 (d)). The steps that can be seen in the merged spectrum

8. Nonlinear Amplification with Feedback in Anomalous Dispersive Fibers

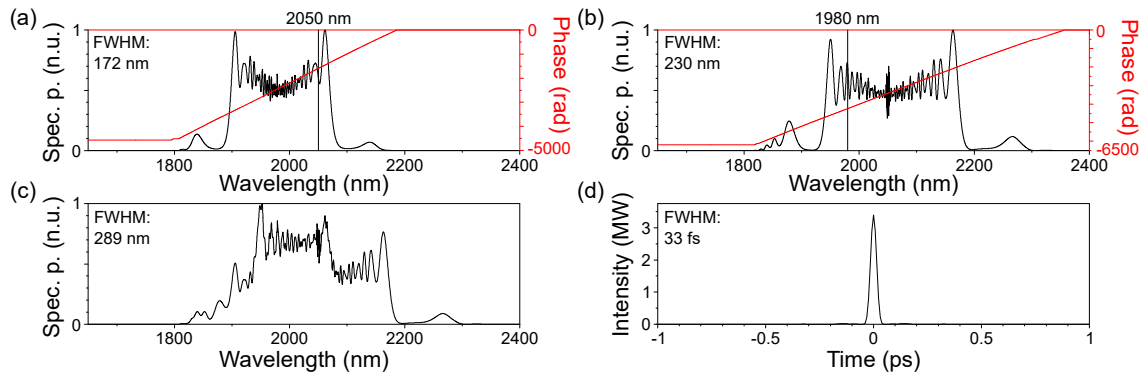


Figure 8.9.: Output parameters for the pulse amplification in a Thulium/Holmium mixed Mamyshev oscillator: (a) Spectrum at the output of arm 1, amplification in a Thulium-doped fiber, succeeding band-pass filter at 2050 nm, (b) spectrum at the output of arm 2, amplification in a Holmium-doped fiber, succeeding band-pass filter at 1980 nm, (c) linear superposition of the two output spectra, (d) Fourier-transformed pulse duration from the spectrum in (c). Spec. p.: Spectral power.

is a result of the asymmetric amplification in the two arms; the output of arm 2 has a higher energy. Mixing the gain of Tm-doped fibers and Ho-doped fibers and coherently combining the output pulses of the two arms enables peak powers of 3.6 MW (Fig. 8.9 (d)). Further broadening towards other gain media, as for example the blue side of Tm around 1750 nm and Er around 1550 nm in additional arms enables the coherent assembly of extremely broad spectra.

8.4. Conclusion and Prospects

Summary In this chapter, the transfer of a Mamyshev oscillator to anomalous dispersive gain fibers was presented experimentally and theoretically. Despite the fact that a parabolic pulse evolution was not possible, pulses with optical spectra of 58 nm and compressed durations below 200 fs could be achieved. In combination with the pulse energy of 6.4 nJ, this oscillator showed excellent pulse parameters. Pulse-to-pulse fluctuations of 0.2% and a long-term stability of 0.35% were measured. The output energy was limited by self-lasing of the excessive amplified spontaneous emission in the gain fibers. A numerical analysis with a good overlap to the experimental results validated the mode-locking mechanism depending on the alternating spectral filtering, despite the use of non-polarization maintaining fibers which could also support nonlinear polarization evolution.

Although ultrafast lasers with higher output pulse energies than the laser system presented here exist in the Thulium-wavelength range, they usually go along with an increased pulse duration. Chernysheva *et al.* reported a pulse energy of 2 nJ, as mentioned in Section 8.1. The spectral width in this case was 24 nm and the pulse duration 300 fs [15]. Engelbrecht *et al.* presented a pulse energy of 4.3 nJ and a pulse duration of 294 fs [25], and Yang *et al.* reported a pulse energy of 10 nJ corresponding to a spectral bandwidth of 8 nm and a pulse duration of 550 fs [146].

In contrast to that, the pulses from the Mamyshev oscillator tend to decrease in duration while increasing in pulse energy, as can be seen from the comparison with the results from

Reference [112]. Pulse energies with more than 6 nJ pulse energy and durations of less than 200 fs have not been found elsewhere, and the output pulse energy of Thulium-doped Mamyshev oscillators is expected to rise with further research efforts.

Prospects The limitation due to the excessive amplified spontaneous emission could be reduced by increasing the seed signal power. The circulating pulse energy is reduced at each splice and very severely at the BPFs. Optimizing the splices and increasing the filter bandwidth promises further power scaling. Furthermore, optimizing the amplification of the pulse in the two arms, e. g. by a backward pumping scheme, could mitigate the amplified spontaneous emission. A backward pumping scheme would provide less gain at points of low signal pulse energy and high gain at the point where the pulse is already amplified. Due to the more efficient amplification, less spontaneous emission occurs. A third possibility would be to shift the maximum gain in the Thulium-doped fiber to ≈ 1960 nm. This can be obtained by pumping with another Thulium-doped fiber laser at a wavelength of ≈ 1830 nm. The ultimate limitation of the pulse energy scaling is expected to be optical wave breaking. It was determined to occur at an output pulse energy of 55 nJ in this setup.

A noticeable increase in stability and a strong simplification of the adjustment is expected for the setup with polarization-maintaining fibers on the one hand. On the other hand, a non-polarization-maintaining setup allows for the simultaneous mode-locking by nonlinear polarization evolution in the case of overlapping band-pass filters. The pulses generated by this method could be used for a self-injection without the need of an additional self-injection arm.

Besides the mere power scaling, the increase of the spectral width to overlap with the gain cross-sections of other laser gain media poses the possibility of the generation of extremely broad coherently combined spectra and subsequently the generation of few-, single-, or even sub-cycle pulses. A numerical study with a flat gain has been shown for the combination of Thulium and Holmium as gain media. Further gain media could be included by additional arms, as mentioned in Section 7.3.

9. Summary and Prospects

Summary This thesis addressed several aspects of the amplification of ultrashort laser pulses in optical fibers. Managing the nonlinear effects is the paramount issue to be considered in a fiber-based pulse amplifier. Two fundamentally different approaches were presented with the target of achieving μJ -level pulse energies along with pulse durations below 150 fs for a further use in material processing. The two concepts were chirped-pulse amplification and self-similar pulse amplification.

Chirped-pulse amplification aims for the suppression of nonlinear effects as strong as possible. By chirping of the pulses prior to the amplification, the pulse peak intensity was reduced and simultaneously the impact of nonlinear effects. After amplification, the pulses were dechirped to achieve short pulse durations with high peak intensities. Additionally, the pulse intensity could be further reduced by a larger mode-field diameter in a photonic crystal fiber. This enables a linear amplification, and pulse energies of 450 nJ at a repetition rate of 66.7 MHz and pulse durations of 293 fs could be achieved after compression. The output pulse energy was limited by the pump power and not sufficient for the intended application of material processing. Although higher pulse energies have been shown from a fiber-based chirped-pulse amplifier and could have been implemented for instance by a reduction of the repetition rate, also the pulse duration was too long for the intended application. The pulse duration was limited by the available optical spectrum of the seed pulse, which could not be corrected for in a chirped-pulse amplifier, but only in a nonlinear post-compression stage in which the spectrum would be nonlinearly broadened. As this is a quite complicated extension of the chirped-pulse amplification system, another approach was chosen instead; the self-similar pulse amplification.

In a self-similar pulse amplifier, nonlinearities are expedited which enable a manipulation of the spectral bandwidth of the pulses, while maintaining a linear chirp. The pulse evolution concepts of self-similarity and gain-managed amplification were employed and investigated. Specifically the use of spectral filtering, parabolic pre-shaping, a long gain fiber with a low doping concentration and a core-diameter of 20 μm were implemented. With this design, pulse energies of 1 μJ and pulse durations of 50 fs at a repetition rate of 11 MHz were achieved. The nonlinear amplification was limited by transverse mode instabilities.

The applicability of the respective amplification concept depends on the seed pulses. While self-similar amplifiers strongly improve pulse parameters like spectral bandwidth and spectral phase of a narrowband input pulse, the amplification is limited to roughly 1 – 2 μJ pulse energy with recompressed pulse durations of less than 100 fs, due to Raman scattering [37]. The linear amplification of chirped pulses on the other side cannot improve pulse parameters, but is more likely to deteriorate the output due to gain narrowing and residual higher order dispersion. Still, the use of high quality, broadband seed pulses allows for the amplification to pulse energies in the mJ-regime with compressed pulse durations in the range of 100s of fs [24]. These seed pulses should incorporate broadband

9. Summary and Prospects

spectra (to precompensate gain narrowing) and relatively high pulse energies (to reduce the amount of necessary amplifier stages).

This kind of high-energy, broadband pulses could be generated by two concatenated nonlinear amplifiers between offset spectral filters, forming a Mamyshev oscillator. In this oscillator design, a small portion of the output of the one amplifier is fed back into the other amplifier, in which it is spectrally regenerated and amplified. The output parameters of this pulse generator are exceptional for a fiber-based oscillator; pulse energies of 650 nJ were achieved with compressed pulse durations of less than 100 fs at a repetition rate of 12.5 MHz at a wavelength around 1 μm . This is to the best of my knowledge the highest output pulse energy from a mode-locked oscillator based on standard fibers. Despite the use of a few-mode amplification fiber in the second amplifier, a very high beam quality along with a high stability could be achieved.

By the use of the Mamyshev oscillator mode-locking concept, ultrashort pulses can be generated that are comparable in performance and even surpass pulses emitted by solid-state lasers. Simultaneously, the advantages of fiber-based systems are preserved, such as the long interaction length of signal, pump and gain medium, low costs, and an environmental robustness due to the use of polarization maintaining fibers.

The concept of this Mamyshev oscillator was transferred to the 2 μm -wavelength regime. A circulation of mode-locked pulses by the use of anomalous dispersive, Thulium-doped gain fibers was established. The concept of the Mamyshev oscillator promises high output pulse energies also in the wavelength range of Thulium-doped fibers. Indeed, the 6.4 nJ pulses in the < 200 fs-regime were the highest pulse energies achieved in this wavelength range.

The nonlinearities, resulting from the high pulse peak intensity, and the dispersion, resulting from the broadband optical spectrum, cause changes in the pulse shape. In order to analyze the final pulse shape, the pulses must be characterized. In this thesis, the concept of dispersion scans (d-scans) was applied to a fiber-based chirped-pulse amplification system, in which the pulses were compressed in a grism compressor. This analysis method proved to be an adequate tool for the pulse characterization. The difficulty to retrieve the unknown exact dispersion of the grism compressor and the pulse shape simultaneously was met by choosing a corresponding retrieval algorithm, the self-calibrating d-scan retrieval [4]. The advantage of the d-scan concept lies within the simultaneous use of the grism as compressor and option for scanning the dispersion. Information on the residual dispersion can furthermore be retrieved from the raw traces, which is advantageous for the optimization of the grism compressor. The disadvantage results from the retrieval algorithm which is still on research-level, and the necessity to use the specific (grism) compressor for the experiments, instead of e. g. a grating compressor that is matched to the amplifier. In a commercial master-oscillator power-amplifier system, the d-scans will be valuable for an online monitoring of the output parameters.

An important part of this thesis was the management of nonlinear effects. As a result, a significant improvement of pulse quality and output pulse parameters could be achieved. It is also important that the pulse performance improvement can only be achieved as long as the nonlinear effects *can* be controlled. For that, innovative solutions are always demanded. Such a solution is the concept of the Mamyshev oscillator, which applies a saturable absorption mechanism with excellent performance, strongly simplifying the management of nonlinearities. Pulses with very high output powers can thus be demon-

strated, that surpass the output parameters of state-of-the-art, Kerr-lens mode-locked Titanium:Sapphire lasers.

Prospects Mamyshev oscillators will continue to be in the focus of research efforts. Improvements could concentrate on multiple aspects, such as the further increase of the output pulse energy, of the spectral bandwidth on the tunability of the repetition rate or the self-starting.

In general, the amplification of ultrashort pulses in optical fibers is always limited by a nonlinear effect. In order to increase the limiting threshold, the pulse propagation in the waveguides can be improved and new possibilities for the handling of the nonlinear effects are required. Examples for innovative waveguides rely on two-dimensional photonic crystals, posing many degrees of freedom to manipulate the pulse propagation. Mode-field diameters of more than 100 μm have been demonstrated in large-pitch fibers [24] for instance, enabling the guidance of higher pulse energies. Nonlinear effects can be handled by a division of the beam in multiple cores in order to further reduce the local intensity and a subsequent recombination [36]. As the Mamyshev oscillator can be viewed as two concatenated nonlinear amplifiers, all those considerations on the increase of the nonlinear threshold can be implemented into the oscillator in order to increase the output pulse energy.

Innovative waveguides can also be used to enhance the Kerr-nonlinearity in order to increase the spectral width. Furthermore, the synthesis of extremely broadband optical spectra and ultimately the reduction of the pulse duration to sub-cycle, directly from a (single) fiber oscillator seems to be very attractive. This could be achieved by the implementation of different gain materials into different arms of the Mamyshev oscillator. Multiple arms can be added in order to bridge the wavelength gaps from Erbium to Thulium and Holmium. Even the bridging from Erbium to Ytterbium should be possible. By the implementation of additional arms into one laser, all the outputs have the same repetition rate which enables the coherent combination of the several output pulses.

The tunability of the repetition rate is an advantage of the Mamyshev oscillator principle. By managing the pump power and the spectral separation of the band-pass filters, the fundamental repetition rate or higher harmonics can be realized. This can be pushed towards extrema: High harmonics in the Gigahertz regime are useful for material processing [56], while the fundamental repetition rate (in combination with a long cavity) in the Megahertz regime is an excellent pulse source for microscopy applications [40].

One important aspect limiting the elegance of the Mamyshev concept is the difficulty of self-starting. Although the mode-locking mechanism by the Faraday instability has already been theoretically investigated and experimentally demonstrated, so far, the Mamyshev oscillators incorporating self-starting by the Faraday instability did not reach the power levels that could be achieved by injection-started oscillators. Having a reliable self-starting mechanism would strongly increase the attractiveness of this oscillator concept.

The work of this thesis is only a small part in the effort for further control of nonlinear effects in glass fibers. "Fiber lasers are beginning to emerge as practical alternatives to bulk solid state lasers with competing performance" [52]. The performance of laboratory Mamyshev oscillators already surpass the performance of commercial solid state lasers in several aspects and future scaling is very probable. The increasing understanding and

9. *Summary and Prospects*

handling opportunities of nonlinear effects in fiber-based systems are attractive for various applications and research on nonlinear dynamics.

Appendix

A. Mode-locking by Nonlinear Polarization Evolution

The generation of ultrashort pulses is supported by a broad gain bandwidth. Yb- and Tm-doped fibers are, therefore, popular active media for ultrashort pulse fiber lasers.

The generation of mode-locked pulses requires a nonlinear element in the laser oscillator. This nonlinear element increases the losses for the cw-operation and decreases the losses for high optical intensities. This is usually achieved by the use of saturable absorbers. Real saturable absorbers absorb light until a threshold is surpassed and then quickly turn transparent. This effect can also be mimicked by nonlinear effects: Nonlinear effects resulting from the high optical intensities alter several parameters of the signal, such as polarization, phase or spectrum. The intensity dependent loss can then be achieved by tuning stationary elements in the laser oscillator to a position, where they are optimized for the nonlinearly altered parameters. These optical elements can be referred to as artificial saturable absorbers. Artificial saturable absorbers use nonlinear effects to introduce high losses to low optical powers and low losses to high powers.

The pulse generation process can be viewed from the process of the pulse shaping and from the process of the locking of the modes. Those two processes act jointly, but differ in the explanation. Here, the generation of ultrashort pulses in glass fibers will be introduced for the example of nonlinear polarization evolution (NPE) which is a well-established technique for saturable absorption.

Pulse Shaping The key feature in NPE is the polarization rotation of the pulse part with high intensity. Polarization sensitive elements act as discriminators to separate the low power background from the high power pulse peaks. The high power pulses can then be further amplified while low intensities are suppressed in the oscillator [128].

Nonlinear contributions to the change of the refractive index depend on the energy in the different polarization axes and can be described as [2]

$$\begin{aligned}\Delta n_x &= n_2 \left(|E_x|^2 + \frac{2}{3} |E_y|^2 \right) \\ \Delta n_y &= n_2 \left(|E_y|^2 + \frac{2}{3} |E_x|^2 \right)\end{aligned}$$

with the nonlinear refractive index n_2 . The first terms in the above equations cause SPM, the second terms result in XPM, because the nonlinear phase shift of the one axis depends on the intensity of the other. The axis-dependent variation of the refractive index induces a nonlinear birefringence into the fiber. In the consequence, energy is transferred between the polarization components, similar to the polarization beating. This causes a rotation of the polarization ellipse [85].

The nonlinear polarization rotation ϕ_{\max} depends on the nonlinear length L_{NL} (cf. Eq. 2.13)

$$\phi_{\max} = \frac{L}{L_{NL}}.$$

In an oscillator, the rotated part can be transmitted by a polarization dependent component like a polarizing beam splitter cube, while the non-rotated parts are dumped. The polarization dependent component therefore cuts off the (low-intensity) flanks of the pulse, hence shortening it each round-trip. As the amplification requires a seed, the pulse is further amplified.

Resulting from random intensity fluctuations in the cw-operation mode, the mode-locking by NPE can be self-starting. At higher intensity, lower losses are experienced and, therefore, these pulse parts are amplified more strongly in the next round-trip.

Mode-Locking As opposed to Q-switched pulses, mode-locked pulses can be much shorter than the cavity length. The loss modulation of the saturable absorber causes a pulse shortening in each roundtrip. Fiber dispersion in combination with nonlinear effects result in an increase of pulse duration in each roundtrip. For a certain pulse width there is a balance between the two processes.

A periodic intensity modulation of the central laser frequency ω_0 with the frequency ω_m generates sidebands at the frequency ω_n around the central carrier frequency.

$$\omega_n = \omega_0 + n\omega_m$$

The spacing of the sidebands depends on the modulation frequency, which does not necessarily coincide with the adjacent longitudinal cavity mode [123]. This sideband generation in the frequency domain can also be derived by the Fourier transform of the amplitude modulation in the temporal domain. The amplitude modulation produces a time-varying transmission given by

$$T_{AM}(t) = \exp(-\Delta_m \cdot (1 - \cos(\omega_m t))) \approx 1 - \Delta_m + \Delta_m \cos(\omega_m t), \quad \Delta_m \ll 1.$$

The peak to peak variation of the amplitude modulation is then $2\Delta_m$, Δ_m being the modulation depth. This means, the input cosine wave is attenuated by the amplitude modulation by the factor $(1 - \Delta_m)$, leading to two sidebands with the amplitudes given by $\delta E_{n+1} = \delta E_{n-1} = (\Delta_m/2)E_n$ [123]. As the sidebands are generated by the amplitude modulation of the central frequency, they are coupled, i. e. mode-locked.

The relative intensity of the generated sidebands in the frequency domain has an effect on the pulse shape in the temporal domain. The same intensity of all modes results in a rectangular spectrum, which results in satellite pulses in the temporal domain. The adaption of the sidebands to a Gaussian shape in the frequency domain, leads to a Gaussian shape in the temporal domain.

B. Grating-Prism Compressors

The impact of third order dispersion (TOD) on pulses is stronger, the shorter the pulse durations are. For pulse durations in the range of ≈ 150 fs, TOD must be compensated in a chirped pulse amplifier [93].

Compared to a simple grating compressor, combining a prism and a grating in the compressor introduces additional degrees of freedom to the compressor. On the one hand, the dispersion properties of the grism rely on the diffraction at the gratings and the refraction in the prisms, thus manipulating and delaying the light differently and allowing for TOD compensation. On the other hand, the additional elements in the compressor can be individually adjusted, thus allowing for a precise control of the relation of β_3/β_2 [59].

Grism compressors can apply reflection gratings in combination with prisms [34, 60] or grating structures directly inscribed on one prism surface [135, 59]. With respect to the efficiency and the adjustment degrees of freedom, nowadays, using transmission gratings that are separated from the prisms is the most common way to set up a grism as also shown in Figure B.1 [33], as transmission gratings usually have higher diffraction efficiencies [67].

The scheme of a grism compressor is presented in Figure B.1. The beam propagation can be traced by ray tracing and calculated using the matrix formalism. The beam is refracted according to Snell's law (cf. Eq. 2.1) at point P_1 and correspondingly at every interface

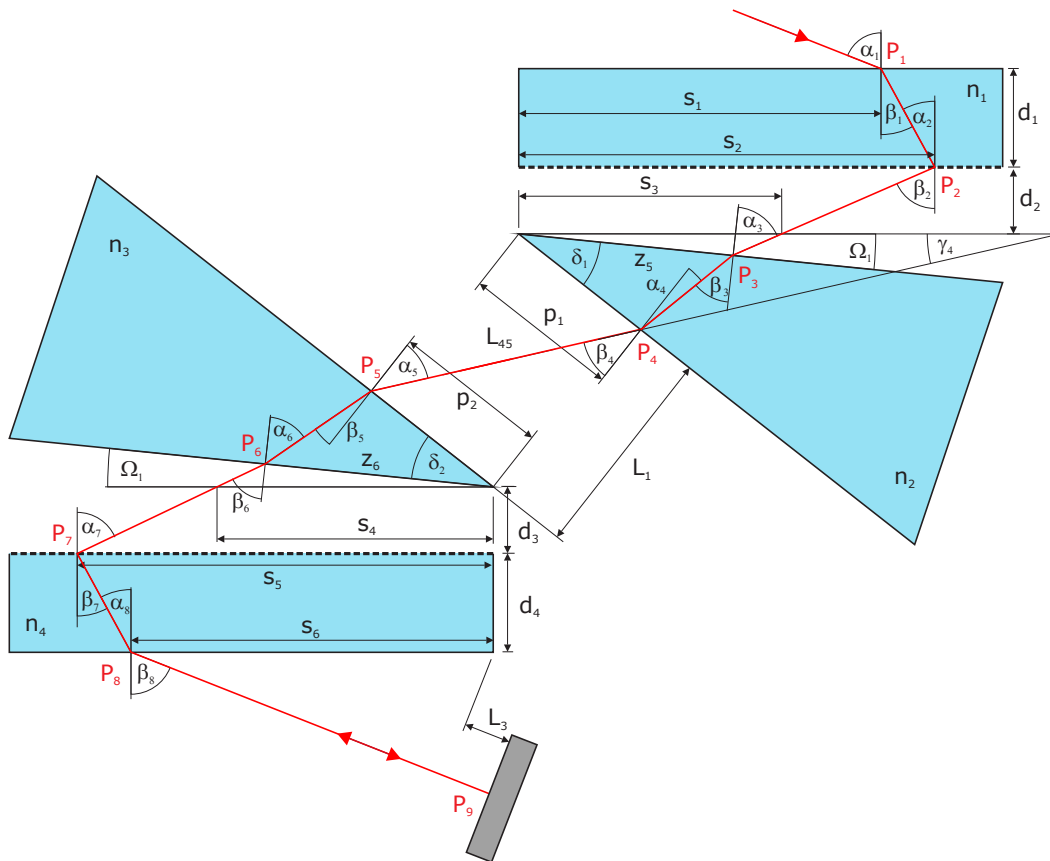


Figure B.1.: Sketch of a transmission grism compressor, picture from Reference [93].

of medium to air. At the points P_2 and P_7 , the beam is diffracted according to the grating equation $\sin(\gamma) + n \sin(\theta) = \lambda/d$, with the incidence angle γ , the diffraction angle θ , the material refractive index n and the grating line separation $d = 1/g$ [93]. For the calculation of the overall dispersion, the wavelength dependence of n , the diffraction at the gratings, and the refraction at the surfaces must be considered. For the explicit calculation, the calculator was already available from the scope of the thesis of D. Mortag [93].

For the dispersion compensation of a fiber stretcher, the relation of β_3 to β_2 of the fiber must be matched by the grism compressor. As there are many parameters which can be adjusted in the grism compressor (cf. Fig. B.1), an important simplification for the compressor is the symmetry between the first grating-prism combination and the second. This can be implemented by a second retroreflector, as shown in Figure B.2.

Furthermore, there are two parameters that are fixed and need to be set in advance: the grating line density and the prism apex angle. In order to match the β_3/β_2 -relation of the fiber, the dispersion of the grism was simulated by a ray tracing program. Following from the specific application, there are various possible configurations, some of which are collected in Table B.1. The dispersion of a standard fused silica fiber at the wavelength of 1030 nm is $\beta_2 = 0.025 \text{ ps}^2$ and $\beta_3 = 6 \cdot 10^{-5} \text{ ps}^3$, leading to a relation $\beta_3/\beta_2 = 2.4 \text{ fs}$.

In order to adjust the β_3/β_2 -ratio of the grism, the prism-grating angle (PGA) can be adjusted as a coarse tuning mechanism; changing PGA has a strong effect on the ratio. Fine tuning can be done by adjusting the prism position parallel to the grating surface,

Table B.1.: Grism parameters for three different configurations. The dimensions belong to the definitions as shown in Figure B.1.

Parameter	Configuration 1	Configuration 2	Configuration 3
Grating line density	600 lines/mm	1000 lines/mm	1500 lines/mm
Incidence angle α	18°	31°	50.6°
Prism material	Fused silica	N-BK7	N-BK7
Prism apex angle δ	45°	54°	66.5°
Prism-grating angle (PGA)	10.3°	3.4°	-1°
Distance d_2	10 mm	10 mm	10 mm
Distance s_3	10 mm	10 mm	10 mm
Distance p_2	70 mm	70 mm	90 mm
β_3/β_2	2.445 fs	2.457 fs	2.431 fs
Comment	Fitting to stretcher fiber lengths of 50 m; compression of $\approx 50 \text{ ps}$ -pulses to $\approx 150 \text{ fs}$ -pulses	Stretcher fiber length of roughly 150 m, grating line density is the most efficient for the wavelength of 1030 nm	For very long stretcher fiber lengths; the required large expansion of the pulse spectrum required large apertures

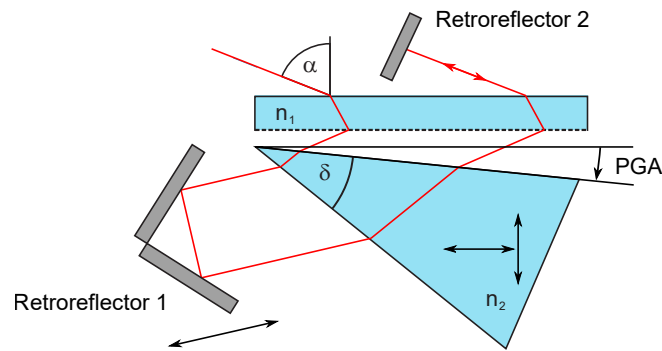


Figure B.2.: Sketch of a simplified transmission grism compressor, picture from Reference [93].

i. e. inducing more or less material into the beam line. Adjusting the Retroreflector 1 (Fig. B.2), corresponds to an adjustment of the prism separation distance in a double grism-compressor (Fig. B.1). The adjustment of the prism separation distance has a very small effect on the β_3/β_2 -ratio, but changes the overall absolute value of dispersion that is induced by the grism compressor. In order to configure the optimum dispersion compensation, the pulse shape behind the grism should be monitored.

Grisms can also be used as pulse stretchers [59]. Owing to the various degrees of freedom, the pulses can be pre-shaped for amplification in order to only use reflection optical components after amplification, which is advantageous for the pulse quality of high energy pulses [21].

C. Established Pulse Analysis Methods

The autocorrelation (AC) [7] is a self-referenced method and was the first solution for the measurement of ultrashort pulses and is still a widely used method. Its principle is to split up a train of pulses and delay one part of each copy with respect to the other copy. Both copies are then spatially overlapped again and the second harmonic is generated from the superposed intensities. The resulting changes in peak power (depending on the delay of the pulse parts) can be measured in an intensity-dependent nonlinear step, usually the generation of the second harmonic. The high peak powers that are required for the nonlinear stage are only achieved when the two pulse copies overlap temporally. According to the beam path, either only the intensity can overlap or the electrical field can also interfere, which results in different traces. The first arrangement, the intensity AC, is schematically shown in Figure 4.1 (a).

Intensity Autocorrelation In the intensity AC, the pulses only overlap in the nonlinear crystal. The generated trace is the convolution of the pulse with itself and does not show the pulse shape [7]. A reliable statement on the pulse duration can only be given, if the actual pulse shape is known.

In some cases, the pulse form can be derived from its generation: a soliton laser for instance generates a pulse envelope with a shape of a squared hyperbolic secant (sech^2) [2]. In other cases, a pulse shape can be assumed from the resulting AC signal. It must be noted,

that both the pulse shape and the resulting pulse duration are only a guess. Usually, in this thesis, a Gaussian pulse shape is assumed. A Gaussian shape, as well as a sech^2 -shape and a Lorentian shape produce AC signals that are also Gaussian-, sech^2 - and Lorentian-shaped, with AC traces that are longer for the factor 1.414, 1.543 and 2, respectively [18].

The intensity AC is the most coarse way to determine the pulse shape [109]. However, there is still the possibility to assert statements on deformation. Double pulses and optical wave breaking can be determined with a relatively high reliability. Double pulses generate satellite pulses in the AC signal, too. The distance between the double pulses is given by the delay of the satellite pulses. Pulse breaking constitutes itself by the generation of several pulse spikes, as introduced in Section 3.2. This complex pulse shape generates an AC signal that shows a broad, noisy, bell-like pedestal with a narrow coherence spike.

Interferometric Autocorrelation As opposed to the intensity AC, in the interferometric AC, the separated beams follow the same path after the delay. Thus, the electrical fields of the two pulses interfere and interference fringes can be seen in the AC signal. As the interference fringes result from the electrical field and due to the sampling rate of the AC devices, this method is suitable for pulses that are shorter than ≈ 500 fs.

The interferometric AC is also called fringe-resolved autocorrelation (FRAC). The interference signal requires a peak to background relation of 8 to 1. This relation results from the fact that the intensity of the second harmonic sum field is measured, involving the fourth power of the electrical field amplitude [18]. A deviation from the peak to background relation is an indication for a misalignment of the beam into the autocorrelator or a broad pedestal under the pulse. This way, a coherence spike over a broad pedestal can be distinguished from a short pulse in the AC trace. Following from the arrangement of the frequency components in the pulse after dispersion or alteration by self-phase modulation, the FRAC-trace shows characteristic interference patterns of the electrical field. The FRAC, therefore, offers more information on the pulse than the intensity AC.

Also FRAC traces are never unambiguous, they can only give a hint on the real pulse duration. For the full characterization of pulses, the phase information is essential. This can be obtained by coupling the information of the AC to a spectral measurement like in FROG-measurements for instance.

Frequency-Resolved Optical Gating Full characterization by coupling spectral information of the pulse to temporal features emerged less than 30 years ago. Today, various methods are available, having different advantages and shortcomings. The review paper by R. Trebino [137], a well-known pioneer in this field, gives an overview of the developments. One of the most popular methods, the frequency-resolved optical gating (FROG) and one of its variations will be briefly introduced here.

The FROG-method is based on measuring the spectrum of a particular temporal component of the pulse. For this, the photodiode in an AC-device is replaced by a spectrometer as schematically shown in Figure 4.1 (b) [58].

From a practical point of view it is also possible to make use of the limited critical phase matching conditions of the second harmonic generation in the nonlinear stage of the process. In this case, only a small part of the pulse is actually detected by the autocorrelator. Owing to the turning angle of the crystal, a spectral dependency of the measured AC is achieved.

The result of the measurement is a spectrogram, a trace that shows the delay from the AC against the spectral information. By measuring the spectral information coupled to the temporal information, the full characterization becomes a two dimensional pulse retrieval problem which essentially yields unique results [57]. Although the pulse shape is completely determined by the FROG-retrieval, some less relevant ambiguities remain in the classical FROG-setup. These are the absolute phase shift of the pulse, the time reversal and a temporal translation of the pulses. If these ambiguities should become relevant, minor changes to the FROG-setup are necessary [137]. Various iterative retrieval algorithms are available, as well in commercial systems as for download for research applications¹.

Grating-eliminated no-nonsense observation of ultrafast incident laser light e-fields

Closely related to the FROG-method is the GRENOUILLE-method, an abbreviation for grating-eliminated no-nonsense observation of ultrafast incident laser light e-fields [99]. In this technique, the FROG-trace is recorded in a single shot: The expanded laser beam is tightly focussed into a narrowband phase matched nonlinear crystal. Due to the angle resulting from the tight focussing, the newly generated frequency components have different angles. The temporal delay is achieved by a so-called biprism, by which the left half of the beam is overlaid in the crystal with the right half. Due to the beam diameter, a delay is imposed. The information on delay and spectrum are multiplexed in two dimensions and can be recorded by a camera. The retrieval algorithm is similar to the one of the FROG-trace.

D. Numerical Model

The numerical analysis of the Thulium-based fiber Mamyshev oscillator was performed with the commercial software Fiberdesk². This software numerically simulates the pulse propagation by solving the generalized Schrödinger equation [2].

$$\begin{aligned}
 \frac{\partial A}{\partial z} = & -\frac{\alpha}{2}A && \rightarrow \text{losses} \\
 & + \int_{-\infty}^{\infty} \frac{g(\omega)}{2} A(\omega) e^{-i\omega t} d\omega && \rightarrow \text{gain} \\
 & + \sum_{n \geq 1} \beta_n \frac{i^{n+1}}{n!} \frac{\partial^n}{\partial t^n} A && \rightarrow \text{dispersion} \\
 & + i\gamma && \rightarrow \text{self-phase modulation} \\
 & \cdot \left(1 + i\tau \frac{\partial}{\partial t} \right) && \rightarrow \text{self-steepening} \\
 & \cdot A(t) \int_{-\infty}^{\infty} R(\tau) |A(t - \tau)|^2 d\tau && \rightarrow \text{Raman response}
 \end{aligned}$$

¹"Code", <https://frog.gatech.edu/code.html>, accessed August 5, 2020

²"Fiberdesk", www.fiberdesk.com/, accessed: August 31, 2020

Here, different terms represent specific effects which can be individually switched on or off. The pulse envelope A during the propagation along the fiber is calculated by the split-step Fourier method. In this method, the dispersive effects are approximated to be independent from the nonlinear effects for the propagation over a short distance. Therefore, analytical solutions can be found, when considering only linear effects in the frequency domain in a first step and only nonlinear in the time domain in a second step; the change of the pulse envelope per propagation step is solved in two steps. Matching of temporal and spectral shape is achieved by Fourier transforms after each propagation step.

A simulation is always an approximation to the experiment, because only a simplified setup is modeled in the simulation. The components forming the Mamyshev oscillator in the experiment are depicted in Figure D.1 (a). The simplified numerical model is shown in Figure D.1 (b). As an example, it is a decent assumption to merge the anomalous and normal dispersive fiber in front of the amplification stages, since nonlinear effects are negligible at the low peak powers at that position right behind the band-pass filtering.

The fiber parameters for the simulation were calculated from the information provided by the suppliers and are presented in Table 8.1. Dispersion is only relevant up to the third order, due to the given optical spectrum and pulse duration.

The simulation was started with the spectral information of the injection seed with a pulse energy of 130 pJ. The circulating pulse converged towards the output parameters presented in Section 8.3 in less than five roundtrips. The experimental data were reproduced with a flat gain of 1.7/m in arm 1 and 3.0/m in arm 2. The maximum pulse energy was achieved with a gain of 2.9/m in arm 1 and 4.6/m in arm 2, the circulation in case of the large spectral band-pass filter separation with a gain of 3.1/m in arm 1 and 4.0/m in arm 2.

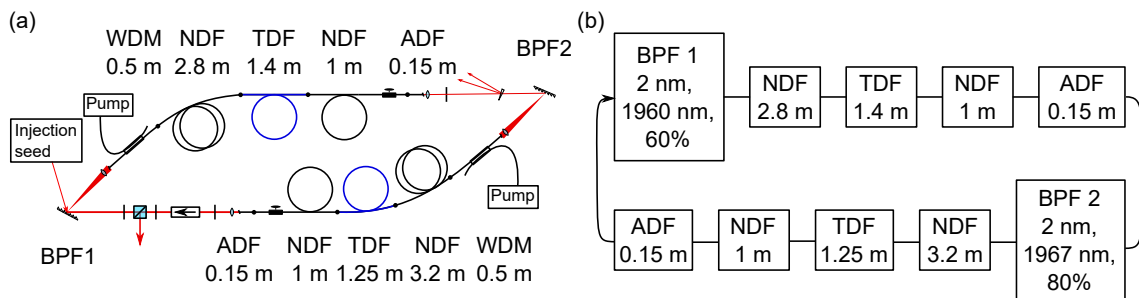


Figure D.1.: Concept for the simulation of the Thulium-based fiber Mamyshev oscillator: (a) experimental setup compared to (b) the numerically simulated setup. The gain in the TDF could be adapted corresponding to the output parameters. The fiber length is given for the individual slots, the BPFs include the transmission bandwidth, central wavelength and transmission ratio. ADF: Anomalous dispersive fiber SMF28, BPF: band-pass filter, NDF: normal dispersive fiber UHNA4, TDF: Thulium-doped fiber TmDF200, WDM: Wavelength-division multiplexer (anomalous dispersive fiber, SMF28).

Bibliography

- [1] AGGER, Søren D. ; POVLSEN, Jorn H.: Emission and absorption cross section of thulium doped silica fibers. In: *Optics Express* 14 (2006), Nr. 1, S. 50. – URL <https://www.osapublishing.org/oe/abstract.cfm?uri=oe-14-1-50>. – ISSN 1094-4087
- [2] AGRAWAL, Govind P.: *Nonlinear Fiber Optics*. 4. Elsevier Inc., 2007. – ISBN 978-0-12-369519-1
- [3] AGUERGARAY, Claude ; HAWKER, Ryan ; RUNGE, Antoine F. J. ; ERKINTALO, Miro ; BRODERICK, Neil G. R.: 120 fs, 4.2 nJ pulses from an all-normal-dispersion, polarization-maintaining, fiber laser. In: *Applied Physics Letters* 103 (2013), Nr. 12, S. 121111. – URL <http://scitation.aip.org/content/aip/journal/apl/103/12/10.1063/1.4821776>. – ISSN 00036951
- [4] ALONSO, Benjamín ; SOLA, Íñigo J. ; CRESPO, Helder: Self-calibrating d-scan: measuring ultrashort laser pulses on-target using an arbitrary pulse compressor. In: *Scientific Reports* 8 (2018), December, Nr. 1, S. 3264. – URL <http://www.nature.com/articles/s41598-018-21701-6>. – ISSN 2045-2322
- [5] ANDERSON, D. ; DESAIX, M ; KARLSSON, M. ; LISAK, M. ; QUIROGA-TEIXEIRO, M. L.: Wave-breaking-free pulses in nonlinear-optical fibers. In: *Journal of the Optical Society of America B* 10 (1993), July, Nr. 7, S. 1185. – URL <https://www.osapublishing.org/abstract.cfm?URI=josab-10-7-1185>. – ISSN 0740-3224
- [6] ANDERSON, D. ; DESAIX, M. ; LISAK, M. ; QUIROGA-TEIXEIRO, M. L.: Wave breaking in nonlinear-optical fibers. In: *Journal of the Optical Society of America B* 9 (1992), August, Nr. 8, S. 1358. – URL <https://www.osapublishing.org/abstract.cfm?URI=josab-9-8-1358>. – ISSN 0740-3224
- [7] ARMSTRONG, J. A.: Measurement of Picosecond Laser Pulse Widths. In: *Applied Physics Letters* 10 (1967), January, Nr. 1, S. 16–18. – URL <http://aip.scitation.org/doi/10.1063/1.1754787>. – ISSN 0003-6951
- [8] ATKIN, D.M. ; SHEPHERD, T.J. ; BIRKS, T.A. ; RUSSELL, P.St.J. ; ROBERTS, P.J.: Full 2-D photonic bandgaps in silica/air structures. In: *Electronics Letters* 31 (1995), October, Nr. 22, S. 1941–1943. – URL <https://digital-library.theiet.org/content/journals/10.1049/el{ }19951306>. – ISSN 0013-5194
- [9] BALCIUNAS, T. ; FOURCADE-DUTIN, C. ; FAN, G. ; WITTING, T. ; VORONIN, A. A. ; ZHELTIKOV, A. M. ; GEROME, F. ; PAULUS, G. G. ; BALTUSKA, A. ; BENABID, F.: A strong-field driver in the single-cycle regime based on self-compression in a kagome fibre. In: *Nature Communications* 6 (2015), may, Nr. 1, S. 6117. – URL <http://www.nature.com/articles/ncomms7117>. – ISSN 2041-1723

Bibliography

- [10] BARENBLATT, Grigory I.: Introduction. In: *Scaling, Self-similarity, and Intermediate Asymptotics*. Cambridge University Press, December 1996, S. 1–27. – URL <https://www.cambridge.org/core/product/identifier/CB09781107050242A008/type/book{ }part>. – ISBN 9781107050242
- [11] BAUER, Franziska ; MICHALOWSKI, Andreas ; KIEDROWSKI, Thomas ; NOLTE, Stefan: Heat accumulation in ultra-short pulsed scanning laser ablation of metals. In: *Optics Express* 23 (2015), January, Nr. 2, S. 1035. – URL <https://www.osapublishing.org/abstract.cfm?URI=oe-23-2-1035>. – ISSN 1094-4087
- [12] BIRKS, T. A. ; KNIGHT, J. C. ; RUSSELL, P. St. J.: Endlessly single-mode photonic crystal fiber. In: *Optics Letters* 22 (1997), July, Nr. 13, S. 961. – URL <https://www.osapublishing.org/abstract.cfm?URI=ol-22-13-961>. – ISBN 0146-9592
- [13] BUDUNOHLU, Ibrahim L. ; ULGÜDÜR, Coskun ; OKTEM, Bulent ; ILDAY, Fatih O.: Intensity noise of mode-locked fiber lasers. In: *Optics Letters* 34 (2009), Nr. 16, S. 2516–2518. – ISSN 1539-4794
- [14] CHANG, Hong ; CHENG, Zhaochen ; SUN, Ruoyu ; PENG, Zhigang ; YU, Miao ; YOU, Yu ; WANG, Min ; WANG, Pu: 172-fs, 27- μ J, Yb-doped all-fiber-integrated chirped pulse amplification system based on parabolic evolution by passive spectral amplitude shaping. In: *Optics Express* 27 (2019), November, Nr. 23, S. 34103. – URL <https://www.osapublishing.org/abstract.cfm?URI=oe-27-23-34103>. – ISSN 1094-4087
- [15] CHERNYSHEVA, Maria A. ; KRYLOV, Alexander A. ; KRYUKOV, Petr G. ; DIANOV, Evgeny M.: Nonlinear amplifying loop-mirror-based mode-locked thulium-doped fiber laser. In: *IEEE Photonics Technology Letters* 24 (2012), Nr. 14, S. 1254–1256. – ISSN 10411135
- [16] CHICHKOV, B. N. ; MOMMA, C. ; NOLTE, S. ; ALVENSLEBEN, F. ; TÜNNERMANN, A.: Femtosecond, picosecond and nanosecond laser ablation of solids. In: *Applied Physics A Materials Science & Processing* 63 (1996), August, Nr. 2, S. 109–115. – URL <http://link.springer.com/10.1007/BF01567637>. – ISSN 0947-8396
- [17] CHONG, Andy ; BUCKLEY, Joel ; RENNINGER, Will ; WISE, Frank: All-normal-dispersion femtosecond fiber laser. In: *Optics Express* 14 (2006), Nr. 21, S. 10095. – URL <https://www.osapublishing.org/oe/abstract.cfm?uri=oe-14-21-10095>. – ISSN 1094-4087
- [18] DIELS, Jean-Claude M. ; FONTAINE, Joel J. ; MCMICHAEL, Ian C. ; SIMONI, Francesco: Control and measurement of ultrashort pulse shapes (in amplitude and phase) with femtosecond accuracy. In: *Applied Optics* 24 (1985), May, Nr. 9, S. 1270. – URL <https://www.osapublishing.org/abstract.cfm?URI=ao-24-9-1270>. – ISSN 0003-6935
- [19] DOCTER, Boudewijn ; POZO, Jose ; BERI, Stefano ; ERMAKOV, Ilya V. ; DANCKAERT, Jan ; SMIT, Meint K. ; KAROUTA, Fouad: Discretely Tunable Laser Based on Filtered Feedback for Telecommunication Applications. In: *IEEE Journal of Selected Topics in Quantum Electronics* 16 (2010), September, Nr. 5, S. 1405–1412. – URL <http://ieeexplore.ieee.org/document/5373898/>. – ISSN 1077-260X

- [20] DORAN, N J. ; WOOD, David: Nonlinear-optical loop mirror. In: *Optics Letters* 13 (1988), January, Nr. 1, S. 56. – URL <https://www.osapublishing.org/ol/abstract.cfm?uri=ol-13-1-56>. – ISBN 0146-9592
- [21] DOU, Tai H. ; TAUTZ, Raphael ; GU, Xun ; MARCUS, Gilad ; FEURER, Thomas ; KRAUSZ, Ferenc ; VEISZ, Laszlo: Dispersion control with reflection gratings of an ultra-broadband spectrum approaching a full octave. In: *Optics Express* 18 (2010), Nr. 26, S. 27900–27909. – ISBN 1094-4087
- [22] EIDAM, Tino ; HADRICH, S. ; ROSER, F. ; SEISE, Enrico ; GOTTSCHALL, Thomas ; ROTHHARDT, Jan ; SCHREIBER, Thomas ; LIMPET, Jens ; TUNNERMANN, A.: A 325-W-Average-Power Fiber CPA System Delivering Sub-400 fs Pulses. In: *IEEE Journal of Selected Topics in Quantum Electronics* 15 (2009), January, Nr. 1, S. 187–190. – URL <http://ieeexplore.ieee.org/document/4773317/>. – ISSN 1077-260X
- [23] EIDAM, Tino ; HANF, Stefan ; SEISE, Enrico ; ANDERSEN, Thomas V. ; GABLER, Thomas ; WIRTH, Christian ; SCHREIBER, Thomas ; LIMPET, Jens ; TUNNERMANN, Andreas: Femtosecond fiber CPA system emitting 830 W average output power. In: *Optics Letters* 35 (2010), January, Nr. 2, S. 94. – URL <https://www.osapublishing.org/abstract.cfm?URI=ol-35-2-94>. – ISBN 9781557528803
- [24] EIDAM, Tino ; ROTHHARDT, Jan ; STUTZKI, Fabian ; JANSEN, Florian ; HADRICH, Steffen ; CARSTENS, Henning ; JAUREGUI, Cesar ; LIMPET, Jens ; TUNNERMANN, Andreas: Fiber chirped-pulse amplification system emitting 3.8 GW peak power. In: *Optics Express* 19 (2011), January, Nr. 1, S. 255. – URL <https://www.osapublishing.org/oe/abstract.cfm?uri=oe-19-1-255>. – ISSN 1094-4087
- [25] ENGELBRECHT, Martin ; HAXSEN, Frithjof ; RUEHL, Axel ; WANDT, Dieter ; KRACHT, Dietmar: Ultrafast thulium-doped fiber-oscillator with pulse energy of 4.3 nJ. In: *Optics Letters* 33 (2008), apr, Nr. 7, S. 690. – URL <https://www.osapublishing.org/abstract.cfm?URI=ol-33-7-690>. – ISSN 0146-9592
- [26] ERKINTALO, Miro ; AGUERGARAY, Claude ; RUNGE, Antoine ; BRODERICK, Neil G R.: Environmentally stable all-PM all-fiber giant chirp oscillator. In: *Optics Express* 20 (2012), September, Nr. 20, S. 22669. – URL <https://www.osapublishing.org/oe/abstract.cfm?uri=oe-20-20-22669>. – ISSN 1094-4087
- [27] FARADAY, Michael: XVII. On a peculiar class of acoustical figures; and on certain forms assumed by groups of particles upon vibrating elastic surfaces. In: *Philosophical Transactions of the Royal Society of London* 121 (1831), December, Nr. August 1827, S. 299–340. – URL <https://royalsocietypublishing.org/doi/10.1098/rstl.1831.0018>. – ISSN 0261-0523
- [28] FENG, Yujun ; NILSSON, Johan ; PRICE, Jonathan H. V.: Robust Phase Retrieval Using Group-Delay-Dispersion-Scanned Second-Harmonic Generation Demonstrated in a Femtosecond Fiber Chirped-Pulse Amplification System. In: *IEEE Journal of Quantum Electronics* 54 (2018), August, Nr. 4, S. 1–11. – URL <https://ieeexplore.ieee.org/document/8395428/>. – ISSN 0018-9197

Bibliography

- [29] FERMANN, M E. ; HABERL, F ; HOFER, M ; HOCHREITER, H: Nonlinear amplifying loop mirror. In: *Optics Letters* 15 (1990), July, Nr. 13, S. 752. – URL <https://www.osapublishing.org/ol/abstract.cfm?uri=ol-15-13-752>. – ISBN 0146-9592
- [30] FERMANN, M. E. ; KRUGLOV, V. I. ; THOMSEN, B. C. ; DUDLEY, J. M. ; HARVEY, J. D.: Self-Similar Propagation and Amplification of Parabolic Pulses in Optical Fibers. In: *Physical Review Letters* 84 (2000), Nr. 26, S. 6010–6013. – URL <https://link.aps.org/doi/10.1103/PhysRevLett.84.6010>. – ISBN 0031-9007 (Print)\r0031-9007 (Linking)
- [31] FERNANDEZ, A. ; JESPERSEN, K. ; ZHU, L. ; GRUNER-NIELSEN, L. ; BALTUSKA, A. ; GALVANAUSKAS, A. ; VERHOEF, A. J.: High-fidelity, 160 fs, 5 μ J pulses from an integrated Yb-fiber laser system with a fiber stretcher matching a simple grating compressor. In: *Optics Letters* 37 (2012), March, Nr. 5, S. 927. – URL <https://www.osapublishing.org/abstract.cfm?URI=ol-37-5-927>. – ISSN 0146-9592
- [32] FINOT, Christophe ; PROVOST, Lionel ; PETROPOULOS, Periklis ; RICHARDSON, David J.: Parabolic pulse generation through passive nonlinear pulse reshaping in a normally dispersive two segment fiber device. In: *Optics Express* 15 (2007), Nr. 3, S. 852
- [33] FORGET, Nicolas ; CROZATIER, Vincent ; TOURNOIS, Pierre: Transmission Bragg-grating grisms for pulse compression. In: *Applied Physics B* 109 (2012), October, Nr. 1, S. 121–125. – URL <http://link.springer.com/10.1007/s00340-012-5126-2>. – ISBN 9781457705335
- [34] FORK, R L. ; CRUZ, C H B. ; BECKER, P C. ; SHANK, C V.: Compression of optical pulses to six femtoseconds by using cubic phase compensation. In: *Optics Letters* 12 (1987), Nr. 7, S. 483–485
- [35] FRANJIC, Kresimir ; COWAN, Michael L. ; KRAEMER, Darren ; MILLER, R. J. D.: Laser selective cutting of biological tissues by impulsive heat deposition through ultrafast vibrational excitations. In: *Optics Express* 17 (2009), December, Nr. 25, S. 22937. – URL <https://www.osapublishing.org/oe/abstract.cfm?uri=oe-17-25-22937>. – ISSN 1094-4087
- [36] FSAIFES, Ihsan ; DANIAULT, Louis ; BELLANGER, Severine ; VEINHARD, Matthieu ; BOURDERIONNET, Jerome ; LARAT, Christian ; LALLIER, Eric ; DURAND, Eric ; BRIGNON, Arnaud ; CHANTELOUP, Jean-Christophe: Coherent beam combining of 61 femtosecond fiber amplifiers. In: *Optics Express* 28 (2020), July, Nr. 14, S. 20152. – URL <https://www.osapublishing.org/abstract.cfm?URI=oe-28-14-20152>. – ISBN 9781557528209
- [37] FU, Walter ; TANG, Yuxing ; MCCOMB, Timothy S. ; LOWDER, Tyson L. ; WISE, Frank W.: Limits of femtosecond fiber amplification by parabolic pre-shaping. In: *Journal of the Optical Society of America B* 34 (2017), March, Nr. 3, S. A37. – URL <https://www.osapublishing.org/abstract.cfm?URI=josab-34-3-A37>. – ISSN 0740-3224
- [38] FU, Walter ; WRIGHT, Logan G. ; SIDORENKO, Pavel ; BACKUS, Sterling ; WISE, Frank W.: Several new directions for ultrafast fiber lasers

- [Invited]. In: *Optics Express* 26 (2018), April, Nr. 8, S. 9432. – URL <https://www.osapublishing.org/abstract.cfm?URI=ol-43-11-2672><https://www.osapublishing.org/abstract.cfm?URI=oe-26-8-9432>. – ISSN 1094-4087
- [39] FU, Walter ; WRIGHT, Logan G. ; WISE, Frank W.: High-power femtosecond pulses without a modelocked laser. In: *Optica* 4 (2017), July, Nr. 7, S. 831. – URL <https://www.osapublishing.org/abstract.cfm?URI=optica-4-7-831>. – ISSN 2334-2536
- [40] FU, Yan ; WANG, Haifeng ; SHI, Riyi ; CHENG, Ji-Xin: Characterization of photo-damage in coherent anti-Stokes Raman scattering microscopy. In: *Optics Express* 14 (2006), Nr. 9, S. 3942. – URL <https://www.osapublishing.org/oe/abstract.cfm?uri=oe-14-9-3942>. – ISSN 1094-4087
- [41] GAIDA, C. ; GEBHARDT, M. ; HEUERMAN, T. ; STUTZKI, F. ; JAUREGUI, C. ; LIMP, J.: Ultrafast thulium fiber laser system emitting more than 1 kW of average power. In: *Optics Letters* 43 (2018), Nr. 23, S. 5853. – ISSN 0146-9592
- [42] GINZBURG, Vladislav ; YAKOVLEV, Ivan ; ZUEV, Alexandr ; KOROBAYNIKOVA, Anastasia ; KOCHETKOV, Anton ; KUZMIN, Alexey ; MIRONOV, Sergey ; SHAYKIN, Andrey ; SHAIKIN, Ilya ; KHAZANOV, Efim ; MOUROU, Gerard: Fivefold compression of 250-TW laser pulses. In: *Physical Review A* 101 (2020), January, Nr. 1, S. 013829. – URL <https://doi.org/10.1103/PhysRevA.101.013829><https://link.aps.org/doi/10.1103/PhysRevA.101.013829>. – ISSN 2469-9926
- [43] HASSAN, M. T. ; LUU, T. T. ; MOULET, A. ; RASKAZOVSKAYA, O. ; ZHOKHOV, P. ; GARG, M. ; KARPOWICZ, N. ; ZHELIKOV, A. M. ; PERVAK, V. ; KRAUSZ, F. ; GOULIELMAKIS, E.: Optical attosecond pulses and tracking the nonlinear response of bound electrons. In: *Nature* 530 (2016), February, Nr. 7588, S. 66–70. – URL <http://www.nature.com/articles/nature16528>. – ISSN 0028-0836
- [44] HILL, K. O. ; FUJII, Y. ; JOHNSON, D. C. ; KAWASAKI, B. S.: Photosensitivity in optical fiber waveguides: Application to reflection filter fabrication. In: *Applied Physics Letters* 32 (1978), May, Nr. 10, S. 647–649. – URL <http://aip.scitation.org/doi/10.1063/1.89881>. – ISSN 0003-6951
- [45] HILL, K. O. ; MALO, B. ; BILODEAU, F. ; JOHNSON, D. C. ; ALBERT, J.: Bragg gratings fabricated in monomode photosensitive optical fiber by UV exposure through a phase mask. In: *Applied Physics Letters* 62 (1993), March, Nr. 10, S. 1035–1037. – URL <http://aip.scitation.org/doi/10.1063/1.108786>. – ISSN 0003-6951
- [46] HINKELMANN, Moritz: *Compact and efficient sub-10 ps pump sources at 2 μm for the generation of coherent mid-infrared radiation*, Gottfried Wilhelm Leibniz Universität, Dissertation, 2020. – 112 S
- [47] HINKELMANN, Moritz ; BAUDISCH, Matthias ; WANDT, Dieter ; MORGNER, Uwe ; ZAWILSKI, Kevin ; SCHUNEMANN, Peter ; NEUMANN, Jörg ; RIMKE, Ingo ; KRACHT, Dietmar: High-repetition rate, mid-infrared, picosecond pulse generation with μJ-energies based on OPG/OPA schemes in 2-μm-pumped ZnGeP₂. In: *Optics Express* 28 (2020), July, Nr. 15, S. 21499. – URL <https://www.osapublishing.org/abstract.cfm?URI=oe-28-15-21499>. – ISSN 1094-4087

Bibliography

- [48] HOCHHEIM, Sven ; BROCKMÜLLER, Eike ; WESSELS, Peter ; KOPONEN, Joonas ; LOWDER, Tyson ; NOVOTNY, Steffen ; NEUMANN, Jörg ; KRACHT, Dietmar: Integrated signal and pump combiner in chirally-coupled-core fibers for all-fiber lasers and amplifiers. In: *OSA Advanced Photonics Congress (AP) 2020 (IPR, NP, NOMA, Networks, PVLED, PSC, SPPCom, SOF)*, OSA, 2020, S. SoTu2H.6. – URL <https://www.osapublishing.org/abstract.cfm?URI=SOF-2020-SoTu2H.6>. – ISBN 978-1-943580-79-8
- [49] HOFFMANN, Mathias ; NAGY, Tamas ; WILLEMSSEN, Thomas ; JUPÉ, Marco ; RISTAU, Detlev ; MORGNER, Uwe: Pulse characterization by THG d-scan in absorbing nonlinear media. In: *Optics Express* 22 (2014), March, Nr. 5, S. 5234. – URL <https://www.osapublishing.org/oe/abstract.cfm?uri=oe-22-5-5234>. – ISSN 1094-4087
- [50] HORTON, Nicholas G. ; WANG, Ke ; KOBAT, Demirhan ; CLARK, Catharine G. ; WISE, Frank W. ; SCHAFFER, Chris B. ; XU, Chris: In vivo three-photon microscopy of subcortical structures within an intact mouse brain. In: *Nature Photonics* 7 (2013), March, Nr. 3, S. 205–209. – URL <http://www.nature.com/articles/nphoton.2012.336>. – ISSN 1749-4885
- [51] HOTZ, David F.: Gain Narrowing in a Laser Amplifier. In: *Applied Optics* 4 (1965), May, Nr. 5, S. 527. – URL <https://www.osapublishing.org/abstract.cfm?URI=ao-4-5-527>. – ISSN 0003-6935
- [52] ILDAY, Ömer: *Theory and Practice of High-Energy Femtosecond Fiber Lasers*, Cornell University, Doctor of Philosophy, 2004. – 134 S
- [53] JOCHER, Christoph ; EIDAM, Tino ; HÄDRICH, Steffen ; LIMPERT, Jens ; TÜNNERMANN, Andreas: Sub 25 fs pulses from solid-core nonlinear compression stage at 250 W of average power. In: *Optics Letters* 37 (2012), November, Nr. 21, S. 4407. – URL <https://www.osapublishing.org/abstract.cfm?URI=ol-37-21-4407>. – ISSN 0146-9592
- [54] KABACIŃSKI, Piotr ; KARDAŚ, Tomasz M. ; STEPANENKO, Yuriy ; RADZEWICZ, Czesław: Nonlinear refractive index measurement by SPM-induced phase regression. In: *Optics Express* 27 (2019), April, Nr. 8, S. 11018. – URL <https://www.osapublishing.org/abstract.cfm?URI=oe-27-8-11018>. – ISSN 1094-4087
- [55] KALAYCIOGLU, H. ; OKTEM, B. ; SENEL, Ç. ; PALTANI, P. P. ; ILDAY, F. : Microjoule-energy, 1 MHz repetition rate pulses from all-fiber-integrated nonlinear chirped-pulse amplifier. In: *Optics Letters* 35 (2010), April, Nr. 7, S. 959. – URL <https://www.osapublishing.org/ol/abstract.cfm?uri=ol-35-7-959>. – ISSN 0146-9592
- [56] KALAYCIOGLU, Hamit ; ELAHI, Parviz ; AKCAALAN, Onder ; ILDAY, Fatih O.: High-Repetition-Rate Ultrafast Fiber Lasers for Material Processing. In: *IEEE Journal of Selected Topics in Quantum Electronics* 24 (2018), may, Nr. 3, S. 1–12. – URL <http://ieeexplore.ieee.org/document/8103327/>. – ISSN 1077-260X
- [57] KANE, D. J. ; TREBINO, R.: Single-Shot Measurement of the Intensity and Phase of a Femtosecond Pulse. In: *Springer Series in Chemical Physics* Bd. 18. URL <http://>

- link.springer.com/10.1007/978-3-642-84910-7{ }36, 1993, S. 138–139. – ISBN 3540564756
- [58] KANE, D.J. ; TREBINO, Rick: Characterization of arbitrary femtosecond pulses using frequency-resolved optical gating. In: *IEEE Journal of Quantum Electronics* 29 (1993), Nr. 2, S. 571–579. – URL <http://ieeexplore.ieee.org/document/199311/>. – ISSN 00189197
- [59] KANE, S ; SQUIER, J: Grism-pair stretcher-compressor system for simultaneous second- and third-order dispersion compensation in chirped-pulse amplification. In: *Journal of the Optical Society of America B* 14 (1997), Nr. 3, S. 661–665
- [60] KANE, S ; SQUIER, J ; RUDD, J V. ; MOUROU, G: Hybrid grating-prism stretcher-compressor system with cubic phase and wavelength tunability and decreased alignment sensitivity. In: *Optics Letters* 19 (1994), November, Nr. 22, S. 1876. – URL <https://www.osapublishing.org/abstract.cfm?URI=ol-19-22-1876>. – ISSN 0146-9592
- [61] KANE, Steve ; SQUIER, Jeff: Grating compensation of third-order material dispersion in the normal dispersion regime: Sub-100-fs chirped-pulse amplification using a fiber stretcher and grating-pair compressor. In: *IEEE Journal of Quantum Electronics* 31 (1995), Nr. 11, S. 2052–2057. – URL <http://ieeexplore.ieee.org/document/469287/>. – ISSN 00189197
- [62] KELLER, U. ; CHIU, T. H. ; FERGUSON, J. F.: Self-starting femtosecond mode-locked Nd:glass laser that uses intracavity saturable absorbers. In: *Optics Letters* 18 (1993), July, Nr. 13, S. 1077. – URL <https://www.osapublishing.org/abstract.cfm?URI=ol-18-13-1077>. – ISSN 0146-9592
- [63] KERSE, Can ; KALAYCIOGLU, Hamit ; ELAHI, Parviz ; AKCAALAN, Önder ; ILDAY, F. .: 3.5-GHz intra-burst repetition rate ultrafast Yb-doped fiber laser. In: *Optics Communications* 366 (2016), S. 404–409
- [64] KERSE, Can ; KALAYCIOGLU, Hamit ; ELAHI, Parviz ; CETIN, Barbaros ; KESIM, Denizhan K. ; AKCAALAN, Onder ; YAVAS, Seydi ; ASIK, Mehmet D. ; OKTEM, Bulent ; HOOGLAND, Heinar ; HOLZWARTH, Roland ; ILDAY, Fatih O.: Ablation-cooled material removal with ultrafast bursts of pulses. In: *Nature* 537 (2016), September, Nr. 7618, S. 84–88. – URL <http://www.nature.com/articles/nature18619>
- [65] KIEU, K. ; WISE, F. W.: Soliton Thulium-Doped Fiber Laser With Carbon Nanotube Saturable Absorber. In: *IEEE Photonics Technology Letters* 21 (2009), February, Nr. 3, S. 128–130. – URL <http://ieeexplore.ieee.org/document/4703254/>. – ISBN 6176321972
- [66] KNIGHT, J. C. ; BIRKS, T. A. ; RUSSELL, P. St. J. ; ATKIN, D. M.: All-silica single-mode optical fiber with photonic crystal cladding: errata. In: *Optics Letters* 22 (1997), April, Nr. 7, S. 484. – URL <https://www.osapublishing.org/abstract.cfm?URI=ol-22-7-484>. – ISSN 0146-9592

Bibliography

- [67] KOBAYASHI, Yohei ; HIRAYAMA, Nozomi ; OZAWA, Akira ; SUKEGAWA, Takashi ; SEKI, Takashi ; KURAMOTO, Yoshiyuki ; WATANABE, Shuntaro: 10-MHz, Yb-fiber chirped-pulse amplifier system with large-scale transmission gratings. In: *Optics Express* 21 (2013), May, Nr. 10, S. 12865. – URL <https://www.osapublishing.org/oe/abstract.cfm?uri=oe-21-10-12865>. – ISSN 1094-4087
- [68] KOPLOW, Jeffrey P. ; KLINER, Davv A. V. ; GOLDBERG, Lew: Single-mode operation of a coiled multimode fiber amplifier. In: *Optics Letters* 25 (2000), April, Nr. 7, S. 442. – URL <https://www.osapublishing.org/abstract.cfm?URI=ol-25-7-442>. – ISSN 0146-9592
- [69] KRUMBUEGEL, Marco A. ; TREBINO, Rick: 8. The FROG Algorithm. In: *Frequency-Resolved Optical Gating: The Measurement of Ultrashort Laser Pulses*. Boston, MA : Springer US, 2000, Kap. 8, S. 157–178. – URL <http://link.springer.com/10.1007/978-1-4615-1181-6>. – ISBN 978-1-4613-5432-1
- [70] KUZNETSOVA, L. ; WISE, F.W. ; KANE, S. ; SQUIER, J.: Chirped-pulse amplification near the gain-narrowing limit of Yb-doped fiber using a reflection grism compressor. In: *Applied Physics B* 88 (2007), September, Nr. 4, S. 515–518. – URL <http://link.springer.com/10.1007/s00340-007-2699-2>. – ISSN 0946-2171
- [71] LEE, Byeong H. ; EOM, Joo B. ; KIM, Jinchae ; MOON, Dae S. ; PAEK, Un-Chul ; YANG, Gil-Ho: Photonic crystal fiber coupler. In: *Optics Letters* 27 (2002), May, Nr. 10, S. 812. – URL <https://www.osapublishing.org/abstract.cfm?URI=ol-27-10-812>. – ISSN 0146-9592
- [72] LI, Jianfeng ; ZHANG, Zuxing ; SUN, Zhongyuan ; LUO, Hongyu ; LIU, Yong ; YAN, Zhijun ; MOU, Chengbo ; ZHANG, Lin ; TURITSYN, Sergei K.: All-fiber passively mode-locked Tm-doped NOLM-based oscillator operating at 2- μm in both soliton and noisy-pulse regimes. In: *Optics Express* 22 (2014), Nr. 7, S. 7875. – ISSN 1094-4087
- [73] LI, Wenqi ; GAN, Zebiao ; YU, Lianghong ; WANG, Cheng ; LIU, Yanqi ; GUO, Zhen ; XU, Lu ; XU, Min ; HANG, Yin ; XU, Yi ; WANG, Jianye ; HUANG, Pei ; CAO, He ; YAO, Bo ; ZHANG, Xiaobo ; CHEN, Lingru ; TANG, Yunhai ; LI, Shuai ; LIU, Xingyan ; LI, Shanming ; HE, Mingzhu ; YIN, Dinjun ; LIANG, Xiaoyan ; LENG, Yuxin ; LI, Ruxin ; XU, Zhizhan: 339 J high-energy Ti:sapphire chirped-pulse amplifier for 10 PW laser facility. In: *Optics Letters* 43 (2018), Nr. 22, S. 5681. – ISSN 0146-9592
- [74] LIN, Q. ; AGRAWAL, Govind P.: Raman response function for silica fibers. In: *Optics Letters* 31 (2006), November, Nr. 21, S. 3086. – URL <https://www.osapublishing.org/abstract.cfm?URI=ol-31-21-3086>. – ISSN 0146-9592
- [75] LINDE, D von der: Characterization of the noise in continuously operating mode-locked lasers. In: *Applied Physics B* 39 (1986), April, Nr. 4, S. 201–217. – URL <http://link.springer.com/10.1007/BF00697487>
- [76] LIU, Chi-Hung ; CHANG, Guoqing ; LITCHINITSER, Natasha ; GALVANAUSKAS, Almantas ; GUERTIN, Doug ; JABOBSON, Nick ; TANKALA, Kanishka: Effectively Single-Mode Chirally-Coupled Core Fiber. In: *Advanced Solid-State Photonics*. Washington, D.C. : OSA, 2007, S. ME2. – URL <https://www.osapublishing.org/abstract.cfm?URI=ASSP-2007-ME2>. – ISBN 1-55752-829-2

- [77] LIU, Wei ; SCHIMPF, Damian N. ; EIDAM, Tino ; LIMPET, Jens ; TÜNNERMANN, Andreas ; KÄRTNER, Franz X. ; CHANG, Guoqing: Pre-chirp managed nonlinear amplification in fibers delivering 100 W, 60 fs pulses. In: *Optics Letters* 40 (2015), January, Nr. 2, S. 151. – URL <https://www.osapublishing.org/abstract.cfm?URI=ol-40-2-151>. – ISSN 0146-9592
- [78] LIU, Wu ; LIAO, Ruoyu ; ZHAO, Jun ; CUI, Jiahua ; SONG, Youjian ; WANG, Chingyue ; HU, Minglie: Femtosecond Mamyshev oscillator with 10-MW-level peak power. In: *Optica* 6 (2019), February, Nr. 2, S. 194. – URL <https://www.osapublishing.org/abstract.cfm?URI=optica-6-2-194>. – ISSN 2334-2536
- [79] LIU, Yang ; LI, Wenxue ; LUO, Daping ; BAI, Dongbi ; WANG, Chao ; ZENG, Heping: Generation of 33 fs 93.5 W average power pulses from a third-order dispersion managed self-similar fiber amplifier. In: *Optics Express* 24 (2016), May, Nr. 10, S. 10939. – URL <https://www.osapublishing.org/abstract.cfm?URI=oe-24-10-10939>. – ISSN 1094-4087
- [80] LIU, Zhanwei ; ZIEGLER, Zachary M. ; WRIGHT, Logan G. ; WISE, Frank. W.: Megawatt peak power from a Mamyshev oscillator. In: *Optica* 4 (2017), June, Nr. 6, S. 649. – URL <https://www.osapublishing.org/abstract.cfm?URI=optica-4-6-649>. – ISSN 2334-2536
- [81] LUO, Daping ; LIU, Yang ; GU, Chenglin ; ZHU, Zhiwei ; DENG, Zejiang ; ZHOU, Lian ; DI, Yuanfeng ; XIE, Gehui ; LI, Wenxue: 130 W, 180 fs ultrafast Yb-doped fiber frequency comb based on chirped-pulse fiber amplification. In: *Optics Express* 28 (2020), February, Nr. 4, S. 4817. – URL <https://www.osapublishing.org/abstract.cfm?URI=oe-28-4-4817>. – ISSN 1094-4087
- [82] MA, Chunyang ; KHANOLKAR, Ankita ; ZANG, Yimin ; CHONG, Andy: Generation of 17 fs pulses from a Mamyshev oscillator with intra-cavity photonic crystal fiber. In: *Conference on Lasers and Electro-Optics*. Washington, D.C. : OSA, 2019, S. STu3L.1. – URL https://www.osapublishing.org/abstract.cfm?URI=CLEO_{_}SI-2019-STu3L.1. – ISBN 978-1-943580-57-6
- [83] MA, Chunyang ; KHANOLKAR, Ankita ; ZANG, Yimin ; CHONG, Andy: Ultrabroadband, few-cycle pulses directly from a Mamyshev fiber oscillator. In: *Photonics Research* 8 (2020), January, Nr. 1, S. 65. – URL <https://www.osapublishing.org/abstract.cfm?URI=prj-8-1-65>. – ISSN 2327-9125
- [84] MA, Xiuquan ; ZHU, Cheng ; HU, I-Ning ; KAPLAN, Alex ; GALVANAUSKAS, Almantas: Single-mode chirally-coupled-core fibers with larger than 50 μ m diameter cores. In: *Optics Express* 22 (2014), April, Nr. 8, S. 9206. – URL <https://www.osapublishing.org/abstract.cfm?URI=oe-22-8-9206>. – ISSN 1094-4087
- [85] MAKER, P. D. ; TERHUNE, R. W. ; SAVAGE, C. M.: Intensity-Dependent Changes in the Refractive Index of Liquids. In: *Physical Review Letters* 12 (1964), May, Nr. 18, S. 507–509. – URL <https://link.aps.org/doi/10.1103/PhysRevLett.12.507>. – ISSN 0031-9007

Bibliography

- [86] MAMYSHEV, P.V.: All-optical data regeneration based on self-phase modulation effect. In: *24th European Conference on Optical Communication. ECOC '98 (IEEE Cat. No.98TH8398)* Bd. 1, Telefonica, 1998, S. 475–476. – URL <http://ieeexplore.ieee.org/document/732666/>. – ISBN 84-89900-14-0
- [87] MARCUSE, Dietrich: Curvature loss formula for optical fibers. In: *Journal of the Optical Society of America* 66 (1976), March, Nr. 3, S. 216. – URL <https://www.osapublishing.org/abstract.cfm?URI=josa-66-3-216>. – ISSN 0030-3941
- [88] MARTINEZ, O.E.: Matrix formalism for pulse compressors. In: *IEEE Journal of Quantum Electronics* 24 (1988), Nr. 12, S. 2530–2536. – URL <http://ieeexplore.ieee.org/document/14385/>. – ISSN 00189197
- [89] MIRANDA, Miguel ; FORDELL, Thomas ; ARNOLD, Cord ; L'HUILLIER, Anne ; CRESPO, Helder: Simultaneous compression and characterization of ultrashort laser pulses using chirped mirrors and glass wedges. In: *Optics Express* 20 (2012), January, Nr. 1, S. 688. – URL <https://www.osapublishing.org/oe/abstract.cfm?u>. – ISBN 1094-4087 (Electronic)\r1094-4087 (Linking)
- [90] MIRANDA, Miguel ; SILVA, Francisco ; L'HUILLIER, Anne ; ARNOLD, Cord L.: Ultrashort Pulse Characterization from Dispersion Scans with a Grating Compressor. In: *Conference on Lasers and Electro-Optics*, URL <https://www.osapublishing.org/abstract.cfm?URI=CLEO{ }AT-2016-JTu5A.67>, 2016. – ISBN 978-1-943580-11-8
- [91] MITSCHKE, F. M. ; MOLLENAUER, L. F.: Ultrashort pulses from the soliton laser. In: *Optics Letters* 12 (1987), jun, Nr. 6, S. 407. – URL <https://www.osapublishing.org/abstract.cfm?URI=ol-12-6-407>. – ISSN 0146-9592
- [92] MOLLENAUER, L. F. ; STOLEN, R. H.: The soliton laser. In: *Optics Letters* 9 (1984), January, Nr. 1, S. 13. – URL <https://www.osapublishing.org/abstract.cfm?URI=ol-9-1-13>. – ISSN 0146-9592
- [93] MORTAG, Dirk: *Investigation of femtosecond fiber laser systems with respect to low repetition rates, pulse energy scaling, and all-fiber-integrability*, Gottfried Wilhelm Leibniz Universität Hannover, Dissertation, 2012. – 129 S
- [94] MÜLLER, Michael ; ALESHIRE, Christopher ; KLENKE, Arno ; HADDAD, Elissa ; LÉGARÉ, François ; TÜNNERMANN, Andreas ; LIMPert, Jens: 10.4 kW coherently combined ultrafast fiber laser. In: *Optics Letters* 45 (2020), June, Nr. 11, S. 3083. – URL <https://www.osapublishing.org/abstract.cfm?URI=ol-45-11-3083>. – ISSN 0146-9592
- [95] NAGY, Tamas ; HÄDRICH, Steffen ; SIMON, Peter ; BLUMENSTEIN, Andreas ; WALTHER, Nico ; KLAS, Robert ; BULDT, Joachim ; STARK, Henning ; BREITKOPF, Sven ; JÓJÁRT, Péter ; SERES, Imre ; VÁRALLYAY, Zoltán ; EIDAM, Tino ; LIMPert, Jens: Generation of three-cycle multi-millijoule laser pulses at 318 W average power. In: *Optica* 6 (2019), November, Nr. 11, S. 1423. – URL <https://www.osapublishing.org/abstract.cfm?URI=optica-6-11-1423>. – ISSN 2334-2536

- [96] NORTH, Thibault ; ROCHETTE, Martin: Regenerative self-pulsating sources of large bandwidths. In: *Optics Letters* 39 (2014), January, Nr. 1, S. 174. – URL <http://www.ncbi.nlm.nih.gov/pubmed/24365851><https://www.osapublishing.org/abstract.cfm?URI=ol-39-1-174>. – ISBN 9781557529992
- [97] OBER, M. H. ; HOFER, M. ; FERMANN, M. E.: 42-fs pulse generation from a mode-locked fiber laser started with a moving mirror. In: *Optics Letters* 18 (1993), mar, Nr. 5, S. 367. – URL <https://www.osapublishing.org/abstract.cfm?URI=ol-18-5-367>. – ISSN 0146-9592
- [98] OLIVIER, Michel ; BOULANGER, Vincent ; GUILBERT-SAVARY, Félix ; SIDORENKO, Pavel ; WISE, Frank W. ; PICHÉ, Michel: Femtosecond fiber Mamyshev oscillator at 1550 nm. In: *Optics Letters* 44 (2019), February, Nr. 4, S. 851. – URL <https://www.osapublishing.org/abstract.cfm?URI=ol-44-4-851>. – ISSN 0146-9592
- [99] O'SHEA, Patrick ; KIMMEL, Mark ; GU, Xun ; TREBINO, Rick: Highly simplified device for ultrashort-pulse measurement. In: *Optics Letters* 26 (2001), June, Nr. 12, S. 932. – URL <https://www.osapublishing.org/abstract.cfm?URI=ol-26-12-932>. – ISSN 0146-9592
- [100] OUELLETTE, François: Dispersion cancellation using linearly chirped Bragg grating filters in optical waveguides. In: *Optics Letters* 12 (1987), October, Nr. 10, S. 847. – URL <https://www.osapublishing.org/abstract.cfm?URI=ol-12-10-847>. – ISSN 0146-9592
- [101] PASCHOTTA, Rüdiger ; NILSSON, Johan ; TROPPER, A.C. ; HANNA, D.C.: Ytterbium-doped fiber amplifiers. In: *IEEE Journal of Quantum Electronics* 33 (1997), July, Nr. 7, S. 1049–1056. – URL <http://ieeexplore.ieee.org/lpdocs/epic03/wrapper.htm?arnumber=594865>. – ISBN 0018-9197
- [102] PAVLOV, I. ; RYBAK, A. ; CENEL, C. ; ILDAY, F. O.: Balancing gain narrowing with self phase modulation: 100-fs, 800-nJ from an all-fiber-integrated Yb amplifier. In: *2013 Conference on Lasers & Electro-Optics Europe & International Quantum Electronics Conference CLEO EUROPE/IQEC Bd. 927*, IEEE, May 2013, S. 1–1. – URL <http://ieeexplore.ieee.org/document/6801340/>. – ISBN 978-1-4799-0594-2
- [103] PEREGO, A. M. ; TARASOV, N. ; CHURKIN, D. V. ; TURITSYN, S. K. ; STALIUNAS, K.: Pattern Generation by Dissipative Parametric Instability. In: *Physical Review Letters* 116 (2016), January, Nr. 2, S. 028701. – URL <https://link.aps.org/doi/10.1103/PhysRevLett.116.028701>. – ISSN 0031-9007
- [104] PERRY, M. D. ; DITMIRE, T. ; STUART, B. C.: Self-phase modulation in chirped-pulse amplification. In: *Optics Letters* 19 (1994), December, Nr. 24, S. 2149. – URL <https://www.osapublishing.org/abstract.cfm?URI=ol-19-24-2149>. – ISSN 0146-9592
- [105] PESSOT, M. ; MAINE, P. ; MOUROU, G.: 1000 times expansion/compression of optical pulses for chirped pulse amplification. In: *Optics Communications* 62 (1987), June, Nr. 6, S. 419–421. – URL <https://linkinghub.elsevier.com/retrieve/pii/0030401887900113>. – ISSN 00304018

Bibliography

- [106] PICHÉ, Michel: Mode locking through nonlinear frequency broadening and spectral filtering. In: PICHÉ, Michel (Hrsg.) ; PACE, Paul W. (Hrsg.): *Mode-locked and Other Ultrashort Laser Designs, Amplifiers, and Applications* Bd. 2041, URL <http://proceedings.spiedigitallibrary.org/proceeding.aspx?articleid=938810>, January 1994, S. 358–365. – ISBN 0819413003
- [107] PIERROT, S. ; SALIN, F.: Amplification and compression of temporally shaped picosecond pulses in Yb-doped rod-type fibers. In: *Optics Express* 21 (2013), August, Nr. 17, S. 20484. – URL <https://www.osapublishing.org/oe/abstract.cfm?uri=oe-21-17-20484>. – ISSN 1094-4087
- [108] POEYDEBAT, Etienne ; SCOL, Florent ; VANVINCQ, Olivier ; BOUWMANS, Geraud ; HUGONNOT, Emmanuel: All-fiber Mamyshev oscillator with high average power and harmonic mode-locking. In: *Optics Letters* 45 (2020), March, Nr. 6, S. 1395. – URL <https://www.osapublishing.org/abstract.cfm?URI=ol-45-6-1395>. – ISSN 0146-9592
- [109] RATNER, Justin ; STEINMEYER, Günter ; WONG, Tsz C. ; BARTELS, Randy ; TREBINO, Rick: Coherent artifact in modern pulse measurements. In: *Optics Letters* 37 (2012), July, Nr. 14, S. 2874. – URL <https://www.osapublishing.org/abstract.cfm?URI=ol-37-14-2874>. – ISSN 0146-9592
- [110] REGELSKIS, Kęstutis ; ŽELUDEVIČIUS, Julijanas ; VISKONTAS, Karolis ; RAČIUKAITIS, Gediminas: Ytterbium-doped fiber ultrashort pulse generator based on self-phase modulation and alternating spectral filtering. In: *Optics Letters* 40 (2015), November, Nr. 22, S. 5255. – URL <https://www.osapublishing.org/abstract.cfm?URI=ol-40-22-5255>. – ISSN 0146-9592
- [111] RENNINGER, William H. ; WISE, Frank W.: Fundamental Limits to Mode-Locked Lasers: Toward Terawatt Peak Powers. In: *IEEE Journal of Selected Topics in Quantum Electronics* 21 (2015), January, Nr. 1, S. 63–70. – URL <http://ieeexplore.ieee.org/document/6832467/>. – ISSN 1077-260X
- [112] REPGEN, Paul ; SCHUHBAUER, Benedikt ; HINKELMANN, Moritz ; WANDT, Dieter ; WIENKE, Andreas ; MORGNER, Uwe ; NEUMANN, Jörg ; KRACHT, Dietmar: Mode-locked pulses from a Thulium-doped fiber Mamyshev oscillator. In: *Optics Express* 28 (2020), April, Nr. 9, S. 13837. – URL <https://www.osapublishing.org/abstract.cfm?URI=oe-28-9-13837>. – ISSN 1094-4087
- [113] REPGEN, Paul ; WANDT, Dieter ; MORGNER, Uwe ; NEUMANN, Jörg ; KRACHT, Dietmar: Sub-50 fs, μ J-level pulses from a Mamyshev oscillator-amplifier system. In: *Optics Letters* 44 (2019), December, Nr. 24, S. 5973. – URL <https://www.osapublishing.org/abstract.cfm?URI=ol-44-24-5973>. – ISSN 0146-9592
- [114] ROCHETTE, Martin ; SUN, Kai ; HERNÁNDEZ-CORDERO, Juan ; CHEN, Lawrence R.: Multiwavelength self-pulsating fibre laser based on cascaded SPM spectral broadening and filtering. In: VALLÉE, Réal (Hrsg.) ; PICHÉ, Michel (Hrsg.) ; MASCHER, Peter (Hrsg.) ; CHEBEN, Pavel (Hrsg.) ; CÔTÉ, Daniel (Hrsg.) ; LAROCHELLE, Sophie (Hrsg.) ; SCHRIEMER, Henry P. (Hrsg.) ; ALBERT, Jacques (Hrsg.) ; OZAKI, Tsuneyuki (Hrsg.): *Photonics North 2008* Bd. 7099, URL <http://proceedings.spiedigitallibrary.org/>

- spiedigitallibrary.org/proceeding.aspx?doi=10.1117/12.805303, June 2008, S. 70990N
- [115] RUSSELL, Philip: Photonic Crystal Fibers. In: *Science* 299 (2003), January, Nr. 5605, S. 358–362. – URL <https://www.sciencemag.org/lookup/doi/10.1126/science.1079280>. – ISSN 00368075
- [116] SALEH, Bahaa E. A. ; TEICH, Malvin C.: *Fundamentals of Photonics*. New York : John Wiley & Sons, Inc., 1991. – 966 S. – ISBN 0-471-83965-5; 0-471-2-1374-8
- [117] SMARTSEV, Igor ; BORDENYUK, Andrey ; GAPONTSEV, Valentin: Environmentally stable seed source for high power ultrafast laser. In: GLEBOV, Alexei L. (Hrsg.) ; LEISHER, Paul O. (Hrsg.): *Components and Packaging for Laser Systems III* Bd. 10085, URL <http://proceedings.spiedigitallibrary.org/proceeding.aspx?doi=10.1117/12.2250641>, February 2017, S. 100850S
- [118] SCARNERA, V. ; GHIRINGHELLI, F. ; MALINOWSKI, A. ; CODEMARD, C. A. ; DURKIN, M. K. ; ZERVAS, M. N.: Modal instabilities in high power fiber laser oscillators. In: *Optics Express* 27 (2019), February, Nr. 4, S. 4386. – URL <https://www.osapublishing.org/abstract.cfm?URI=oe-27-4-4386>. – ISSN 1094-4087
- [119] SCOTT, R.P. ; LANGROCK, C. ; KOLNER, B.H.: High-dynamic-range laser amplitude and phase noise measurement techniques. In: *IEEE Journal of Selected Topics in Quantum Electronics* 7 (2001), Nr. 4, S. 641–655. – URL <http://ieeexplore.ieee.org/document/974236/>. – ISSN 1077260X
- [120] SIDORENKO, Pavel ; FU, Walter ; WISE, Frank: Nonlinear ultrafast fiber amplifiers beyond the gain-narrowing limit. In: *Optica* 6 (2019), October, Nr. 10, S. 1328. – URL <https://www.osapublishing.org/abstract.cfm?URI=optica-6-10-1328>. – ISSN 2334-2536
- [121] SIDORENKO, Pavel ; FU, Walter ; WRIGHT, Logan G. ; OLIVIER, Michel ; WISE, Frank W.: Self-seeded, multi-megawatt, Mamyshev oscillator. In: *Optics Letters* 43 (2018), June, Nr. 11, S. 2672. – URL <https://www.osapublishing.org/abstract.cfm?URI=ol-43-11-2672>. – ISSN 0146-9592
- [122] SIDORENKO, Pavel ; WISE, Frank: Generation of 1 μ J and 40 fs pulses from a large mode area gain-managed nonlinear amplifier. In: *Optics Letters* 45 (2020), July, Nr. 14, S. 4084. – URL <https://www.osapublishing.org/abstract.cfm?URI=ol-45-14-4084>. – ISSN 0146-9592
- [123] SIEGMAN, Anthony E. ; KELLY, Aidan (Hrsg.): *Lasers*. 1. Mill Valley, CA 94941 : University Science Books, 1986. – ISBN 0-935702-11-5
- [124] SNYDER, Allan W. ; YOUNG, William R.: Modes of optical waveguides. In: *Journal of the Optical Society of America* 68 (1978), March, Nr. 3, S. 297. – URL <https://www.osapublishing.org/abstract.cfm?URI=josa-68-3-297>. – ISBN 4953340450

Bibliography

- [125] SOBON, Grzegorz ; SOTOR, Jaroslaw ; MARTYNKIEN, Tadeusz ; ABRAMSKI, Krzysztof M.: Ultra-broadband dissipative soliton and noise-like pulse generation from a normal dispersion mode-locked Tm-doped all-fiber laser. In: *Optics Express* 24 (2016), March, Nr. 6, S. 6156. – URL <https://www.osapublishing.org/abstract.cfm?URI=oe-24-6-6156>. – ISSN 1094-4087
- [126] SONG, Huanyu ; LIU, Bowen ; CHEN, Wei ; LI, Yuan ; SONG, Youjian ; WANG, Sijia ; CHAI, Lu ; WANG, Chingyue ; HU, Minglie: Femtosecond laser pulse generation with self-similar amplification of picosecond laser pulses. In: *Optics Express* 26 (2018), October, Nr. 20, S. 26411. – URL <https://www.osapublishing.org/abstract.cfm?URI=oe-26-20-26411>. – ISSN 1094-4087
- [127] SQUIER, Jeff ; BARTY, Chris P. J. ; SALIN, François ; LE BLANC, Catherine ; KANE, Steve: Use of mismatched grating pairs in chirped-pulse amplification systems. In: *Applied Optics* 37 (1998), March, Nr. 9, S. 1638. – URL <https://www.osapublishing.org/abstract.cfm?URI=ao-37-9-1638>. – ISSN 0003-6935
- [128] STOLEN, R. H. ; BOTINEAU, J. ; ASHKIN, A.: Intensity discrimination of optical pulses with birefringent fibers. In: *Optics Letters* 7 (1982), October, Nr. 10, S. 512. – URL <https://www.osapublishing.org/abstract.cfm?URI=ol-7-10-512>. – ISSN 0146-9592
- [129] STRICKLAND, Donna ; MOUROU, Gerard: Compression of amplified chirped optical pulses. In: *Optics Communications* 55 (1985), October, Nr. 6, S. 447–449. – URL <http://linkinghub.elsevier.com/retrieve/pii/0030401885901518>. – ISBN 0030-4018
- [130] SZCZEPANEK, Jan ; KARDAŚ, Tomasz M. ; MICHALSKA, Maria ; RADZEWICZ, Czesław ; STEPANENKO, Yuriy: Simple all-PM-fiber laser mode-locked with a non-linear loop mirror. In: *Optics Letters* 40 (2015), August, Nr. 15, S. 3500. – URL <https://www.osapublishing.org/abstract.cfm?URI=ol-40-15-3500>. – ISSN 0146-9592
- [131] SZCZEPANEK, Jan ; KARDAŚ, Tomasz M. ; RADZEWICZ, Czesław ; STEPANENKO, Yuriy: Nonlinear Polarization Evolution of ultrashort pulses in Polarization Maintaining fibers. In: *Optics Letters* 29 (2018), April, Nr. 21, S. 2548–2550. – URL <https://arxiv.org/ftp/arxiv/papers/1804/1804.04352.pdf>
- [132] TAJALLI, Ayhan ; CHANTEAU, Bruno ; KRETSCHMAR, Martin ; KURZ, Heiko.G. ; ZUBER, David ; KOVAČEV, Milutin ; MORGNER, Uwe ; NAGY, Tamas: Few-cycle optical pulse characterization via cross-polarized wave generation dispersion scan technique. In: *Optics Letters* 41 (2016), November, Nr. 22, S. 5246. – URL <https://www.osapublishing.org/abstract.cfm?URI=ol-41-22-5246>. – ISSN 0146-9592
- [133] TANG, Yuxing ; CHONG, Andy ; WISE, Frank W.: Generation of 8 nJ pulses from a normal-dispersion thulium fiber laser. In: *Optics Letters* 40 (2015), May, Nr. 10, S. 2361. – URL <https://www.osapublishing.org/abstract.cfm?URI=ol-40-10-2361>. – ISSN 0146-9592
- [134] TARASOV, Nikita ; PEREGO, Auro M. ; CHURKIN, Dmitry V. ; STALIUNAS, Kestutis ; TURITSYN, Sergei K.: Mode-locking via dissipative Faraday instability. In: *Nature Communications* 7 (2016), August, S. 12441. – URL <http://www.nature.com/>

- doifinder/10.1038/ncomms12441. – ISBN 2041-1723 (Electronic)\r2041-1723 (Linking)
- [135] TOURNOIS, P.: New diffraction grating pair with very linear dispersion for laser pulse compression. In: *Electronics Letters* 29 (1993), Nr. 16, S. 1414. – ISSN 00135194
- [136] TREACY, E.: Optical pulse compression with diffraction gratings. In: *IEEE Journal of Quantum Electronics* 5 (1969), September, Nr. 9, S. 454–458. – URL <http://ieeexplore.ieee.org/document/1076303/>. – ISBN 0018-9197
- [137] TREBINO, Rick ; BOWLAN, Pamela ; GABOLDE, Pablo ; GU, Xun ; AKTURK, Selcuk ; KIMMEL, Mark: Simple devices for measuring complex ultrashort pulses. In: *Laser & Photonics Review* 3 (2009), April, Nr. 3, S. 314–342. – URL <http://doi.wiley.com/10.1002/lpor.200810032>. – ISSN 18638880
- [138] TREBINO, Rick ; ZEEK, Erik: Ultrashort Laser Pulses. In: *Frequency-Resolved Optical Gating: The Measurement of Ultrashort Laser Pulses*. Boston, MA : Springer US, 2000, S. 11–35. – URL http://link.springer.com/10.1007/978-1-4615-1181-6_{_}2. – ISSN 1539-3755
- [139] TURITSYN, Sergei K. ; BALE, Brandon G. ; FEDORUK, Mikhail P.: Dispersion-managed solitons in fibre systems and lasers. In: *Physics Reports* 521 (2012), December, Nr. 4, S. 135–203. – URL <https://linkinghub.elsevier.com/retrieve/pii/S0370157312002657>. – ISSN 03701573
- [140] WADSWORTH, W.J. ; KNIGHT, J.C. ; RUSSELL, P.S.J.: In: *Technical Digest. Summaries of papers presented at the Conference on Lasers and Electro-Optics. Postconference Technical Digest (IEEE Cat. No.01CH37170)*. – ISBN 1-55752-662-1
- [141] WANG, Pan ; YAO, Shunyu ; GRELU, Philippe ; XIAO, Xiaosheng ; YANG, Changxi: Pattern formation in 2- μm Tm:Mamyshev oscillators associated with the dissipative Faraday instability. In: *Photonics Research* 7 (2019), November, Nr. 11, S. 1287. – URL <https://www.osapublishing.org/abstract.cfm?URI=prj-7-11-1287>. – ISSN 2327-9125
- [142] WEN, Xin ; TANG, Guowu ; YANG, Qi ; CHEN, Xiaodong ; QIAN, Qi ; ZHANG, Qinyuan ; YANG, Zhongmin: Highly Tm³⁺ doped germanate glass and its single mode fiber for 2.0 μm laser. In: *Scientific Reports* 6 (2016), April, Nr. 1, S. 20344. – URL <http://www.nature.com/articles/srep20344>. – ISSN 2045-2322
- [143] WIENKE, Andreas ; WANDT, Dieter ; MORGNER, Uwe ; NEUMANN, Jörg ; KRACHT, Dietmar: Comparison Between Tm:YAP and Ho:YAG Ultrashort Pulse Regenerative Amplification. In: *Advanced Solid State Lasers*. Washington, D.C. : OSA, 2015, S. ATh2A.39. – URL <https://www.osapublishing.org/abstract.cfm?URI=ASSL-2015-ATh2A.39>. – ISBN 978-1-943580-02-6
- [144] XING, Lou ; TUAN, Tong ; SAINI, Than ; NGUYEN, Hoa ; SUZUKI, Takenobu ; OHISHI, Yasutake: Linear Er-doped fiber Mamyshev regenerator with high pulse energy generation. In: DONG, Liang (Hrsg.) ; ZERVAS, Michalis N. (Hrsg.): *Fiber Lasers XVII: Technology and Systems* Bd. 4360, SPIE, February 2020, S. 86.

Bibliography

- URL <http://proceedings.spiedigitallibrary.org/proceeding.aspx?doi=10.1117/12.959089>. – ISBN 9781510632837
- [145] YABLON, Andrew D.: *Springer Series in Optical Sciences*. Bd. 103: *Optical Fiber Fusion Splicing*. Berlin/Heidelberg : Springer-Verlag, 2005. – URL <http://link.springer.com/10.1007/b137759>. – ISBN 3-540-23104-8
- [146] YANG, Lih-Mei ; WAN, Peng ; PROTOPOPOV, Vladimir ; LIU, Jian: 2 μ m femtosecond fiber laser at low repetition rate and high pulse energy. In: *Optics Express* 20 (2012), February, Nr. 5, S. 5683. – URL <https://www.osapublishing.org/oe/abstract.cfm?uri=oe-20-5-5683>. – ISSN 1094-4087
- [147] ZAOUTER, Y. ; BOULLET, J. ; MOTTAY, E. ; CORMIER, E.: Transform-limited 100 μ J, 340 MW pulses from a nonlinear-fiber chirped-pulse amplifier using a mismatched grating stretcher-compressor. In: *Optics Letters* 33 (2008), July, Nr. 13, S. 1527. – URL <https://www.osapublishing.org/abstract.cfm?URI=ol-33-13-1527>. – ISSN 0146-9592
- [148] ZAOUTER, Y. ; PAPADOPOULOS, D. N. ; HANNA, M. ; BOULLET, J. ; HUANG, L. ; AGUERGARAY, C. ; DRUON, F. ; MOTTAY, E. ; GEORGES, P. ; CORMIER, E.: Stretcher-free high energy nonlinear amplification of femtosecond pulses in rod-type fibers. In: *Optics Letters* 33 (2008), January, Nr. 2, S. 107. – URL <https://www.osapublishing.org/abstract.cfm?URI=ol-33-2-107>. – ISSN 0146-9592
- [149] ŽELUDEVĪČIUS, Julijanas ; MICKUS, Marijus ; REGELSKIS, Kęstutis: Investigation of different configurations and operation regimes of fiber pulse generators based on nonlinear spectral re-shaping. In: *Optics Express* 26 (2018), October, Nr. 21, S. 27247. – URL <https://www.osapublishing.org/abstract.cfm?URI=oe-26-21-27247>. – ISSN 1094-4087
- [150] ZHAO, Wei ; HU, Xiaohong ; WANG, Yishan: Femtosecond-Pulse Fiber Based Amplification Techniques and Their Applications. In: *IEEE Journal of Selected Topics in Quantum Electronics* 20 (2014), September, Nr. 5, S. 512–524. – URL <http://ieeexplore.ieee.org/document/6747992/>. – ISSN 1077-260X
- [151] ZHOU, Shian ; KUZNETSOVA, Lyuba ; CHONG, Andy ; WISE, Frank W.: Compensation of nonlinear phase shifts with third-order dispersion in short-pulse fiber amplifiers. In: *Optics Express* 13 (2005), Nr. 13, S. 4869. – URL <https://www.osapublishing.org/oe/abstract.cfm?uri=oe-13-13-4869>. – ISSN 1094-4087

Publications

Reviewed Journal Articles

1. Paul Reppen, Dieter Wandt, Uwe Morgner, Jörg Neumann, and Dietmar Kracht. *Sub-50 fs, μ J-level pulses from a Mamyshev oscillator-amplifier system*. Optics Letters **44** (24), p. 5973 (2019).
2. Paul Reppen, Benedikt Schuhbauer, Moritz Hinkelmann, Dieter Wandt, Andreas Wienke, Uwe Morgner, Jörg Neumann, and Dietmar Kracht. *Mode-locked pulses from a Thulium-doped fiber Mamyshev oscillator*. Optics Express **28** (9), p. 13837 (2020).

Conference Contributions

1. Paul Reppen, Ayhan Tajalli, Dieter Wandt, Uwe Morgner, Jörg Neumann, Dietmar Kracht. *Characterization of ultrafast pulses of an Yb-doped fiber amplifier via dispersion scans after compression in a grism compressor*. SPIE Photonics West 2018, 10512-38 (2018)
2. Paul Reppen, Dieter Wandt, Uwe Morgner, Jörg Neumann, Dietmar Kracht. *High-Energy Ultrafast Yb-Fiber Laser System Based on a Mamyshev Regenerator*. CLEO/Europe-EQEC Conference, CJ-7.2 (2019)
3. Paul Reppen, Dieter Wandt, Uwe Morgner, Jörg Neumann, and Dietmar Kracht. *Amplification of ultrafast pulses in an extended Mamyshev regenerator*. In L. Dong & M. N. Zervas (Eds.), Fiber Lasers XVII: Technology and Systems (p. 24). SPIE Photonics West 2020 (2020)
4. Paul Reppen, Dieter Wandt, Andreas Wienke, Uwe Morgner, Jörg Neumann, Dietmar Kracht. *High-energy pulses from an Yb-doped fiber Mamyshev oscillator by the use of a few-mode amplification fiber*. Europhoton 2020, Tu-M2.5 (2020)
5. Paul Reppen, Benedikt Schuhbauer, Moritz Hinkelmann, Dieter Wandt, Andreas Wienke, Uwe Morgner, Jörg Neumann, Dietmar Kracht. *Generation of high-energy pulses in a Thulium-doped fiber Mamyshev oscillator*. Europhoton 2020, Tu-M2.6 (2020)
6. Paul Reppen, Dieter Wandt, Andreas Wienke, Uwe Morgner, Jörg Neumann, Dietmar Kracht. *Yb-doped fiber Mamyshev oscillator with a few-mode gain fiber*. SPIE Photonics West 2021, Paper number LA102-43 (2021)
7. Paul Reppen, Benedikt Schuhbauer, Moritz Hinkelmann, Dieter Wandt, Andreas Wienke, Uwe Morgner, Jörg Neumann, Dietmar Kracht. *Dispersion-managed Thulium-doped fiber Mamyshev oscillator*. SPIE Photonics West 2021, Paper number LA102-44 (2021)

Curriculum Vitae

Personal Details

Name	Paul Christoph Reppen
Date of birth	26.05.1991
Place of birth	Düsseldorf
Nationality	German

Education

Jun 2010	Abitur, St.-Ursula-Gymnasium Attendorn
----------	--

Community Service

Aug 2010 – Jul 2011	Volunteer for the German Development Service at the Adwoki Technical School, Uganda
---------------------	---

University Education

Oct 2011 – Sep 2014	Studies of Physics at the Westfälische Wilhelms-Universität Münster, degree: Bachelor of Science Thesis title: <i>Spontane Ramanstreuung als Kontrast in einem konfokalen Mikroskop</i>
Oct 2014 – Nov 2016	Studies of Physics at the Westfälische Wilhelms-Universität Münster, degree: Master of Science Thesis title: <i>Investigations on an All-PM, Fiber-Based, Yb³⁺-Doped Master-Oscillator Power-Amplifier System</i>
Oct 2017 – present	Ph.D. student in Physics at the Leibniz Universität Hannover

Professional Affiliations

Aug 2014 – Aug 2015	Student assistant at zeb consulting Münster
Oct 2015 – Sep 2016	Teaching assistant for internships in Physics for medical students at Westfälische Wilhelms-Universität Münster
Jan 2017 – present	Research scientist at Laser Zentrum Hannover

Acknowledgement

At this point, I want to thank those people who supported the origin of this thesis. First of all, I want to thank Prof. Dr. Uwe Morgner for his support and supervision of my work in general and this thesis in particular. Furthermore, I want to thank Prof. Dr. Detlev Ristau and Prof. Dr. Ömer Ilday for their evaluation of this thesis.

For proofreading, I would further like to thank Dr. Andreas Wienke, Dr. Moritz Hinkelmann, Dr. Dieter Wandt, and Dr. Jörg Neumann. I would like to thank Dr. Dietmar Kracht, Dr. Jörg Neumann, and Dr. Dieter Wandt for the opportunity to work at the Laser Zentrum in the Laser Development Department in the 2+2-project "OPUMAC".

Dr. Dieter Wandt and Dr. Andreas Wienke offered valuable input as heads of the Ultrafast Photonics Group. My fellow PhD-students and colleagues were always available for fruitful discussions. Thank you for that.

